Air–Sea CO_2 Cycling in the Southeastern Beaufort Sea

Brent Gordon Thomas Else

Department of Environment and Geography

University of Manitoba

A thesis submitted to the Faculty of Graduate Studies of

The University of Manitoba

in partial fulfilment of the degree of

Doctor of Philosophy

© B.G.T. Else, August 20, 2012

For Nancy,
my partner in this journey
and many others.

Acknowledgements

An interdisciplinary work such as this is not possible without the help of a great many people. I am very thankful for the data collection efforts of Bruce Johnson, Sarah Woods, Kyle Swystun, Gauthier Carnat, Elizabeth Shadwick, Keith Johnson, Jens Ehn, Silvia Gremes-Cordero, Sylvain Blondeau, Luc Michaud and many others. I also benefited greatly from the assistance of Ryan Galley, Lisa Miller, Al Mucci, Helmuth Thomas, Will Drennan, C.J. Mundy, Matthew Asplin and Michel Gosselin, who each guided me and provided practical assistance when I waded into their areas of expertise. I am also very grateful for the help of the Captains and crew of the CCGS *Amundsen*, my thesis advisory committee, and of course my supervisor, Tim Papakyriakou.

This work also required tremendous financial support. Much of that support came through the resources and opportunities provided by the International Polar Year-Circumpolar Flaw Lead System Study (IPY-CFL 2008), which was funded by the Canadian IPY Federal program office, NSERC, Fisheries and Oceans Canada and many other contributors. I also benefited from involvement in ArcticNet, which is funded in part by NCE Canada, NSERC, CIHR and SSHRC. I personally received generous financial support from a Vanier Canada Graduate Scholarship and a Duff Roblin Fellowship, and received logistical support from the Northern Scientific Training Program and the Centre for Earth Observation

Science. I also wish to acknowledge the successes that key members of the Arctic research community have achieved in establishing a wealth of infrastructure and opportunities for graduate students studying the Arctic in Canada. For their past and ongoing efforts to these ends, thanks are due to Dave Barber, Louis Fortier, Martin Fortier, Gary Stern, Jody Deming and the many others who have been instrumental in securing funding for projects such as IPY-CFL and ArcticNet.

Finally, this work required a great deal of personal support. Much of that support came from my wife and from our immediate families. However, an incredible amount of support came from the people we built relationships with here in Winnipeg. Specifically, I am thankful for the friendships of Lauren Hope and Brendon Boland, Christopher and Joanna Neufeld, Jeff and Charlotte Ehlers, Matthew and Laura Asplin, Marc Cadieux, and the congregation of Central Baptist Church. Those people (amongst many others) have made Winnipeg a great place for us to live, work, and raise a family. And for that I am most thankful.

"For unto whomsoever much is given, of him shall much be required; and to whom men have committed much, of him they will ask the more."

Luke 12:48

Abstract

During the fourth International Polar Year, an interdisciplinary study was conducted to examine the couplings between sea ice, ocean, atmosphere, and ecosystem in the southeastern Beaufort Sea. This thesis examines components of the system that control the air–sea exchange of carbon dioxide. Using eddy covariance measurements, we found enhanced CO_2 exchange associated with new ice formation in winter flaw leads. This exchange was typically directed towards the surface, although we also measured one instance of outgassing. Sea surface dissolved CO_2 measurements (pCO_{2sw}) in Amundsen Gulf showed significant undersaturation with respect to the atmosphere at freeze–up, followed by a slow increase over the winter until spring phytoplankton blooms caused strong undersaturation at break–up. Over the summer, pCO_{2sw} increased until becoming slightly supersaturated due to surface warming. Along the southern margins of Amundsen Gulf and on the Mackenzie Shelf we found pCO_{2sw} supersaturations in the fall due to wind–driven coastal upwelling. In the spring, this upwelling occurred along the landfast ice edges of Amundsen Gulf. By combining observations of enhanced winter gas exchange with observations of pCO_{2sw} in Amundsen Gulf, we derived an annual budget of air–sea CO_2 exchange for the region. This exercise showed that uptake through the winter season was as impor-

tant as the open water season, making the overall annual uptake of CO_2 about double what had previously been calculated.

Prior to this work, the prevailing paradigm of airsea CO_2 cycling in Arctic polynya regions posited that strong CO_2 absorption occurs in the open water seasons, and that a potential outgassing during the winter is inhibited by the sea ice cover. As a new paradigm, we propose that the spatial and temporal variability of many processes – including phytoplankton blooms, sea surface temperature and salinity changes, upwelling, river input, continental shelf processes, and the potential for high rates of winter gas exchange – need to be considered in order to understand the carbon source/sink status of a given Arctic polynya region. A paradigm that considers such varied processes is useful in understanding how climate change in the Arctic can impact ai–sea CO_2 exchange.

Contents

List of Tables

LIST OF TABLES

List of Figures

Use of Copyrighted Material

Chapter 2 of this thesis is reproduced with minor modifications from Else et al. [2011, Wintertime CO_2 fluxes in an Arctic polynya using eddy covariance: Evidence for enhanced air-sea gas transfer during ice formation, *Journal of Geophysical Research*, 116, CO00G03, doi:10.1029/2010JC006760], with permission from the American Geophysical Union.

Chapter 3 of this thesis is reproduced with minor modifications from Else et al. [2012, Annual cycles of pCO_{2sw} in the southeastern Beaufort Sea: New understandings of air–sea CO_2 exchange in Arctic polynyas, *Journal of Geophysical Research*, 117, C00G13, doi:10.1029/2011JC007346], with permission from the American Geophysical Union.

Chapter 4 of this thesis is reproduced with minor modifications from Else et al. [in press, Sea surface pCO_2 cycles and CO_2 fluxes at landfast sea ice edges in Amundsen Gulf, Canada, *Journal of Geophysical Research*, doi:10.1029/2012JC007901], with permission from the American Geophysical Union.

Chapter 5 of this thesis is reproduced with minor modifications from Else et al. [in review, Annual and interannual variability of air-sea CO_2 exchange in an Arctic polynya region, *Global Biogeochemical Cycles*, MS#2012GB004425], with permission from the American Geophysical Union.

Chapter 1

Introduction

1.1 Motivation

1.1.1 The Global Ocean CO_2 Sink: Grace Running Out?

In recent years, an important debate has emerged regarding where humanity should attempt to stabilize atmospheric CO_2 levels. The target agreed to in principle under the United Nations Framework Convention on Climate Change is 450 ppm, a level commonly (although debatably) cited as the highest we can go while avoiding catastrophic climate change [Hansen et al., 2007]. It is therefore interesting to consider that the 450 ppm target is only possible because of the role the global oceans play in offsetting our CO_2 emissions. Since industrialization, oceans have absorbed nearly 50% of fossil fuel and cement–manufacturing carbon emissions [Sabine et al., 2004], and without that sink atmospheric CO_2 levels would have exceeded 450 ppm at some point in 2011. Given our hesitation to commit resources towards meeting CO_2 targets, it can be argued that the ocean carbon sink has quite literally bought us time.

The question then emerges as to whether or not this grace period afforded by the oceans will continue, or if at some point the ocean sink will cease to be as effective. The pre-industrial global ocean is thought to have been a net source of atmospheric CO_2 [Sarmiento and Sundquist, 1992], acting as a component in a near-equilibrium system where carbon was released to the atmosphere by the oceans, absorbed from the atmosphere by terrestrial vegetation, and then delivered back to the oceans by rivers carrying eroded soil carbon [Watson et al., 2011]. The subsequent transition to an ocean carbon sink was a direct result of the rapid accumulation of CO_2 in the atmosphere, which inverted the mean air–sea CO_2 gradient. Therefore, one might think that as atmospheric CO_2 concentrations continue to increase, an even stronger ocean carbon sink will emerge. While this seems to have been the case for most of the period since industrialization [Sarmiento et al., 1998], evidence is emerging that the ocean sink is no longer keeping up with carbon emissions [Denman et al., 2007; Sarmiento et al., 1998].

Part of this slow down is due to inevitable changes in ocean carbon chemistry, but in some regions additional changes can be linked to climate processes. For example, instead of increasing, the Southern Ocean CO_2 sink has remained constant over the last two decades as a result of increased wind–driven upwelling [Le Quéré et al., 2007]. As a further example, the North Atlantic CO_2 sink weakened over the period 1990–2006 due to a reduction in vertical transport and a stagnation of surface water, which allowed it to approach equilibrium with the atmosphere [Schuster and Watson, 2007]. In both of these cases, variability in air–sea CO_2 exchange can be linked to large–scale climate variability, which provides a convincing argument that climate change may impact the ability of certain oceans to absorb CO_2 [Watson et al., 2011]. Part of the challenge for predicting the future of the ocean carbon sink therefore lies

in understanding the processes which control regional CO_2 exchange, and predicting how those processes may be impacted by climate change.

1.1.2 The Arctic Ocean: A Changing CO_2 Sink?

Nowhere is the potential impact of climate change on marine carbon cycling greater than in the Arctic. Over recent decades, surface air temperature in the Arctic has increased at nearly twice the global average rate [ACIA, 2004]. Positive feedbacks associated with sea ice loss appear to be the main cause of this "Arctic amplification" [Screen and Simmonds, 2010; Serreze et al., 2009], although other processes such as increasing poleward atmospheric heat transport [Graversen et al., 2008], changing cloud cover [Schweiger et al., 2008], and changes in atmospheric water vapour content [Francis and Hunter, 2007] have also been implicated. In their review paper, Bates and Mathis [2009] found that most Arctic seas act as relatively strong sinks for CO_2, but they also identified many pathways by which the Arctic marine carbon cycle is vulnerable to this amplified signal of climate change.

The rapid decrease in minimum sea ice extent (e.g. Comiso et al. [2008]) observed over the past three decades probably has the widest reaching implications. Most notably, this loss of ice coverage has exposed large areas of the Arctic ocean to the atmosphere, removing potential restrictions on air–sea gas exchange. Bates et al. [2006] estimated that the sink of CO_2 in the Arctic Ocean has tripled as a result of this ice loss, although subsequent studies have found that the ability for these exposed waters to absorb CO_2 may be limited [Cai et al., 2010]. Ice loss has also increased photosynthetic production in the Arctic, both by exposing a larger expanse of the surface ocean to light penetration, and by extending the growing season in other seasonally ice free regions [Arrigo et al., 2008; Pabi et al., 2008]. An increase

in primary productivity should reduce surface CO_2 concentrations, but the strength of that effect largely depends on whether organic carbon can be effectively exported from the surface.

Implied in the observation of decreasing summer sea ice extent is an increasing area which undergoes freeze–thaw cycles every year. This has two important implications for air–sea gas exchange. First, there is evidence that a strong pulse of CO_2 uptake occurs during initial ice formation [Anderson et al., 2004], which may become more important as the seasonal ice area expands. Second, the formation and melt of sea ice has been linked to a process known as the "sea ice pump". This mechanism was proposed by Rysgaard et al. [2007], who observed high alkalinity relative to dissolved inorganic carbon (DIC) in Arctic sea ice. The likely cause of this enrichment is the formation of calcium carbonate ($CaCO_3$) crystals which are are retained in brine pockets and channels while DIC is removed by brine drainage. The subsequent flushing by spring melt dissolves the $CaCO_3$ crystals, releasing alkalinity and reducing surface CO_2 concentrations.

Also associated with sea ice loss are notable changes in the physical properties of the surface ocean. Significant increases in surface ocean temperature have been observed in most areas of the Arctic, with particularly strong warming in areas where summer ice extent has experienced dramatic reductions [Steele et al., 2008]. Since water temperature has a direct effect on CO_2 concentrations [Takahashi et al., 1993], this warming must be reducing to some extent the uptake capacity of these waters. Remarkable freshening of the Canada basin sector of the Arctic Ocean has also been observed [McPhee et al., 2009; Morison et al., 2012], largely associated with a change in circulation that is redirecting runoff from Siberian rivers and causing a compensating increase of salinity in the Eurasian sector. Freshening reduces the

surface ocean's buffering capacity (e.g. Yamamoto-Kawai et al. [2009]) and modifies the solubility of CO_2, but it also has indirect impacts. A warmer and fresher ocean is more stable, which reduces the vertical transport of nutrient and CO_2–rich water, in turn limiting primary production (e.g. Tremblay et al. [2008]).

With these overarching issues providing the motivation, research on Arctic marine carbon cycling is at an interesting point. So far, studies of the processes controlling air–sea CO_2 exchange have been limited, providing mostly snapshots of certain regions in certain seasons. Those snapshots show interesting potential links with climate change, but we lack more complete studies of air–sea carbon exchange (e.g. over larger spatial domains or over annual cycles), which would allow us to identify which processes are most important, and therefore where climate change is likely to have its biggest impact. The objectives of this thesis are designed to work towards addressing that deficiency.

1.2 Thesis Objectives

Polynya regions (areas which host unseasonable open water or thin ice at some point in their annual cycle) have long been cited as useful microcosms for studying air–sea gas exchange in polar oceans. Interactions between components of the physical and biogeochemical systems are amplified in these regions, and the seasonal ice cycles that they undergo can be used as analogues for areas of the Arctic Ocean that are becoming seasonally ice free under the influence of climate change. Although gas exchange studies of polynya regions are sparse, a general hypothesis has been formulated to describe their annual air–sea CO_2 exchange cycle [Yager et al., 1995]. The hypothesis posits that during the late spring, summer, and early fall, surface water CO_2 concentrations are typically low and ice coverage is minimal, permitting

uptake of atmospheric CO_2 by the ocean. During winter, when surface water CO_2 concentrations increase, a more complete ice cover prevents the release of CO_2 from the ocean to the atmosphere. The hypothesis states that the imbalance between uninhibited uptake during the open water season, and restricted outgassing during the ice covered season, results in polynya regions acting as strong annual sinks for CO_2.

The overarching goal of this thesis is to test this hypothesis in three polynya regions of the southeastern Beaufort Sea: the Mackenzie Shelf, the Banks Island Shelf and Amundsen Gulf. Couplings between the atmosphere, ice, ocean and ecosystem were intensely studied in these areas over an annual cycle in 2007–08 as part of the International Polar Year projects of ArcticNet and the Circumpolar Flaw Lead System Study. The objectives of this thesis focus on the components of the system which control air–sea CO_2 exchange, and are as follows:

1. Observe the rate of CO_2 exchange under varying ice, ocean and atmospheric conditions, and examine the processes that control that rate.

2. Observe the air–sea CO_2 concentration gradient in the study region over an annual cycle, and examine the physical and biogeochemical processes that determine its magnitude.

3. Calculate seasonal and annual budgets of CO_2 exchange for the study regions.

4. Discuss the potential for using results obtained in this region as a model for other Arctic regions.

5. Discuss how this system (and by extension other similar systems) may be affected by climate change.

1.3 Thesis Outline

This thesis is composed of four research papers, each of which makes up an individual chapter. The first paper (Chapter 2) describes eddy covariance measurements of CO_2 exchange rates made during the fall and early winter seasons. This work primarily addresses objective 1, and it has been peer–reviewed and published in *Journal of Geophysical Research – Oceans*:

Else, B.G.T., Papakyriakou, T.N., Galley, R.J., Drennan, W.M., Miller, L.A., and H. Thomas (2011). Wintertime CO_2 fluxes in an Arctic polynya using eddy covariance: Evidence for enhanced air-sea gas transfer during ice formation. *J. Geophys. Res.*, 116, C00G03, doi:10.1029/2010JC006760.

The second paper (Chapter 3) describes measurements of the sea surface partial pressure of CO_2 and analyses of the processes controlling its variability in each of the three study regions. This work addresses objective 2, and it has been peer–reviewed and published in *Journal of Geophysical Research – Oceans*:

Else, B.G.T., Papakyriakou, T.N., Galley, R.J., Mucci, A., Gosselin, M., Miller, L.A., Shadwick, E., and H. Thomas (2012). Annual cycles of pCO_{2sw} in the southeastern Beaufort Sea: New understandings of air-sea CO_2 exchange in Arctic polynya regions. *J. Geophys. Res.*, 117, C00G13, doi: 10.1029/2011JC007346.

The third paper (Chapter 4) describes measurements of the sea surface partial pressure of CO_2 and calculated CO_2 fluxes along the landfast ice regions of southern Amundsen Gulf. This work primarily addresses objective 2 and 3, and it is currently in press at *Journal of Geophysical Research – Oceans*:

Else, B.G.T., Galley, R.J., Papakyriakou, T.N., Miller, L.A., Mucci, A., and D. Barber (in press). Sea surface pCO_2 cycles and CO_2 fluxes at landfast sea ice edges in Amundsen Gulf, Canada. *J. Geophys. Res.*, doi:10.1029/2012JC007901.

The final paper (Chapter 5) combines results presented in Chapters 3 and 4 to derive a budget of air–sea CO_2 exchange in Amundsen Gulf. These results are then placed in the context of long–term variability in the processes that control air–sea CO_2 flux, and the potential impacts of climate change are presented. This work addresses objectives 3, 4 and 5, and has been submitted to *Global Biogeochemical Cycles*:

Else, B.G.T., Papakyriakou, T.N., Galley, R.J., Miller, L.A., Mucci, A., Asplin, M.G. and D. Barber. An annual air–sea CO_2 flux budget for the Cape Bathurst polynya region (in review). Submitted to *Global Biogeochem. Cy.*.

In Chapter 6 the results of Chapters 2–5 are summarized, limitations and future work are discusssed, and concluding remarks are presented.

Chapter 2

Wintertime CO_2 Fluxes in an Arctic Polynya Using Eddy Covariance: Evidence for Enhanced Air–Sea Gas Transfer During Ice Formation

Journal of Geophysical Research – Oceans, 116, C00G03,

doi: 10.1029/2010JC006760

Brent G.T. Else*[1], Tim N. Papakyriakou[1], Ryan J. Galley[1], Will M. Drennan[2], Lisa A. Miller[3], and Helmuth Thomas[4]

[1]Centre for Earth Observation Science, Department of Environment and Geography, University of Manitoba, Winnipeg, Manitoba, Canada

[2]Division of Applied Marine Physics, Rosenstiel School of Marine and Atmospheric Science, University of Miami, Miami, Florida, USA

[3]Centre for Ocean Climate Chemistry, Institute of Ocean Sciences, Fisheries and Oceans Canada, Sidney, British Columbia, Canada

[4]Department of Oceanography, Dalhousie University, Halifax, Nova Scotia, Canada

Abstract

Between November 1 2007 and January 31 2008, we calculated the air–sea flux of CO_2, sensible heat, and water vapour in an Arctic polynya system (Amundsen Gulf, Canada) using eddy covariance equipment deployed on the research icebreaker CCGS *Amundsen*. During this time period, Amundsen Gulf was a dynamic sea ice environment composed primarily of first year ice with open water coverage varying between 1–14%. In all cases where measurements were influenced by open water we measured CO_2 fluxes that were 1–2 orders of magnitude higher than those expected under similar conditions in the open ocean. Fluxes were typically directed towards the water surface with a mean flux of -4.88 μmol m^{-2} s^{-1} and a maximum of -27.95 μmol m^{-2} s^{-1}. One case of rapid outgassing (mean value +2.10 μmol m^{-2} s^{-1}) was also observed. The consistent patten of enhanced gas exchange over open water allows us to hypothesize that high water–side turbulence is the main cause of these events. Modification of the physical and chemical properties of the surface seawater by cooling and brine rejection may also play a role. A rough calculation using an estimate of open water coverage suggests that the contribution of these events to the annual regional air–sea CO_2 exchange budget may make the winter months as important as the open water months. Although high, the uptake of CO_2 fits within mixed layer dissolved inorganic carbon budgets derived for the region by other investigators.

2.1 Introduction

In order to properly forecast the effects of climate change, general circulation models need to adequately account for sources and sinks of CO_2. The global marine

system plays a major role in cycling CO_2 and presently absorbs about 2.2 PgC year^{-1}[Denman et al., 2007], which offsets about 30% of present anthropogenic emissions. However, the rate of CO_2 uptake is not consistent across all oceans. On an annual basis a given region may behave anywhere on the spectrum from a strong source of CO_2 to a strong sink, and significant inter- and intra-annual variability may also exist [Takahashi et al., 2009]. This spatio-temporal variability arises from variability in the processes controlling CO_2 fluxes.

For the open ocean, research has advanced to the point where these processes are known well enough to make reasonable flux estimates at a wide range of scales (see review by Wanninkhof et al. [2009]). Typically, estimates of CO_2 flux (F_{CO_2}) are computed using a form of the bulk flux equation:

$$F_{CO_2} = \alpha k(p\mathrm{CO}_{2sw} - p\mathrm{CO}_{2air}) \tag{2.1}$$

where α is the solubility of CO_2 in water, $p\mathrm{CO}_{2sw}$ is the partial pressure of CO_2 in the surface seawater, $p\mathrm{CO}_{2air}$ is the partial pressure of CO_2 in the atmosphere and k is the gas transfer velocity. Using this approach, the air-sea gradient of CO_2 ($p\mathrm{CO}_{2sw} - p\mathrm{CO}_{2air}$, commonly denoted $\Delta p\mathrm{CO}_2$) determines the potential for exchange, while the transfer velocity encompasses the processes that control the rate at which the exchange can occur. The main determinant of transfer velocity is water-side turbulence, which itself is mainly determined by wind velocity through its relationship with momentum flux [Jähne, 1987]. Many other factors influence water-side turbulence, such as wave state [Bock et al., 1999; Zappa et al., 2004], surface films [Frew, 1997; Frew et al., 2004; Jähne, 1987], rain [Ho et al., 2004; Takagaki and Komori, 2007; Zappa et al., 2009], tides [Zappa et al., 2007], and buoyancy [McGillis et al., 2004]. In addition, several processes not directly related

to turbulence also affect transfer velocity, such as chemical enhancement [Bolin, 1960; Kuss and Schneider, 2004] and bubbles from breaking waves [Asher et al., 1996; Woolf, 1997; Woolf et al., 2007]. Despite the myriad processes affecting gas exchange, wind velocity alone is typically used to estimate transfer velocity in the open ocean with mature wave fields [Wanninkhof et al., 2009]. As such, numerous parameterizations to estimate k from wind speed have been created based on tank experiments [Liss and Merlivat, 1986], modelling exercises [Sweeney et al., 2007; Wanninkhof, 1992], and field studies conducted primarily at low and mid–latitudes [Ho et al., 2006; Nightingale et al., 2000; Wanninkhof and McGillis, 1999].

At high latitudes (e.g. the Arctic), the processes that control CO_2 fluxes are not well known. Depending on the season and location, a given region of the Arctic Ocean may be ice free or it may be covered by sea ice of variable concentration, thickness and thermodynamic state. During the open water season it is reasonable to assume that what we understand about open-ocean fluxes would be applicable, but as soon as sea ice is present existing parameterizations of transfer velocity are likely invalid. Although sea ice is permeable to gas exchange under certain conditions [Gosink et al., 1976], the mechanisms that control the rate of exchange are very different from the open ocean. Furthermore, the open water that does remain in an icescape experiences different controls on near-surface turbulence; fetch limitations [Woolf, 2005] imposed by surrounding ice floes and the generation of turbulence due to ice formation [McPhee and Stanton, 1996] are two examples of those unique controls.

The initial freeze-up and growth of sea ice has generated considerable interest, since the process significantly modifies the chemistry of the surface ocean and because dissolved inorganic carbon (DIC) may be driven down from the surface with

rejected brines in what has been termed a sea ice CO_2 pump [Anderson et al., 2004; Rysgaard et al., 2009, 2007] . A water column study by Anderson et al. [2004] in Svalbard found high DIC and elevated chlorofluorocarbon levels in deep waters, which they hypothesized originated from enhanced air-sea exchange of CO_2 during ice formation. Some support for this enhanced exchange was recently presented in a tank study by Loose et al. [2009]. In this paper, we describe the first eddy covariance observations of such flux enhancements over a natural sea ice surface.

2.2 Study Area

The data presented in this paper were collected between November 1, 2007 and January 31, 2008 during the International Polar Year Circumpolar Flaw Lead System Study (CFL) in Amundsen Gulf and the southeastern Beaufort Sea (Figure 2.1). The region is subject to a complex annual ice cycle which has been summarized by Galley et al. [2008]. The open water season (defined as sea ice concentration $\leq 20\%$) typically lasts 10 weeks, starting in late July. Freeze-up occurs in early October and is characterized by initial landfast ice growth along the coastal margins. The ice which forms offshore in Amundsen Gulf typically remains mobile during the time period of this study (shaded areas in Figure 2.1), creating an icescape which is characterized by small transient leads and polynyas. Later in the winter the eastern half of Amundsen Gulf may become landfast, and on some occasions the western portion becomes landfast as well. The Beaufort Sea pack ice remains mobile throughout the winter, rotating with the predominant Beaufort gyre to create persistent linear flaw lead features (Figure 2.1). The mean spring breakup for Amundsen Gulf is early June, which creates the feature commonly referred to as the Cape Bathurst polynya (Figure 2.1) which in some years extends well into eastern Amundsen Gulf.

Figure 2.1: Map of the Banks Island flaw lead/polynya complex. The light grey line shows the ship track. The shaded grey area represents the region which usually remains mobile through the time period under consideration, and the dotted line shows the areas typically associated with the Cape Bathurst polynya and flaw lead.

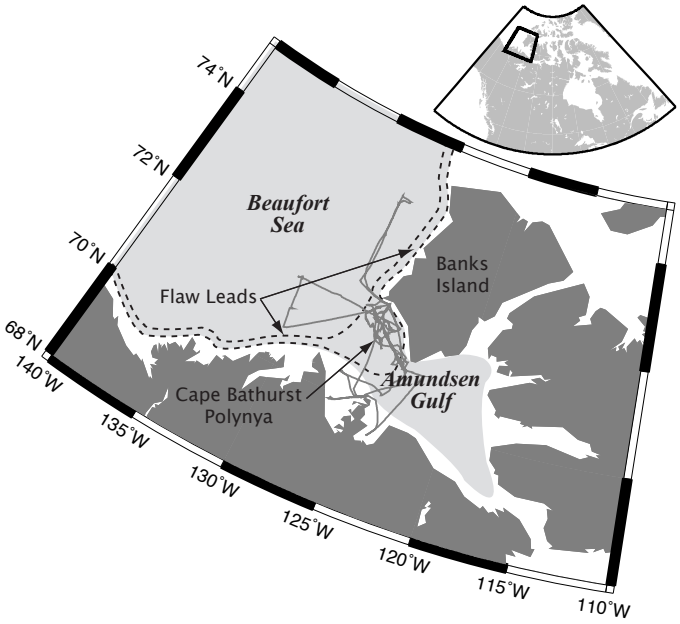

Observations have shown that the region experiences significant air-sea pCO_2 gradients in the fall. Mucci et al. [2010] observed ΔpCO_2 ranging from -138 to -28 μatm from September–November 2003, and Murata and Takizawa [2003] observed gradients of similar magnitude during three years of cruises in August–September, 1998–2000. Observations made during the CFL study showed that significant undersaturation (ΔpCO_2 typically around -70 μatm) persisted through the end of January 2008 in offshore Amundsen Gulf [Else et al., 2012b; Shadwick et al., 2011].

During the winter season, the persistent flaw leads and polynyas in combination with strong local pCO_2 gradients make this study area an ideal location for examining the effect of freezing sea ice on gas exchange.

2.3 Methods

2.3.1 Atmospheric Instrumentation

For the duration of the experiment a guyed open-lattice tower at the bow of the ship was instrumented with eddy covariance and meteorological equipment. The flux instrumentation consisted of a Gill Windmaster Pro sonic anemometer/thermometer, a LI-COR LI-7500 open path CO_2/H_2O gas analyzer and a Systron Donner MotionPak. The flux instrumentation was located at a height of 14 m above the surface (7 m above the deck of the ship), with the exception of the MotionPak which was located at the midpoint of the tower.

The meteorological equipment consisted of a conventional anemometer for wind speed and direction (RM Young 05103, height=15 m), a temperature/relative humidity probe (Vasailla HMP45C212, height=14 m) and a pressure sensor (RM Young 61205V). An array of radiation sensors was deployed on top of the wheelhouse of the ship, consisting of a photosynthetically active radiation (PAR) sensor (Kipp & Zonen PARlite), an incoming shortwave radiation sensor (Eppley PSP) and an incoming longwave radiation sensor (Eppley PIR).

2.3.2 Surface Water pCO_2 Instrumentation

Surface water from a dedicated scientific intake line (depth ~5 m) was continuously sampled for pCO_{2sw} using a shower-type equilibrator which cycled headspace air through a LI-COR LI-7000 CO_2/H_2O gas analyzer [Körtzinger et al., 1996]. The gas analyzer was calibrated daily using ultra-high purity N_2 as a zero gas and a CO_2/air mixture traceable to WMO standards as a span gas. The instrument was located in the engine room very close to the water intake, but a slight warming of the sample

water relative to results from CTD casts was detected by a thermocouple in the equilibrator. This warming effect was very consistent, allowing correction of pCO_{2sw} for thermodynamic effects following Takahashi et al. [1993] (see chapter 3.3.1 for a more complete description). After correction, the pCO_{2sw} measurements showed good agreement ($r^2 = 0.9$, mean difference = 19 μatm, no statistically significant bias) with independent calculations from DIC/TA measurements (see Shadwick et al. [2011] for a description of the DIC/TA dataset and methods).

2.3.3 Study Design

The CFL study was a unique over-wintering experiment because the research vessel remained mobile through the entire winter. The goal of this strategy was to create a time series of the seasonal evolution of the flaw lead/polynya system. Logistically, this meant that the specific location and operation of the vessel was highly opportunistic; when ice conditions allowed the ship to move freely, spatial sampling was conducted, but when ice conditions were more severe the ship was positioned in large consolidated floes and allowed to drift. These floes were typically occupied for 1 – 7 days, depending on the stability of the floe and whether or not it was drifting outside of the study area. When repositioning was necessary, the ship would break out of the floe and either break ice or transit through small cracks until a more suitable floe was located.

2.3.4 Eddy Covariance

The study design allowed us to examine a sea ice system which would otherwise be inaccessible, but it does have implications for the eddy covariance technique which is best suited for a stationary tower over a homogenous surface. To help address these

issues, we filtered the data to ensure that each eddy covariance run was not subject to significant changes either in ship operation or atmospheric conditions. If the ship was under power, ship velocity and course over ground were required to be consistent (within $\pm$ 3.7 km hr^{-1} of mean for velocity and $\pm$ 27.5° of mean for course). Relative wind direction was also required to be consistent within $\pm$27.5° of the mean, and it was further restricted to within $\pm$ 90° of the bow of the ship to reduce the effects of flow distortion. To help with the issue of non–homogeneous surfaces, we found it useful to break the data up into individual case studies during time periods where flux data collection was consistent and the ship location, atmospheric conditions and sea ice conditions were fairly uniform (see Table 2.1, Figure 2.2).

Filtering was also necessary to remove instances where atmospheric conditions negatively impacted the flux instruments. The LI-7500 outputs a diagnostic value that warns of lens obstruction, which during this study was most often caused by accretion of rime. We filtered out all instances where the diagnostic value exceeded its normal operating range, creating a fairly significant loss of data. The sonic anemometer was less influenced by riming, but filtering was carried out based on the characteristically erratic performance of the instrument that occurs under such circumstances.

The LI-7500 used in this study makes high frequency (10Hz) measurements of the molar concentrations of CO_2 and water vapour (c_{co_2} and c_v respectively). By combining these measurements with high frequency vertical wind velocity (w) measurements from the sonic anemometer, the flux of CO_2 is calculated over an averaging period (in this case, 30 minutes) via:

$$F_c = \overline{w'c'_{co_2}} + \frac{\overline{c}_{co_2}}{\overline{c}_d}\left[\overline{w'c'_v} + \overline{c_a}\frac{\overline{w'T'}}{\overline{T}}\right] \tag{2.2}$$

Figure 2.2: Measured CO_2 fluxes (including sensor heating correction) for the study period. The numbers along the top axis indicate the sample cases, the most interesting of which are discussed in the text, with the red brackets denoting their time frame. The inset shows observations made between December 1–2 with an extended scale on the y-axis. The horizontal grey lines show the estimated noise level of the eddy covariance system as discussed in section 2.5.1

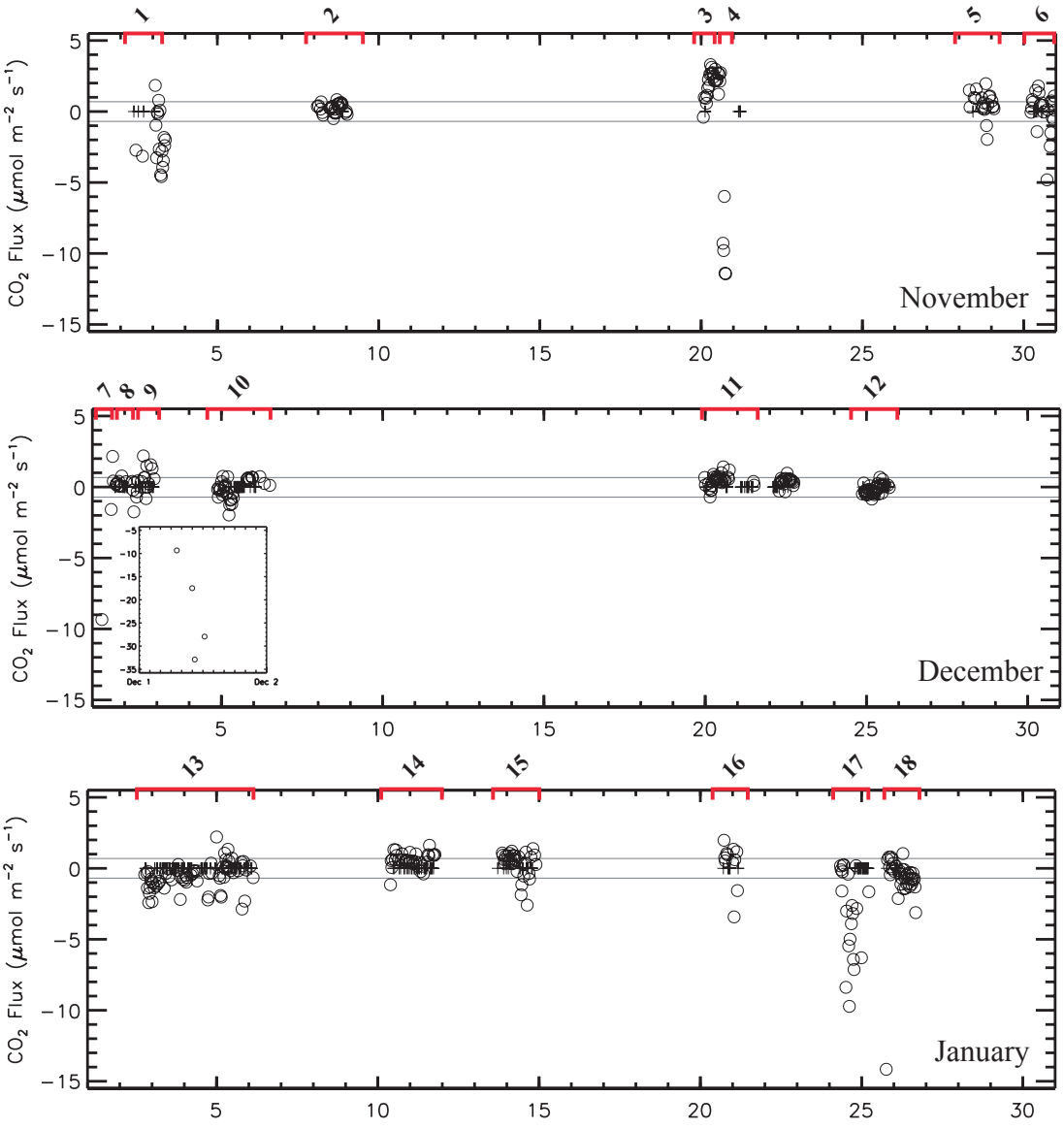

Table 2.1: Summary of conditions experienced during each sample case. [a]Ship was in transit, or drifting significantly; reported value is the midpoint .

Case	Date	(Lat/Lon)	F_{CO_2} (μmol/m^{2}s)	ΔCO_2 (μatm)	H Flux (W/m^2)	E Flux (W/m^2)	Air T (°C)	U Vel. (m/s)	U Dir. (deg)	Sea Ice Conditions
1	11/2 04:30 - 11/3 09:30	71.185[a] −129.096	−1.81	−80	+43.3	+4.1	−7.5	8.7	029.0	Newly forming grease ice
2	11/8 02:15 - 11/9 00:50	69.498 −123.930	+0.23	+146.5	+7.3	+3.7	−18.9	5.5	131.1	Newly formed fast ice. Estimated thickness: 30-40cm
3	11/20 01:30 - 11/20 14:45	71.038 −123.297	+2.10	−77.5	+53.8	+9.9	−15.2	12.5	098.4	Mobile ice with upwind leads, thickness: 37cm
4	11/20 16:00 - 11/20 18:30	71.071 −123.430	−9.58	−66.7	+111.4	+11.3	−14.2	11.8	110.8	Mobile ice with upwind leads, thickness: 37cm
5	11/28 07:30 - 11/29 02:00	70.419[a] −126.372	+0.55	+15.8	−2.3	+0.8	−16.0	8.0	254.6	Consolidated mobile ice, thickness: 52 cm
6	11/30 05:15 - 11/30 23:30	71.053[a] −123.954	−0.03	−52.1	+1.3	−1.1	−15.8	11.5	314.1	Consolidated, ridged ice floe
7	12/1 07:00 - 12/1 12:30	71.590[a] −124.656	−26.88	N/A	+33.4	−10.4	−16.6	7.3	003.4	Transit through active lead with open water and grease ice
8	12/1 13:45 - 12/2 02:45	71.901 −125.441	+0.31	−63.6	−2.9	+0.0	−19.7	5.1	037.3	Land fast ice
9	12/2 05:30 - 12/2 22:15	71.725 −125.597	+0.35	−69.4	+1.3	−0.3	−18.2	3.4	047.1	Consolidated ice floe, thickness: 35cm

Table 2.1: Summary of conditions experienced during each sample case (cont.)

Case	Date	(Lat/Lon)	F_{CO_2} (μmol/m^{2}s)	ΔCO_2 (μatm)	H Flux (W/m^2)	E Flux (W/m^2)	Air T (°C)	U Vel. (m/s)	U Dir. (deg)	Sea Ice Conditions
10	12/4 21:00 - 12/6 12:15	71.402[a] −124.875	−0.09	−86.7	+15.8	+2.0	−18.0	5.1	267.3	Consolidated ice floes, varying thicknesses: 25–45cm
11	12/19 23:15 - 12/22 18:15	71.915 −125.433	+0.42	−49.8	−0.6	+3.3	−22.0	4.6	108.8	Land fast ice
12	12/24 20:45 - 12/25 17:15	71.262 −124.383	−0.14	−51.0	+5.5	+1.3	−20.7	5.9	123.2	Consolidated mobile ice, thickness: 30cm
13	1/2 18:15 - 1/6 03:30	71.306[a] −124.722	−0.50	−52.0	−7.9	+5.3	−21.8	11.6	117.9	Thick consolidated ice floe, thickness: 105cm
14	1/10 09:15 - 1/11 18:45	71.653[a] −126.101	+0.58	−78.3	+2.9	+1.2	−21.3	7.0	123.3	Consolidated mobile ice
15	1/13 16:00 - 1/14 22:00	71.494[a] −124.638	+0.34	−73.8	+3.2	+1.0	−25.0	8.0	062.4	Consolidated mobile ice
16	1/20 17:00 - 1/21 04:30	71.579 −125.104	+0.34	*N/A*	−2.9	+2.8	−18.9	6.4	123.6	Consolidated mobile ice, thickness: 91cm
17	1/24 08:00 - 1/25 05:30	71.203 −125.184	−3.15	−38.4	+16.4	+5.6	−20.3	11.9	291.7	Consolidated mobile ice, upwind leads
18	1/25 18:00 - 1/26 16:30	71.172 −125.014	−0.86	−8.6	+9.4	+2.0	−25.7	8.7	298.5	Consolidated mobile ice

where the overbars denote averaged quantities, the primes indicate fluctuations around a mean value, T is air temperature, c_d is the dry air molar concentration, and c_a is the moist air molar concentration [Leuning, 2004]. The second term on the right hand side of equation 2.2 is the so-called WPL correction (or dilution correction) that must be used for open path sensors [Webb et al., 1980]. The necessary high frequency T measurements are determined from sonic temperature (measured by the sonic anemometer), which were converted to T following Kaimal and Gaynor [1991]. The MotionPak provides 3-axis measurements of acceleration and angular velocity which were used to correct w for ship motion. The techniques for this correction were first adapted for ships by Mitsuta and Fujitani [1974], and later refined by other investigators [Anctil et al., 1994; Dugan et al., 1991; Edson et al., 1998; Fujitani, 1981].

The utility of open path sensors for measuring CO_2 fluxes has recently been debated for conditions where low fluxes are expected [Amiro, 2010; Burba et al., 2008; Ono et al., 2008] and in the marine environment [Prytherch et al., 2010]. During the non-growing season over several terrestrial ecosystems, significant uptakes of CO_2 have been observed and identified as artifacts of the LI-7500 gas analyzer [Amiro, 2010; Hirata et al., 2007; Ono et al., 2008]. Work by Burba et al. [2008] have shown that a heat flux generated by the electronics of the LI-7500 is likely the most significant contributor to this bias, especially at low air temperatures. Other suggestions include pressure fluctuations at high wind velocities that are not usually included in the WPL correction [Järvi et al., 2009] and incomplete WPL corrections due to poor energy balance closure [Ono et al., 2008]. The magnitude of these discrepancies are usually on the order of 1 μmol m^{-2} s^{-1}, which in most terrestrial systems during the growing season is a small percentage of the total flux. However, typical magnitudes

of CO_2 flux in the open ocean are less than 1 μmol m^{-2} s^{-1} (e.g., McGillis et al. [2001]).

A further difficulty of working with an open path analyzer in a marine environment is an apparent sensitivity to contamination of the sensor lens by impurities (most likely salt particles) [Kohsiek, 2000; Prytherch et al., 2010]. The contamination appears to cause a portion of water vapour fluctuations to be mis–recorded as fluctuations of CO_2 (an effect known as "crosstalk"), and can lead to CO_2 fluxes an order of magnitude higher than expected [Prytherch et al., 2010].

Corrections have been proposed for both the sensor heating and H_2O crosstalk issues. Burba et al. [2008] proposed several ways in which the heat flux of the LI-7500 can be estimated and added to the WPL correction. In this study, we have adopted their multivariate regression model for determining the sensor heat flux from air temperature, wind velocity and incoming longwave/shortwave radiation. Prytherch et al. [2010] proposed a correction for the H_2O crosstalk (termed the "PKT" correction) in which an iterative approach is used to remove unwanted correlation between the CO_2 and H_2O signals. This correction has also been adopted for this study, but as we discuss in section 2.5.1 we found it to be unreliable. Thus, all CO_2 flux values reported herein include only the Burba et al. [2008] correction along with the usual WPL corrections.

2.3.5 RADARSAT-1 Imagery

To aid in the identification of ice conditions and to quantify the amount of open water within the study area over the period, fourteen RADARSAT-1 ScanSAR narrow beam images acquired between November 6 2007 and January 28 2008 were classified. RADARSAT-1 ScanSAR narrow beam mode has a resolution of 50 m and

a nominal coverage area of 300 x 300 km. Each of the images were geo-referenced and calibrated to σ°, then geographically cropped using latitudinal bounds 70° and 71.5°N and longitudinal bounds 122° and 126°W. The calibrated, geo-referenced sub-images were then subjected to a median filter with a 3x3 window size to reduce the "speckle" noise common to synthetic aperture RADAR (SAR) imagery while preserving edges. Edge preservation is very important when linear features such as leads are the predominant form of open water at this time of year. Finally, each sub-image was manually classified according to the principles set forth by the Canadian Ice Service (CIS) SAR ice interpretation guide [*Canadian Ice Service*, unpublished].

2.4 Results

2.4.1 Observations of High CO_2 Flux Events

Case 1: November 2 04:30 - November 3 09:30

On November 2, the ship conducted a transect across the mouth of Amundsen Gulf. A RADARSAT-1 image was acquired on November 2 at 01:54 (all times herein reported as UTC) just prior to the start of the transect, which clearly shows that the region was a mix of open water, old ice floes, and newly forming grease ice (Figure 2.3). Due to the ice in the area the intake line for the pCO_{2sw} system was clogged so that we could not obtain measurements of ΔpCO_2. However, samples collected in the region in the previous two days showed that the ΔpCO_2 was around -80 μatm.

Over this time period, we measured a flux of up to -4.26 μmol m^{-2} s^{-1}, with a mean value of -1.81 μmol m^{-2} s^{-1}. Associated with this strong CO_2 uptake was a high sensible heat flux from the ocean to the atmosphere (up to 100 W m^{-2}, mean

Figure 2.3: RADARSAT-1 image collected on November 2 at 01:53, just prior to sample case 1. The inset map shows the location of the imaged area, red lines indicate the ship's track, the green X indicates the location of the ship at the time of image acquisition, and the green arrow shows the mean wind direction.

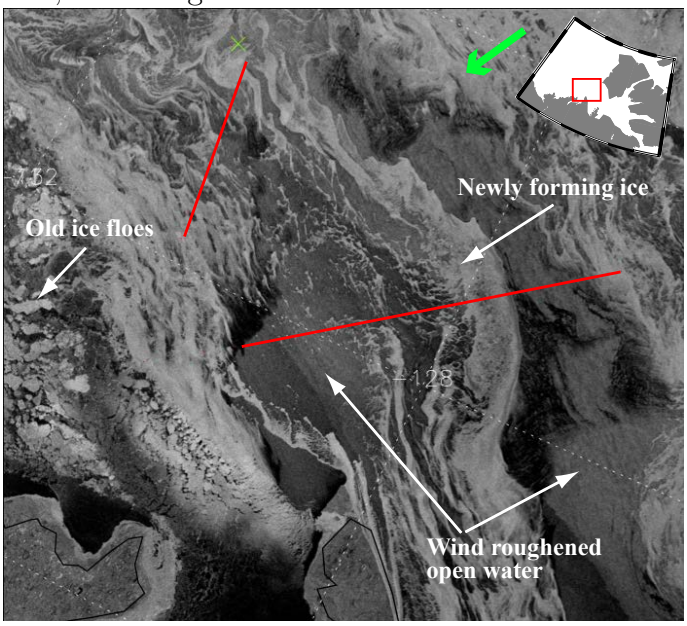

of 43.3 W m^{-2}, Figure 2.4b). This heat flux must have been driven by open water, over which a strong temperature gradient forms due to the relative warmth of the ocean. We therefore interpret the strong CO_2 fluxes to likewise be a signal of open water gas exchange.

Case 3: November 20 01:30 – 14:45

The second instance where we observed particularly high CO_2 fluxes was on November 20, near the southern tip of Banks Island. At this point ice concentration in Amundsen Gulf was very high, and the ship was parked in a 36 cm thick ice floe. Prior to this time, a strong wind event from November 16-17 (wind velocities peaking at about 24 m s^{-1}) created significant ice motion and fracture in the region. This was followed by very low winds (about 5 m s^{-1}), allowing the open water fea-

Figure 2.4: Time series of atmospheric measurements made during sample case 1. (a) Measured CO_2 flux with sensor heating correction added (open circles), and the estimated noise level of the system as discussed in section 2.5.1 (horizontal grey lines), (b) measured sensible heat flux (red open circles) and latent heat flux (blue open circles), (c) 1 minute averages of air temperature (dashed line) and wind velocity (solid line).

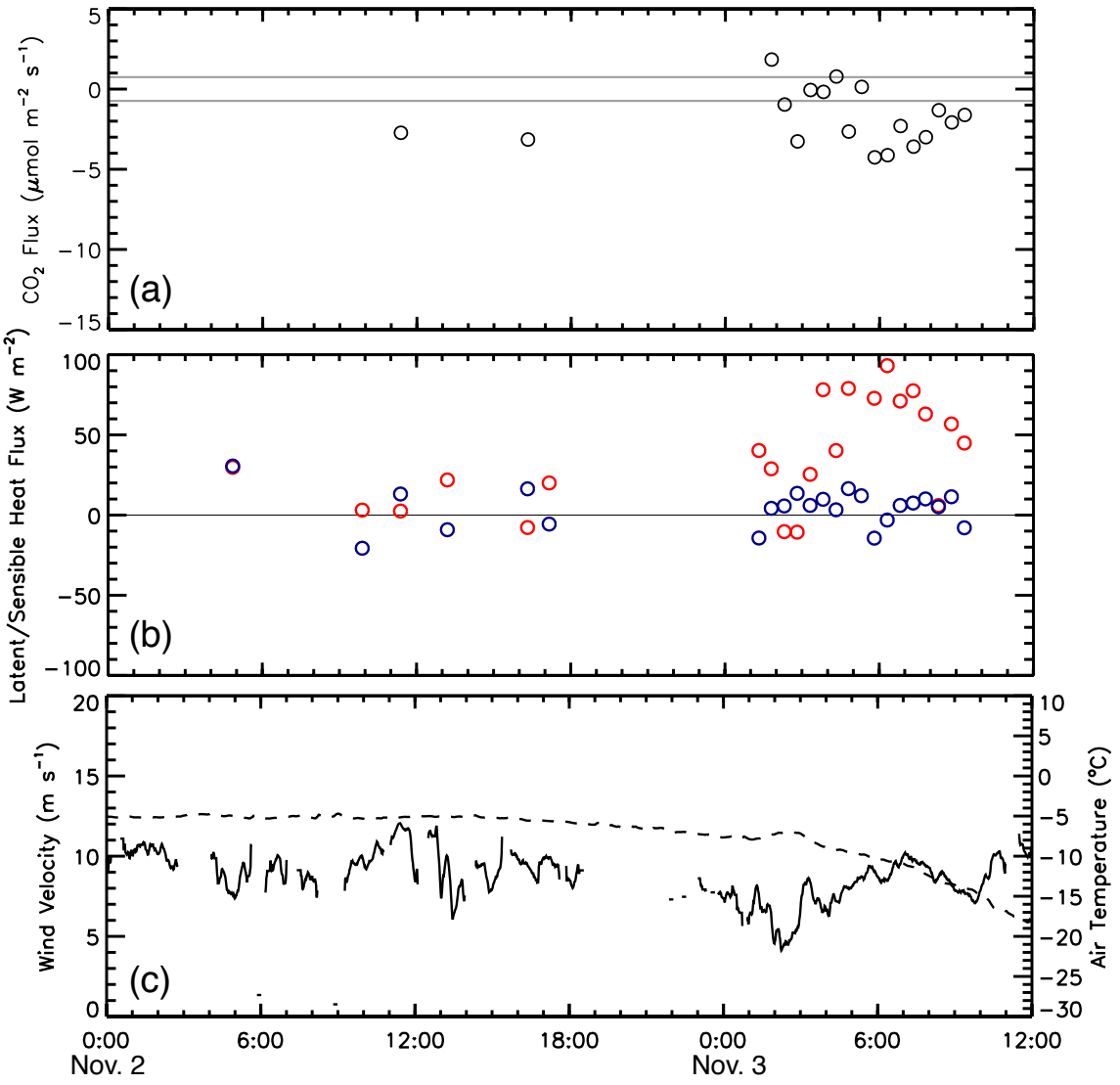

tures to appear obviously on a RADARSAT-1 image acquired on November 20 at 01:29 as dark features (Figure 2.5). Early on November 20, easterly winds picked up quickly to about 13 m s^{-1} and persisted through the sample case (Figure 2.6c). This wind induced significant ice motion (the ship drifted at a mean velocity of 0.6 km hr^{-1}, increasing steadily from 0.4 to 1.1 km hr^{-1}), which would have expanded the open water leads. A signal of open-water fluxes was clearly evident in the heat flux measurements, reaching nearly +100 W m^{-2} (Figure 2.6b) with a mean value of +53.8 W m^{-2} (Table 2.1).

Figure 2.5: RADARSAT-1 image collected on November 20 at 01:29, just prior to cases 3 and 4. The inset map shows the location of the imaged area, red lines indicate the ship's track, the green X indicates the location of the ship at the time of image acquisition, and the green arrow shows the mean wind direction.

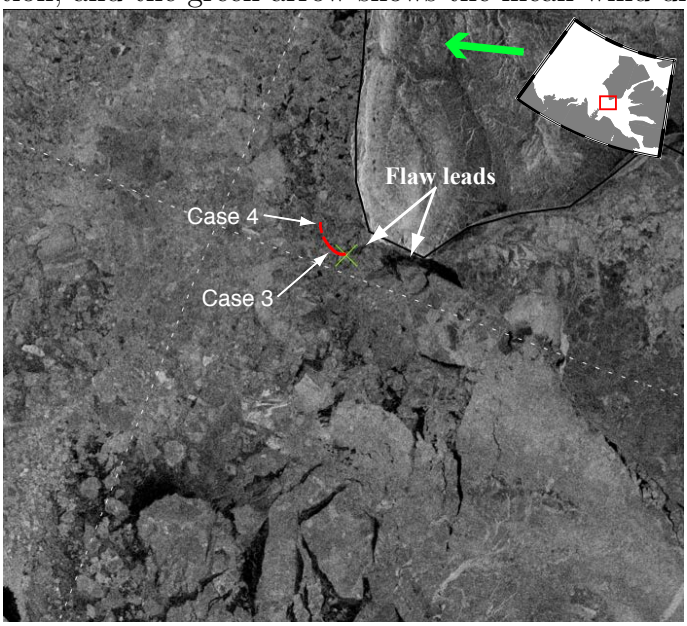

During this case, rapid outgassing of CO_2 was observed at a mean rate of +2.10 μmol m^{-2} s^{-1}. The outgassing was somewhat surprising given that the pCO_{2sw} system recorded undersaturation of -75 μatm (Table 2.1), but the surface water upwind of the ship may have been supersaturated. This result shows that at times

our eddy covariance measurements (which are an integrated flux from the upwind surfaces) are difficult to reconcile with the pCO_{2sw} data (which measures at the same location as the tower).

Case 4: November 20 16:00 – 18:30

Case 4 is an extension of Case 3, but we split the two because the ship repositioned (approximately 1.5 km north) to a new ice floe (Figure 2.5), and the CO_2 flux changed markedly. The heat flux measurements from Case 4 were still heavily influenced by an open water signal, with even higher values than in case 3 (mean and maximum values of +111.4 and +140.7 W m^{-2} respectively, Figure 2.6b). This is in agreement with ship-board observations that the area was a mixture of ice and open water under strong wind forcings.

After the ship repositioned, a very strong negative flux of CO_2 was observed (mean and maximum values of -9.58 and -11.43 μmol m^{-2} s^{-1} respectively, Figure 2.6a). This flux direction is in better agreement with the ΔpCO_2 gradient observed in the area, and may be a result of a change in the upwind surface to lower (i.e. undersaturated) pCO_{2sw} as the ship moved around the southern tip of Banks Island (Figure 2.5).

Case 7: December 1 07:00 – 12:30

The strongest CO_2 fluxes that we measured were on December 1 during a transit along the southwest coast of Banks Island. Immediately prior to this transit, the ship was drifting south in an ice floe under fairly high winds (mean 11.8 m s^{-1}). This drifting event made up Case 6, where no strong CO_2 fluxes or heat fluxes were observed (Table 2.1). The ship eventually broke out of this drift, and transited

Figure 2.6: Time series of atmospheric measurements made during sample cases 3 and 4 (division between the two cases is denoted by the dashed vertical line). (a) Measured CO_2 flux with sensor heating correction added (open circles), range of bulk CO_2 flux estimates (brackets), and the estimated detection limit of the system as discussed in section 2.4.2 (horizontal grey lines), (b) measured sensible heat flux (red open circles) and latent heat flux (blue open circles), (c) 1 minute averages of air temperature (dashed line) and wind velocity (solid line).

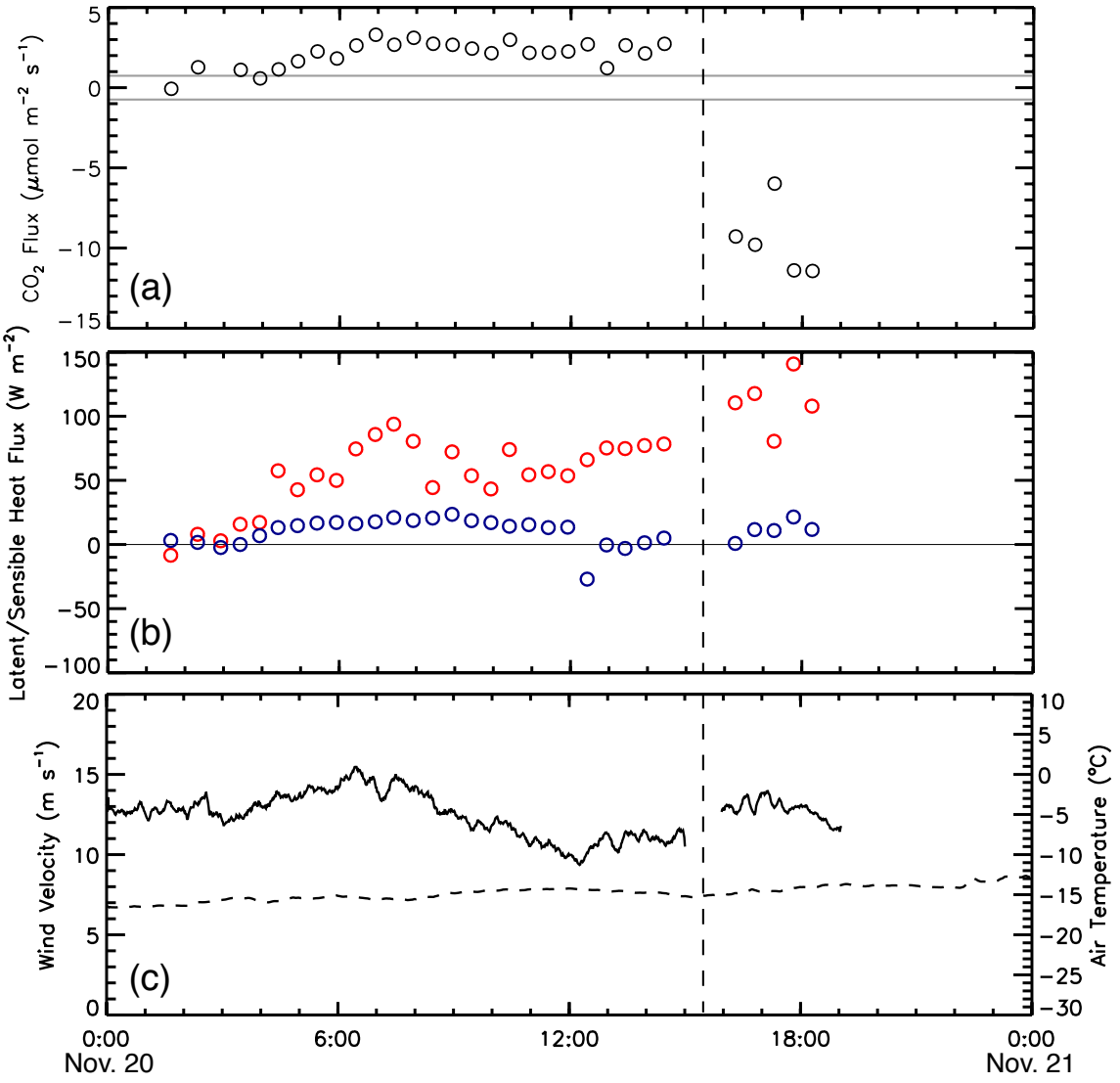

through an active wind-roughened flaw lead. This flaw lead event was captured in a RADARSAT–1 image taken shortly after the end of case 7 (Figure 2.7).

Figure 2.7: RADARSAT-1 image collected on December 1, 14:45, just after case 7. The inset map shows the location of the imaged area, red lines indicate the ship's track, the green X indicates the location of the ship at the time of image acquisition, and the green arrow shows the mean wind direction.

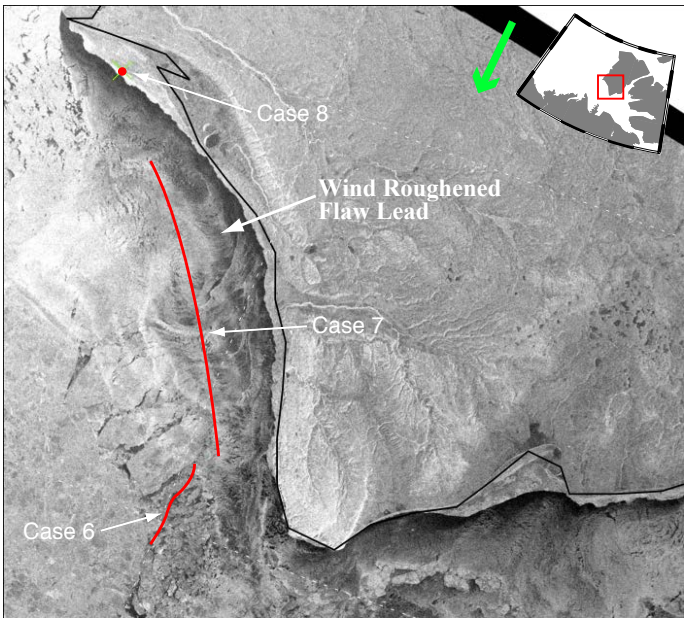

The transit was very short, and only four 30 minute samples passed our quality control tests. However, all of these samples showed very high CO_2 uptake, with flux values ranging from -9.33 to -27.95 μmol m^{-2} s^{-1} (Figure 2.8a). Once again, these fluxes were accompanied by high sensible heat fluxes indicative of open water (Figure 2.8b). No pCO_{2sw} measurements were available during the transit due to a clogged intake line, but based on the ΔpCO_2 during the cases bracketing this one (-52.1 and -63.6 μatm for cases 6 and 8, respectively, Table 2.1), the direction of the flux appeared to be in agreement with the gradient.

Figure 2.8: Time series of atmospheric measurements made during sample case 7. (a) Measured CO_2 flux with sensor heating correction added (open circles), and the estimated noise level of the system as discussed in section 2.5.1 (horizontal grey lines), (b) measured sensible heat flux (red open circles) and latent heat flux (blue open circles), (c) 1 minute averages of air temperature (dashed line) and wind velocity (solid line).

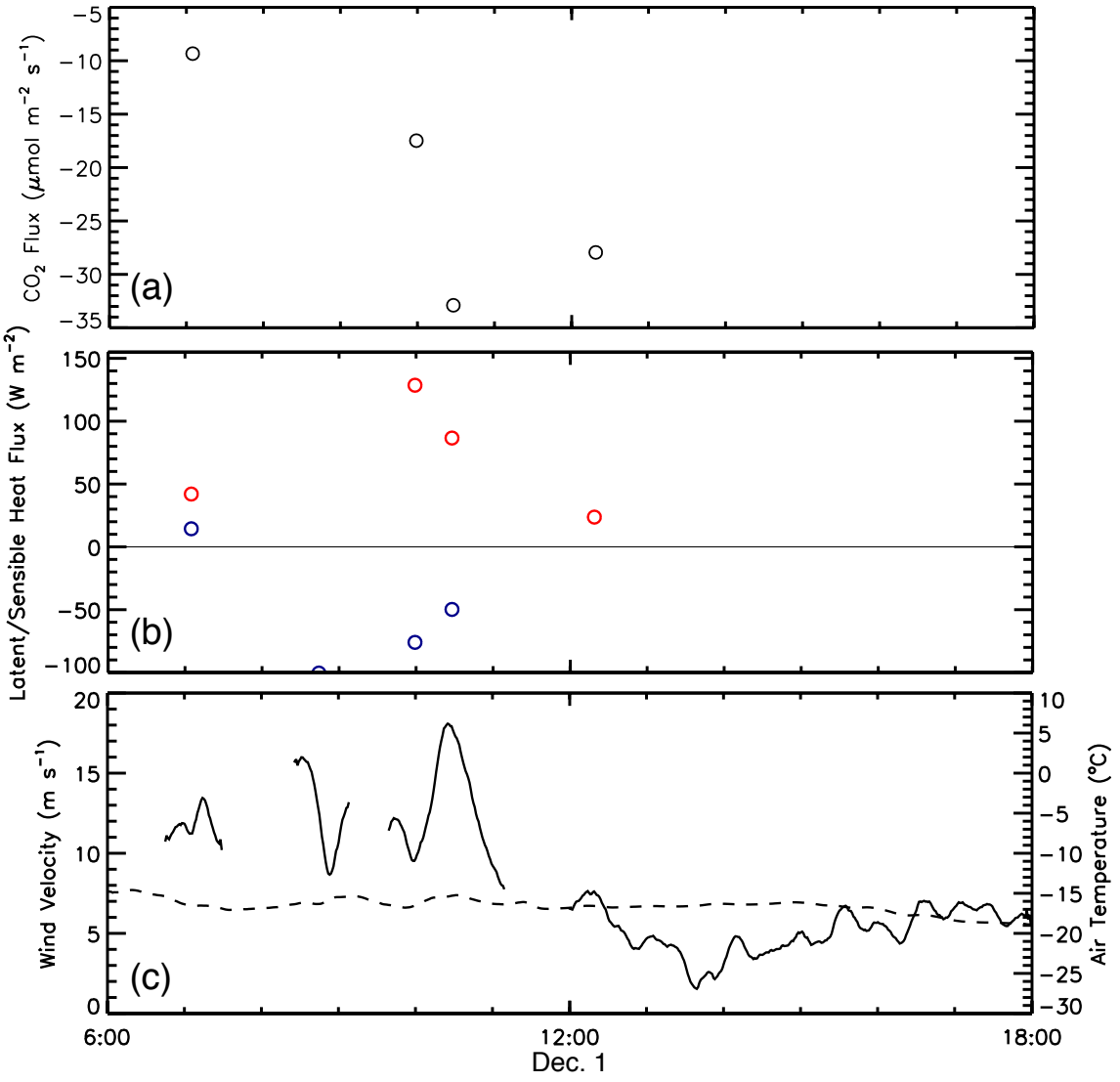

Case 17: January 24. 08:00 - January 25 05:30

The final instance where we measured unusually strong CO_2 fluxes was during case 17 in late January. During this time, the ship was drifting in an ice floe with a thickness of about 100 cm. A RADARSAT image collected at 01:33 on January 24 showed considerable fracturing upwind of the ship (Figure 2.9).

This case was characterized by high wind velocities (up to 19 m s^{-1}, Figure 2.10c) which caused ice drift up to 1.4 km hr^{-1}. These strong winds and ice motion drove significant open water, as observed in heat flux measurements approaching 100 W m^{-2} (Figure 2.10b). Associated with this sensible heat signal was a strong, consistent CO_2 uptake (Figure 2.10a) with a mean flux of -3.15 μmol m^{-2} s^{-1}, in agreement in direction with an observed ΔpCO_2 gradient of -38.5 μatm.

Figure 2.9: RADARSAT-1 image collected on January 24, 01:33, just prior to case 17. The inset map shows the location of the imaged area, red lines indicate the ship's track, the green X indicates the location of the ship at the time of image acquisition, and the green arrow shows the mean wind direction.

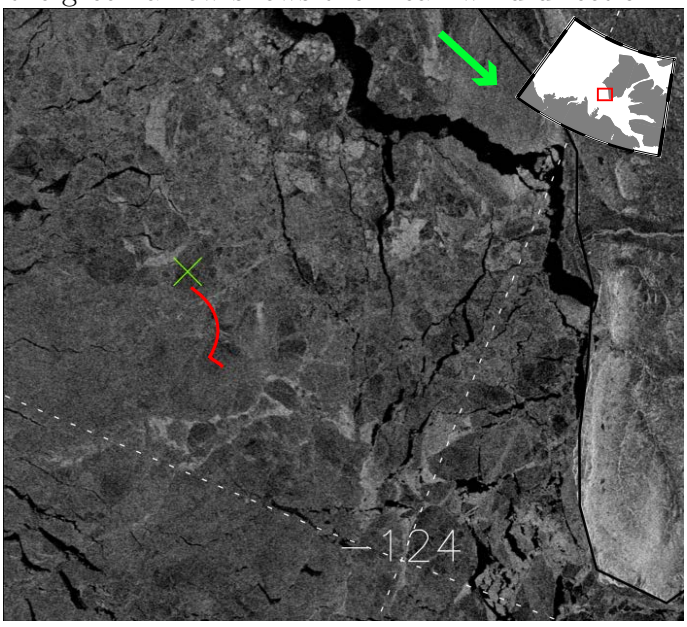

Figure 2.10: Time series of atmospheric measurements made during sample case 17. (a) Measured CO_2 flux with sensor heating correction added (open circles), and the estimated noise level of the system as discussed in section 2.5.1 (horizontal grey lines), (b) measured sensible heat flux (red open circles) and latent heat flux (blue open circles), (c) 1 minute averages of air temperature (dashed line) and wind velocity (solid line).

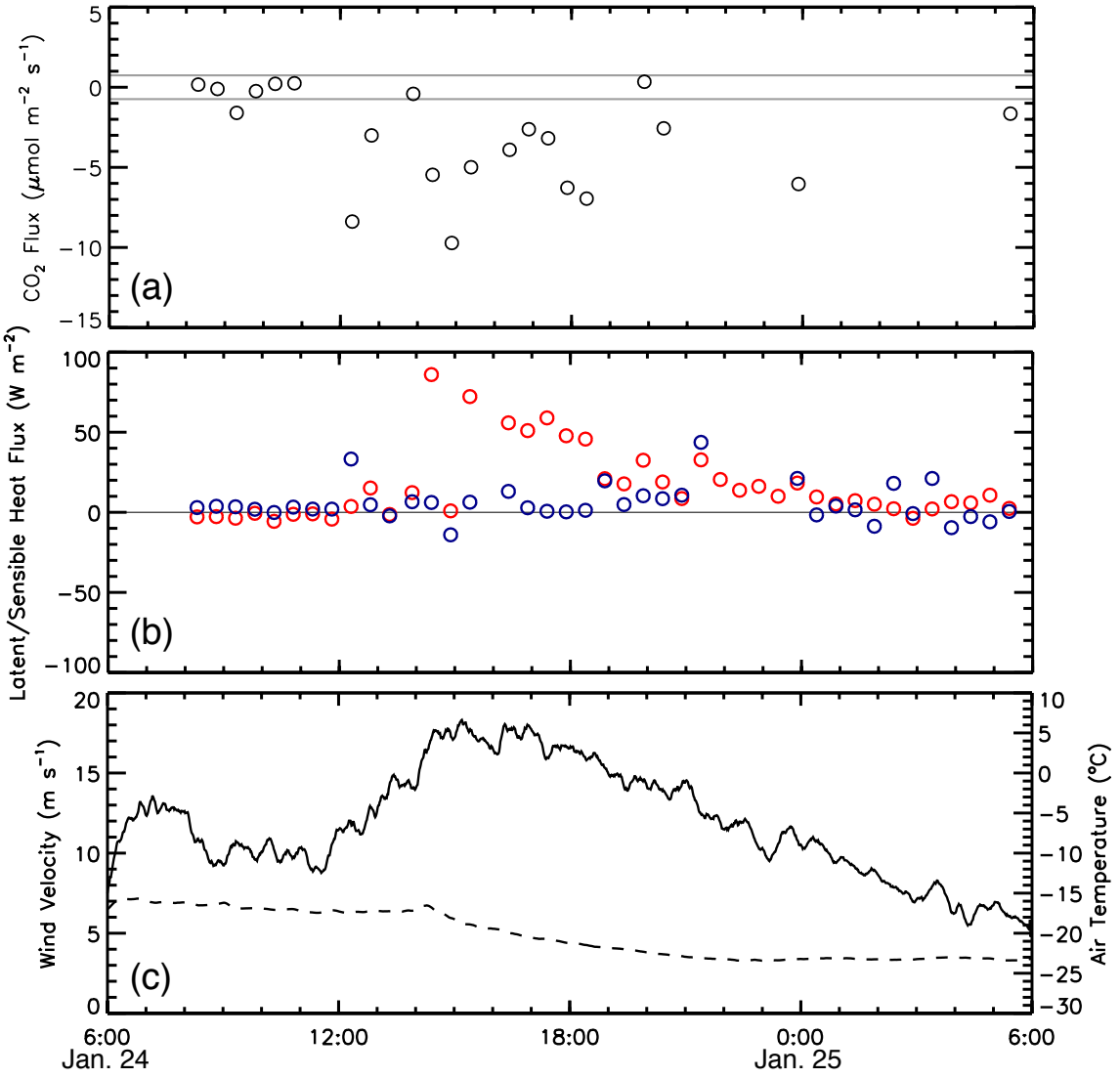

2.4.2 Observations of Low CO_2 Fluxes

Observations in Land Fast Ice

Flux measurements were made in land fast sea ice on three occasions: case 2 (November 8 02:15 – November 9 00:50, 69.50 °N/123.93 °W), case 8 (December 1 13:45 – December 2 02:45, 71.90 °N/125.44 °W), and case 11 (December 19 23:15 – 18:15, 71.91 °N/125.43 °W). The minimum ice thickness for all of these samples was an estimated 40 cm (case 2), and the ice was much thicker (approaching 100 cm) in the other two cases. Sensible heat flux in all cases was small (Table 2.1), and in all three cases the wind direction was such that the upwind fetch was composed of fast ice, confirming that what we were measuring was indeed a land fast ice signal. In these cases, mean fluxes were between +0.23 – +0.42 μmol m^{-2} s^{-1} (Table 2.1 and Figure 2.2). If these measurements are reliable, they would suggest a flux of CO_2 at a climatologically significant rate. However, we will show in section 2.5.1 that these low fluxes likely cannot be distinguished from the noise and biases inherent in our eddy covariance system.

Observations in High Concentration Mobile Ice

A second scenario in which we typically observed non-resolvable CO_2 fluxes was when the ship was drifting in highly concentrated mobile sea ice. These conditions were observed during case 6 (November 30 05:15 – 23:00), case 9 (December 2 05:30 – 22:15), case 13 (January 2 18:15 – January 6 03:30), case 14 (January 10 09:15 – January 11 18:45), case 15 (January 13 16:00 – January 14 00:00) and case 16 (January 20 17:00 – January 21 04:30). As Table 2.1 shows, all of these cases had

very low sensible heat fluxes (highest mean flux was +3.2 W m^{-2}, case 15), and mean CO_2 fluxes ranged from -0.50 – +0.58 μmol m^{-2} s^{-1} (Table 2.1, Figure 2.2).

Observations in Thin Ice

A final scenario which is perhaps more interesting is the observation of non-detectable CO_2 fluxes in cases where other observations (field data and heat flux measurements) suggest that thin ice may be present. Only case 10 (December 4 23:00 – December 6 12:15) falls into this category. RADARSAT–1 images (not shown) acquired shortly before (December 4, 01:21) and after this run (December 7 01:33) do not show a lot of obvious thin ice, but ice cores taken from the surrounding floe were only 26 cm thick. The heat flux measurements (Figure 2.11b) were consistently positive (mean value of +15.8 W m^{-2}), but lower than those observed in section 2.4.1. Thin ice transfers heat at significant rates, but does so less vigorously than open water [Maykut, 1978]. Although winds were moderate (5 – 7 m s^{-2}, Figure 2.11c) the ΔpCO_2 gradient was quite high (mean value of -86.7 μatm). If a flux enhancement was occurring similar to those described in section 2.4.1, we would expect to be able to detect it in our CO_2 flux measurements. However, Figure 2.11a clearly shows that fluxes were not distinctly above the uncertainty inherent in the system. These findings suggest that open water – not just thin ice – is required to drive CO_2 flux at the levels shown in section 2.4.1.

Figure 2.11: Time series of atmospheric measurements made during sample case 10. (a) Measured CO_2 flux with sensor heating correction added (open circles), and the estimated noise level of the system as discussed in section 2.5.1 (horizontal grey lines), (b) measured sensible heat flux (red open circles) and latent heat flux (blue open circles), (c) 1 minute averages of air temperature (dashed line) and wind velocity (solid line).

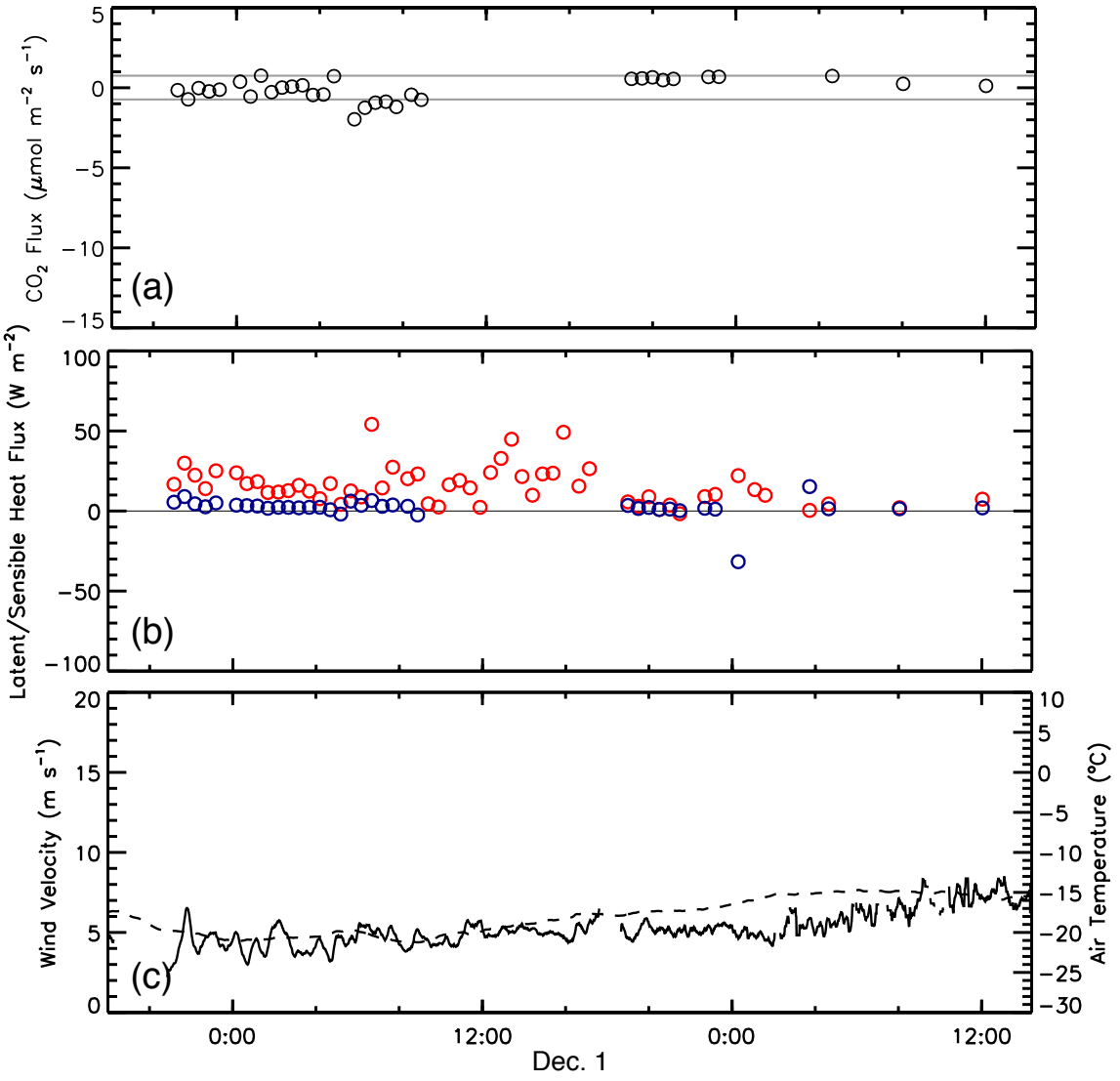

2.5 Discussion

2.5.1 Sensor Uncertainties

The results obtained in land fast and consolidated ice (sections 2.4.2 & 2.4.2) provide an opportunity to test the noise and bias inherent in our eddy covariance system. There is in fact good reason to expect that CO_2 fluxes over these surfaces (thick, cold, consolidated sea ice) should be zero. At surface ice temperatures below ∼-5°C and typical brine salinity, the brine volume drops below 5% which inhibits liquid transport through the ice [Golden et al., 1998]. Loose et al. [2010] examined the transport of gases near this liquid transport threshold, and found the gas transfer velocity to be very small relative to seawater. Similarly, Nomura et al. [2006] measured small CO_2 fluxes (maximum ∼ $+0.01 \mu$mol m^{-2} s^{-1}) over thin laboratory ice well above the liquid transport threshold. At ice temperatures that reduce brine volume to below 5%, these small rates of gas exchange should be effectively shut off.

After November 28, 2007 (when most of the measurements described in sections 2.4.2 & 2.4.2 were made) surface ice temperatures were consistently well below -5°C and brine volumes were typically below 5% [G. Carnat, unpublished data]. We would therefore expect any deviation of the mean CO_2 fluxes over these surfaces from zero to be indicative of bias, and any variation around that mean to be noise in the measurement system. To this end, we calculated the mean and standard deviation of the raw, sensor heating corrected, and crosstalk (PKT) corrected CO_2 fluxes from cases 2, 6, 8, 9, 11 & 13–16 (Table 2.3).

The uncorrected fluxes show a negative bias (-0.45 μmol m^{-2} s^{-1}), which is in the direction predicted by both sensor heating and water vapour crosstalk effects. The standard deviation of CO_2 fluxes around this mean was 0.76 μmol m^{-2} s^{-1},

Table 2.3: Noise and bias in the eddy covariance system, including the effect of various corrections. Bias is calculated as the mean CO_2 flux from cases where near-zero flux is expected, noise is one standard deviation around that mean. The number of eddy covariance sample runs is 274 for raw and sensor heating corrected, 151 for crosstalk corrected.

	Bias (μmol m^{-2} s^{-1})	Noise (μmol m^{-2} s^{-1})
Raw (uncorrected)	-0.45	$\pm$0.76
Sensor heating corrected	0.13	$\pm$0.77
Water vapor crosstalk correction	-0.21	$\pm$1.32

indicating that noise is quite high in the system. By applying only the sensor heating correction, the bias moved to +0.13 μmol m^{-2} s^{-1} – a reduction in the magnitude of the bias, but a slight overcorrection. Fortunately, this correction did not add a lot of additional noise to the system, as the standard deviation remained relatively unchanged (0.77 μmol m^{-2} s^{-1}).

The PKT correction, however, was more troublesome. We found that 55% of the samples from these cases produced what we determined to be an "unreasonable" correction (magnitude of correction >5.5 μmol m^{-2} s^{-1}). Of the remaining samples, the net effect of the correction was to actually make the CO_2 flux more negative, counter to the expected direction. Furthermore, the correction added additional noise as evidenced by an increase in standard deviation to 1.30 μmol m^{-2} s^{-1}. Since no negative bias remains in the mean flux after the sensor heating correction, we conclude that crosstalk contamination must have been small for our system even prior to applying the PKT correction. Arguments for a low crosstalk error in this environment have a strong physical basis, because latent heat fluxes were very small (typically <5 W m^{-2}) compared to the examples discussed by Prytherch et al. [2010] ($\sim$60 W m^{-2}). From an eddy covariance standpoint, a low latent heat flux means that water vapour is not highly correlated with vertical wind velocity, and thus

should not cause significant spurious correlation between CO_2 and vertical wind velocity. For these reasons, we decided not to include the PKT correction in our results.

We propose that our system has an overall uncertainty of ± 0.77 μmol m^{-2} s^{-1} and a bias of $+0.13$ μmol m^{-2} s^{-1} based on the results of the sensor heating corrected fluxes. This level of uncertainty shows that our measurements of high CO_2 flux (section 2.4.1) are above the noise level of the system, and are not the result of a strong systematic bias.

2.5.2 Enhanced Gas Flux by Sea Ice Formation

Our results from section 2.4.1 indicate that in the winter mixed ice environment of Amundsen Gulf, the presence of open water drives a very rapid exchange of CO_2. For comparison, under the typical ΔpCO_2 ($\sim$-70 μatm) and wind velocity ($\sim$8 ms^{-1}) conditions we encountered, the bulk flux approach (equation 2.1) would predict fluxes in the range of -0.10 to -0.12 μmol m^{-2} s^{-1}. Even using the maximum wind velocities observed (19 ms^{-1}), we would not expect fluxes to exceed about -1.5 μmol m^{-2} s^{-1}. Our measured fluxes are therefore at times 1–2 orders of magnitude higher than what might be expected under similar conditions in the open ocean.

Several authors have suggested that an enhancement of gas exchange due to sea ice formation may exist [Anderson et al., 2004; Loose et al., 2009; Rysgaard et al., 2007], but none have described in detail the physical and chemical processes which may account for it. Our study likewise lacks the necessary ancillary observations to show conclusively what processes are responsible for enhanced gas transfer, but in this section we propose two key hypotheses to explain it: (1) enhanced water side turbulence driven by rapid cooling and brine rejection, and (2) modification of

the carbonate system of the surface seawater. These hypotheses are summarized in Figure 2.12 and discussed below.

Figure 2.12: Schematic summarizing the important processes occurring during a wind–driven lead event. The processes highlighted in blue/red are those which likely have a direct effect on air–sea gas exchange. Processes in red are associated with frazil ice formation, and those in blue are associated with the surface cooling.

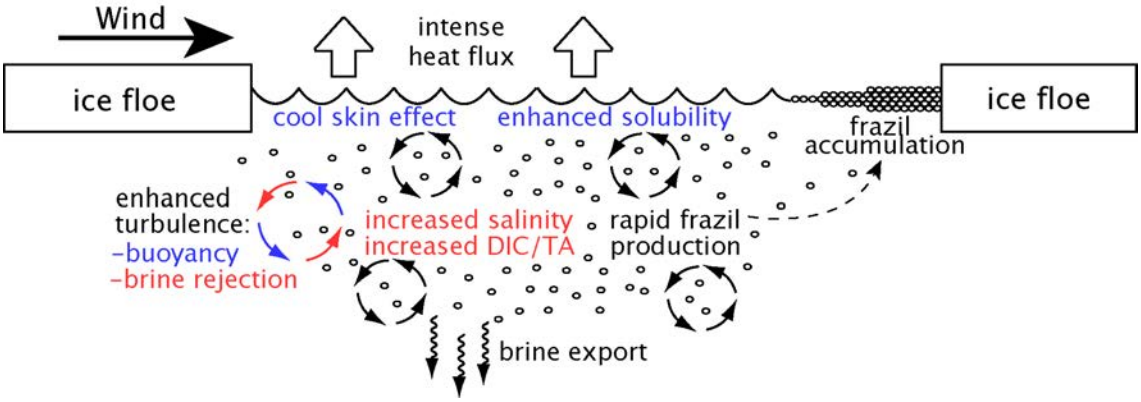

Enhanced Water Side Turbulence

At the upwind side of a crack or flaw lead, a significant heat flux occurs due to the exposure of the relatively warm (i.e. $\sim$ -1.8 °C) water to the very cold atmosphere ($\sim$ -10 – -25 °C). This cooling creates a destabilization of the water surface and generates buoyancy fluxes that may enhance turbulence. McGillis et al. [2004] observed a 40% enhancement of CO_2 fluxes during modest nighttime cooling (sensible heat fluxes on the order of 1-10 W m^{-2}) in the equatorial pacific, which was attributed mostly to these buoyancy fluxes. In a situation such as the one shown in Figure 2.12 where sensible heat fluxes are 1–2 orders of magnitude higher, this enhancement is likely to be much more pronounced.

A second process that may drive high turbulence is the rejection of dense brines by frazil ice formation. Frazil ice is small, unconsolidated ice crystals that are

primarily generated just below the surface [Ushio and Wakatsuchi, 1993]. It is easily transported away from the open water site, creating a region of rapid ice formation but persistent open water. Frazil ice crystals are thought to be essentially pure [Omstedt, 1985] which means that their formation results in the rejection of any solutes, which must create density instabilities and drive enhanced turbulence similar to the effect of heat loss.

Unfortunately, turbulence in these systems has not been well studied. Between November 16 – December 18, one of our collaborators collected 175 profiles of turbulent kinetic energy dissipation rate (ϵ) from a minimum depth of 10 m using a vertical microstructure turbulence profiler (VMP, see Bourgault et al. [2008] for instrument details). ϵ at 10 m reached values of $O(10^{-5})$ W kg^{-1} on a few ($\sim$ 4) profiles, with an approximately exponential decrease with depth [Bourgault et al., 2011]. Extrapolating above 10 m suggests surface dissipation rates that may have occasionally reached $O(10^{-4})$ W kg^{-1}. These values are considerably higher than ϵ measured under refrozen leads at a similar depth by McPhee and Stanton [1996] ($O(10^{-8})$ – $O(10^{-7})$ W kg^{-1}). The exponential shape of the dissipation measurements points to surface turbulence generation, but given that the dominant ice cover must restrict wind and wave action, sea ice processes (likely including ice drift and brine rejection) must play an important role in this system. Zappa et al. [2007] showed that ϵ is a better predictor of gas transfer velocity than wind in systems where turbulence is generated from other sources. Our maximum predicted surface ϵ values are similar to the highest ϵ measurements made by Zappa et al. [2007] in coastal zones and tidal estuaries, but they are not high enough to account for the rate of gas transfer we observed. However, the VMP was almost always deployed when the ship was stationary in ice floes, and it therefore may not have captured

the nature of the transient leads that we hypothesize to be the cause of our high observed CO_2 fluxes.

Modification of the Surface Seawater Carbonate System

pCO_{2sw} is ultimately controlled by the equilibrium condition of the seawater carbonate system. DIC, TA, salinity and water temperature all affect this equilibrium, and thus exert a control on pCO_{2sw}. In terms of gas exchange, it is actually the carbonate system properties of the very thin mass diffusive layer that determines the air–sea ΔpCO_2.

The most obvious modification by lead formation is cooling of the sea surface, which will reduce pCO_{2sw} and increase solubility. Although the seawater will be near its freezing point, cooling beyond the freezing point (supercooling) occurs before ice formation begins. If no particles are available for the nucleation of ice crystals, supercooling can easily exceed 2° C [Tsang and Hanley, 1985]; a condition which can be created in the laboratory, but is not likely to exist in the Arctic. Observations of supercooling in the field are sparse, but Skogseth et al. [2009] observed a supercooling of ∼0.04 °C in the bulk surface water of an open coastal polynya in Svalbard. Given that the heat loss is at the surface, this would likely translate into an even more significant cooling of the diffusive mass boundary layer; in essence, the rapid sensible heat flux would drive a very pronounced cool–skin effect. This cool–skin effect would enhance uptake when the sea surface was undersaturated due to increased solubility and decreased pCO_{2sw}, but would actually act to restrict exchange when the surface was supersaturated. Given that we measured one instance of intense outgassing (case 3, section 2.4.1), this process alone cannot account for the high exchange rates.

Frazil ice formation and the accompanying rejection of brines also has the potential to modify the near–surface chemistry. A decrease in solubility driven by salt rejection and rising DIC/TA concentrations may either suppress or enhance gas exchange, depending on the saturation state. When the sea surface is supersaturated, the added DIC/TA and reduced solubility should enhance outgassing. When the sea surface is undersaturated, these combined effects should suppress uptake. However, whether or not this has an influence on gas exchange depends on where the brines ultimately end up. On the nearby Beaufort Sea Shelf, Melling and Moore [1995] showed that deep penetration to the pycnocline of brine does occur at times, which suggests that modification of the near–surface chemistry may not be important. Shadwick et al. [2011] did measure long–term surface increases in salinity, and DIC/TA in Amundsen Gulf over the winter, but we do not have measurements that capture the evolution of these properties on the timescale of an individual lead event. On these short timescales, we hypothesize that the effects of brine rejection will be minor. Since most of the frazil ice formation is occurring below the ocean skin, there will not be much immediate modification of the chemistry of the mass diffusive layer. Ushio and Wakatsuchi [1993] also showed that the brine rejection from frazil crystals is concentrated in thin streamers that rapidly descend downwards. If leads are small and short-lived, there would be a significant amount of unmodified water available laterally and vertically to replace those descending brines, keeping the surface water properties near–constant.

Ultimately, we cannot draw any firm conclusions regarding the short timescale modifications to the seawater carbonate system. However, given the manner in which the carbonate system is entwined with many of the processes that occur with lead formation, this should be a major focus of future studies.

2.5.3 Significance to the Amundsen Gulf Region

The total winter CO_2 flux through open water in Amundsen Gulf depends on not only the rate at which it occurs, but also on the areal extent of open water. In this section, we combine estimates of these two variables for the purpose of computing area–averaged fluxes. By calculating these fluxes, we can estimate the significance of winter CO_2 exchange relative to the open water season (i.e. late spring/summer/early fall), and we can determine if the fluxes are reasonable based on the water column DIC budget for the region devised by Shadwick et al. [2011].

As described in section 2.3.5, we used RADARSAT–1 imagery to estimate the open water fraction in a bounding box (122–126°W, 70–71.5°N) consistent with the one used by Shadwick et al. [2011]. RADARSAT–1 images that captured this area were available approximately every week, and the open water fraction calculated for each image are shown in Figure 2.13. The amount of open water during the study was highly variable, which probably relates to storm events in the area. To allow comparisons with the results of Shadwick et al. [2011], monthly averages of open water fraction were calculated, and are displayed in Table 2.4.

To estimate the rate of gas exchange over the area we would ideally have some way of scaling our flux measurements using ΔpCO_2 and an easily-obtainable variable like wind speed, but at this point our dataset is too limited to work towards parameterization. Therefore, we simply calculated the mean uptake rate from cases 1,4,7 & 17 (those with substantial uptake; the outgassing observed during case 3 was omitted because the offshore Amundsen Gulf was undersaturated through the entire winter [Shadwick et al., 2011]) to be -4.88 μmol m^{-2} s^{-1}. This rate was multiplied by the average monthly open water fraction to calculate the mean monthly fluxes shown in Table 2.4.

Figure 2.13: Open water percentage for Amundsen Gulf (122–126°W, 70–71.5°N) during the study period, as determined by classification of near-weekly RADARSAT-1 imagery.

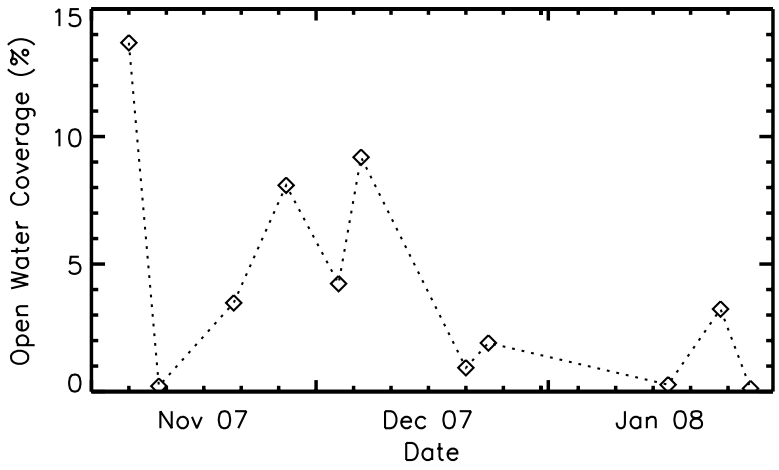

To address the question of whether these fluxes are reasonable we integrated the flux over each month, and calculated the net change in DIC (denoted $\Delta\text{DIC}_{as-enh}$ in Table 2.4) that would occur assuming a 50m mixed–layer depth. Shadwick et al. [2011] budgeted month-by-month changes in DIC in the Amundsen Gulf mixed layer via:

$$\Delta\text{DIC}_{obs} = \Delta\text{DIC}_{bio} + \Delta\text{DIC}_{fw} + \Delta\text{DIC}_{as} + \Delta\text{DIC}_{vd} \tag{2.3}$$

where ΔDIC_{obs} was the observed monthly change in DIC, and the right hand terms are monthly changes in DIC due to biological activity (ΔDIC_{bio}), freshwater fluxes (ΔDIC_{fw}), air–sea exchange (ΔDIC_{as}) and vertical diffusion (ΔDIC_{vd}). ΔDIC_{fw} and ΔDIC_{vd} were calculated from in situ data, and ΔDIC_{as} was calculated using a bulk flux approach scaled for ice concentration. No direct method was available to measure the biological contribution, so it was calculated as a difference of the 4 other terms. With no other constraint on the biological contribution to ΔDIC_{obs}, an air–sea exchange of CO_2 which is enhanced beyond ΔDIC_{as} would be mis-allocated

Table 2.4: Summary of monthly lead fraction, CO_2 fluxes and resulting change in mixed layer DIC. [a]Calculated from RADARSAT-1 image classification (Figure 2.13), [b]calculated from mean of cases 1,4,7 & 17, multiplied by lead percentage and integrated over the month, [c]calculated change in DIC concentration over a 50 m mixed–layer using $F_{CO_{2sw-mon}}$, [d]calculated change in DIC concentration over a 50 m mixed–layer using bulk–flux estimates scaled for open water percentage (from), [e]calculated change in DIC concentration over a 50 m mixed–layer due to biological activity (from).

	November	December	January
[a]Mean Open Water (%)	6.4	4.1	1.2
[b]$F_{CO_{2sw-mon}}$ (μmol m^{-2} s^{-1})	-0.31	-0.20	-0.06
[c]ΔDIC_{as-enh} (μmol kg^{-1})	16.19	10.72	3.13
[d]ΔDIC_{as} (μmol kg^{-1})	1.0	2.0	0.1
[e]ΔDIC_{bio} (μmol kg^{-1})	3.0 $\pm$ 10.0	13.0 $\pm$ 10.0	16.0 $\pm$ 10.0

into ΔDIC_{bio}. Thus if our calculated ΔDIC_{as-enh} fits within the sum of ΔDIC_{as} and ΔDIC_{bio} it can be considered to fit in the budget. Table 2.4 shows that this is the case in all months under consideration, except November. This shows that although the fluxes associated with this enhanced air–sea exchange are very high, they are not unrealistic from the standpoint of the DIC budget.

With respect to significance for the Amundsen Gulf region, the fluxes calculated accounting for enhanced air–sea exchange are more than an order of magnitude higher than those calculated by Shadwick et al. [2011] using a bulk flux approach scaled for ice concentration (Table 2.4). In fact, these fluxes place the air–sea exchange rates on par with the open water season rates calculated by Shadwick et al. [2011]. This is a significant consideration, because the typical model of a polynya's annual air–sea budget is characterized by open water uptake during the autumn storm season (utilizing an initial biological pCO_{2sw} drawdown in the spring) which is then capped by ice over the winter [Yager et al., 1995]. The strength of annual uptake by a polynya was thought to be constrained by whether or not the spring undersaturation could be utilized by open water air–sea exchange, but the results

from this study show that uptake may proceed beyond ice formation. It should be noted, however, that not every polynya may remain undersaturated through the winter; in polynyas where this is not the case, winter outgassing through open water may tip the annual balance away from net uptake.

2.5.4 Potential Significance to the Arctic Ocean

As well as creating a need to re-think the seasonal evolution of gas exchange for polynyas, enhanced winter gas exchange may play an important role in the broader Arctic and Antarctic Oceans. Omar et al. [2005] used a simple extrapolation of winter air–sea CO_2 exchange estimated in Storfjorden to show that Arctic polynyas are likely a significant sink for atmospheric CO_2. Our study confirms that at least one other Arctic polynya behaves as they predict, an important step in validating their larger scale estimates. In addition to polynyas, we hypothesize that leads may act as important centres for winter gas exchange. Leads are typically a small fraction of the Arctic icescape during winter; Lindsay and Rothrock [1995] estimated the percentage to be 2–3% for the central Arctic and 6–9% for the peripheral seas. However, our findings suggest that even at low fractions these features may dominate the winter gas exchange budget much in the same way that they dominate heat fluxes [Andreas, 1980; Maykut, 1978]. Also of note are the large areas of the Arctic and Antarctic ocean which are seasonally ice-free. In the Arctic, this makes up an area of 6.4×10^6 km^2 and in the Antarctic 15.2×10^6 km^2 (Wadhams [2000], 1979-87 averages). As discussed by Omar et al. [2005], the seasonal formation of sea ice over these areas may create short but intense CO_2 fluxes which could be important to the annual air-sea CO_2 exchange budget of the Arctic and Southern Oceans.

Ongoing and anticipated changes in the polar oceans may further increase the importance of this effect. The rapidly decreasing summer ice extent in the Arctic (e.g. Stroeve et al. [2007]) means that a larger area will be subject to annual ice formation, and significant positive trends in sea ice motion [Hakkinen et al., 2008] may create more winter–time open water. Our results show that this will permit larger annual air–sea gas exchange, but whether this will result in a larger net sink of CO_2 is complicated. Surface seawater that is undersaturated in pCO_{2sw} can only absorb a finite amount of CO_2, depending on the state of the carbonate equilibrium (i.e. the Revelle factor). A debate is currently emerging regarding whether the ocean surface exposed by recent sea ice loss has the capacity to take up significant amounts of CO_2 [Bates et al., 2006; Cai et al., 2010]. A similar debate needs to be had regarding uptake capacity of the Arctic Ocean at freeze–up in order to understand the potential for gas exchange enhanced by ice formation. A net annual sink also requires export of absorbed CO_2 to depth, a process that appears to occur effectively on the shelves where deep water formation occurs but not necessarily in the Arctic Ocean basins [Omar et al., 2005]. Clearly, a lot of work remains to be done before we can fully understand the interplay between enhanced gas exchange and future changes to the Arctic Ocean.

2.6 Summary and Conclusions

This paper has provided the first direct, in situ observations of enhanced gas exchange during sea ice formation. Eddy covariance calculations of CO_2 flux in Amundsen Gulf (a polynya with a dynamic winter sea ice cover) showed periods of intense uptake (mean flux -4.88, maximum -27.95 μmol m^{-2} s^{-1}) and one case of outgassing (mean flux +2.10 μmol m^{-2} s^{-1}). These periods of high gas exchange

were observed coincidentally with high heat fluxes, which we confirmed from satellite imagery to be the result of open water (i.e. leads). Conversely, we measured no fluxes above the uncertainty of our instruments over consolidated sea ice.

We presented several hypotheses to explain our observations of enhanced gas transfer. In a winter lead, we expect high water–side turbulence to occur as a result of rapid heat loss and salt rejection. Since turbulence is the first–order control on gas exchange, we hypothesize that this high turbulence is a major cause of enhanced gas exchange. We also discussed the modification of surface properties (temperature, salinity, DIC/TA) and their effect on the seawater carbonate system. The potential of these modifications to influence the rate of gas exchange depends on the saturation state of CO_2 with respect to the atmosphere, and at times may actually be contradictory to high fluxes. In support of these hypotheses, we were only able to provide limited evidence of high turbulence in the region.

By comparing our flux values with DIC measurements we were able to show that although high, they do fit within surface DIC budgets. A rough calculation of the integrated CO_2 uptake over the months of November–January showed that winter gas exchange may in fact be as important as the open water (i.e. late spring/summer/early fall) seasons. These results have wide reaching implications for understanding the annual air–sea CO_2 budgets of polynyas and other seasonally ice–free seas.

Chapter 3

Annual Cycles of pCO_{2sw} in the Southeastern Beaufort Sea: New Understandings of Air–Sea CO_2 Exchange in Arctic Polynya Regions

Journal of Geophysical Research – Oceans, 117, C00G13

doi: 10.1029/2011JC007346

Brent G.T. Else*[1], Tim N. Papakyriakou[1], Ryan J. Galley[1], Al Mucci[2], Michel Gosselin[3], Lisa A. Miller[4], Elizabeth Shadwick[5,6], Helmuth Thomas[5]

[1]Centre for Earth Observation Science, Department of Environment and Geography, University of Manitoba, Winnipeg, Manitoba, Canada

[2]GEOTOP, Department of Earth and Planetary Science, McGill University, Montreal, Québec, Canada.

[3]ISMER, Université du Québec à Rimouski, Rimouski, Québec, Canada

[4]Centre for Ocean Climate Chemistry, Institute of Ocean Sciences, Fisheries and Oceans Canada, Sidney, British Columbia, Canada

[5]Department of Oceanography, Dalhousie University, Halifax, Nova Scotia, Canada

[6]now at Antarctic Climate and Ecosystems Cooperative Research Center, University of Tasmania, Hobart, Tasmania, Australia

Abstract

From October 23, 2007 to August 1, 2008, we made continuous measurements of sea surface partial pressure of CO_2 (pCO_{2sw}) in three regions of the southeastern Beaufort Sea (Canada): Amundsen Gulf, the Banks Island Shelf, and the Mackenzie Shelf. All three regions are seasonally ice covered, with mobile winter ice and an early spring opening that defines them as polynya regions. Amundsen Gulf was characterized by undersaturated pCO_{2sw} (with respect to the atmosphere) in the late fall, followed by an under–ice increase to near–saturation in winter, a return to undersaturation during the spring and an increase to near–saturation in summer. The Banks Island Shelf acted similarly, while the Mackenzie Shelf experienced high supersaturation in the fall, followed by a spring undersaturation and a complex, spatially heterogeneous summer season. None of these patterns are similar to the annual cycle described or proposed for other Arctic polynya regions. We hypothesize that the discrepancy reflects the influence of several previously unconsidered processes including fall phytoplankton blooms, upwelling, winter air–sea gas exchange, the continental shelf pump, spring nutrient limitation, summer surface warming, horizontal advection and riverine input. In order to properly predict current and future rates of air–sea CO_2 exchange in such regions, these processes must be considered on a location–by–location basis.

3.1 Introduction

Polynyas are recurring areas of open water or thin ice in polar seas that persist under conditions where a complete ice cover would otherwise be expected [Barber and Massom, 2007]. The persistence of open water can be caused by removal of ice by wind and currents, by warm water upwelling, or by some combination of the two [Smith et al., 1990]. Although accounting for a small fraction of the Arctic Ocean icescape, polynyas play a disproportionately large role in heat budgets [Maykut, 1978], are often centres of intense biological activity [Massom, 1988], and generate a significant amount of ice relative to established ice covers [Smith et al., 1990]. Because they are ice free, they provide a direct link between ocean and atmosphere and thus serve as conduits for air-sea gas exchange. Also of interest is the role that sea ice may play in modulating air–sea gas exchange in polynya regions (a term that we use to describe a geographic area that hosts a polynya at some point during the year) during the ice–covered or partially ice–covered portions of the annual cycle.

Yager et al. [1995] proposed that these regions act as a strong annual sink of atmospheric CO_2 because the seasonal cycle of sea surface partial pressure of CO_2 (pCO_{2sw}) is in phase with seasonal ice cycles; pCO_{2sw} is lower than the overlying atmosphere (undersaturated) due to phytoplankton blooms in spring and summer when ice concentrations are lowest, and higher than the atmosphere (supersaturated) due to excess respiration in the winter when ice concentrations are highest. They assumed that the winter ice cover would prevent any outgassing, leaving only the uptake of CO_2 during the open water season to contribute to the net annual exchange – a cycle they termed "seasonal rectification". This hypothesis is far–reaching,

because it can also be applied to other regions of the Arctic that are seasonally ice–free.

Although this hypothesis is elegant, relatively little data exist to support it. In the Northeast Water (NEW) Polynya, Yager et al. [1995] only observed the summer undersaturation and hypothesized that a stormy fall season would drive enough gas exchange to replace the CO_2 absorbed by the spring bloom. Observations from the North Water (NOW) Polynya [Miller et al., 2002] provided more evidence for the seasonal rectification hypothesis by documenting a brief period of supersaturation at ice-breakup and a subsequent reduction of pCO_{2sw} by a strong spring bloom. In this case, the undersaturation persisted until the fall freeze–up, and no data were collected during the subsequent winter.

Another important characteristic of Arctic polynyas is their frequent occurance on continental shelves [Barber and Massom, 2007] whose role in air–sea CO_2 exchange has been the source of much discussion over recent years [Borges et al., 2005; Cai et al., 2006; Chen and Borges, 2009; Thomas et al., 2004; Tsunogai et al., 1999]. Shelves are at the distal end of the complex coupling between marine and terrestrial carbon cycles that begins where rivers enter the ocean. Near their discharge point, rivers are typically supersaturated in pCO_{2sw} due to net heterotrophy sustained by their high terrestrial carbon load and relatively low alkalinity, but most of the excess CO_2 is outgassed in the inner estuaries and the near–shore coastal environments [Chen and Borges, 2009]. Seaward of these outgassing regions, most mid– and high–latitude shelves act as sinks for atmospheric CO_2 [Borges et al., 2005; Cai et al., 2006; Chen and Borges, 2009]. This net sink occurs offshore because of high biological productivity during spring and summer promoted by the delivery of upwelled and riverine nutrients, and the export of decay products to the deep basins

during winter. This export is driven by the formation of dense water that sinks and exits the shelf below the pycnocline [Tsunogai et al., 1999], or by the sinking of particulate organic carbon to either the sediments (where some portion becomes sequestered), or to deeper layers where it is respired and eventually exported [Thomas et al., 2004]. This so–called "continental shelf pump" is thought to be particularly important on Arctic shelves where brine production and rapid winter cooling enhance the formation and export of dense water [Anderson et al., 2010], and a large fraction of primary production occurs in episodic blooms that tend to have higher vertical carbon export ratios [Sarmiento and Gruber, 2006].

Yager et al. [1995] wrote that "as more data become available for the NEW Polynya and other Arctic regions, the [seasonal rectification] hypothesis will be tested rigorously". In this paper, we make a significant contribution towards this effort by describing the annual pCO_{2sw} cycle in three polynya regions of the southeastern Beaufort Sea: the Mackenzie Shelf, the Banks Island Shelf and Amundsen Gulf. Our study expands on the work of Shadwick et al. [2011], who provided an overview of the annual pCO_{2sw} cycle in Amundsen Gulf as part of their work on inorganic carbon cycling. The expanded dataset presented here allows us to improve upon their discussion of processes controlling pCO_{2sw} in Amundsen Gulf, and to place it in the context of pCO_{2sw} cycling on the other continental shelf seas of the southeastern Beaufort Sea. The spatiotemporal resolution and coverage of our dataset allows for a rigorous test of the Yager et al. [1995] hypothesis in a complex Arctic polynya region.

3.2 Study Area

This study was conducted from October 23, 2007 to August 1, 2008 in the southeastern Beaufort Sea (Figure 3.1) as part of the fourth International Polar Year Circumpolar Flaw Lead System Study (CFL) and ArcticNet projects onboard the research icebreaker CCGS *Amundsen*. The goal of these projects was to conduct a multi-disciplinary sampling program overwintering in the southeastern Beaufort Sea. The ship conducted transects in Amundsen Gulf and on the Mackenzie and Banks Island shelves during the fall and early winter of 2007. The overwintering was done in the mobile ice of Amundsen Gulf with the ship drifting in ice floes and repositioning by travelling through leads and thin ice. In the spring and summer of 2008, the fall sampling locations were revisited to construct a near–complete annual cycle.

As shown in Figure 3.1, the portion of the southeastern Beaufort Sea discussed in this paper can be subdivided into several distinct regions. The Mackenzie Shelf is a broad continental shelf with a mean depth of 35 m and a shelf break about 120 km offshore. The entire shelf is seasonally affected by the outflow from the Mackenzie River, which modulates salinity, turbidity, temperature, nutrient concentrations and circulation [Carmack and Macdonald, 2002; Carmack et al., 1989; Macdonald et al., 1987]. Phytoplankton productivity is low in the winter, intensifies following an ice algae bloom in April and May and becomes highest during a modest open water bloom that is nutrient limited due to surface stratification [Carmack et al., 2004]. As a result of these blooms, Mucci et al. [2010] observed strong undersaturations of $p\mathrm{CO}_{2sw}$ in the summer and fall.

Figure 3.1: Map of study area with bathymetry (contour interval = 100 m). The regions discussed in the text are outlined with a dashed line, and the black bounding box delineates the region used to create Figures 3.3 & 3.4. The coloured dots indicate the location of CTD casts described in Table 3.1: red – November 5, yellow – March 2, green – May 31, blue – July 11. The inset map shows the locations of the Northeast Water (NEW) and North Water (NOW) polynyas in relation to the study area (black box).

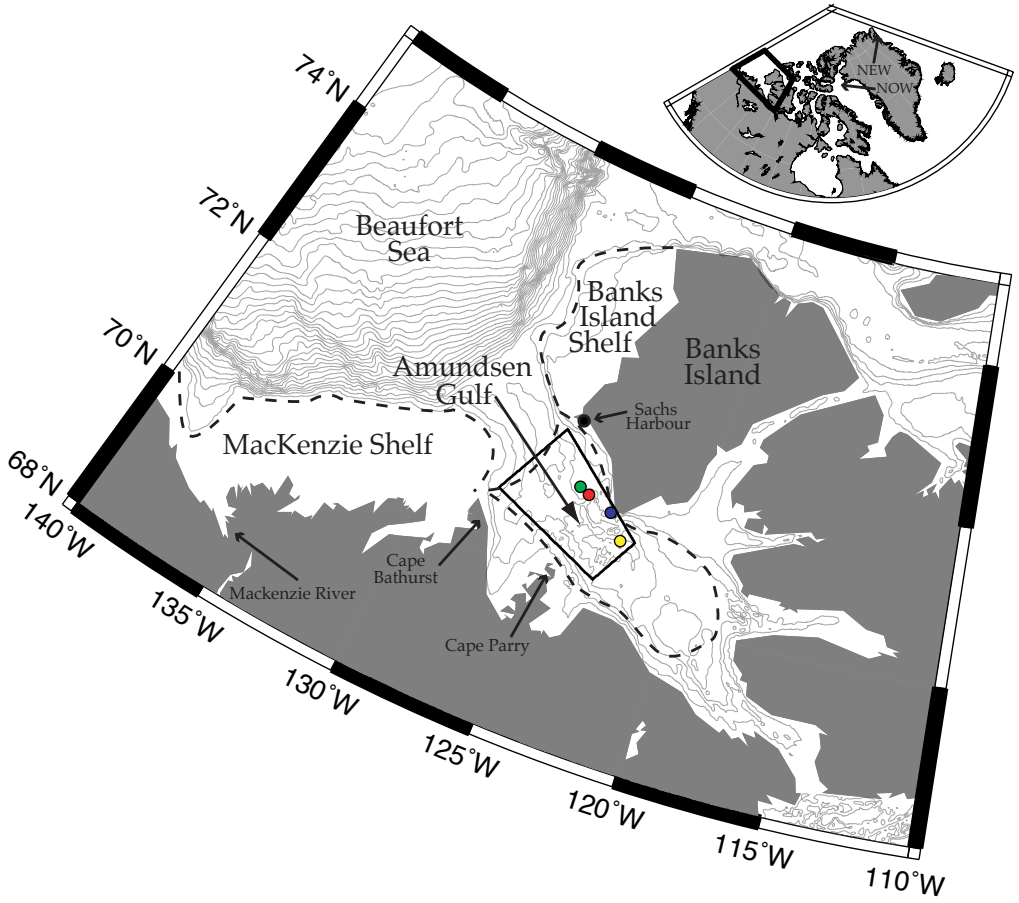

Amundsen Gulf is deeper than the Mackenzie Shelf (max depth of ∼500 m) and is not strongly affected by the Mackenzie River outflow at most times of the year [Chierici et al., 2011; Magen et al., 2010; Thomas et al., 2011; Tremblay et al., 2008]. The region is nutrient–limited due to surface stratification (mostly from sea ice melt), and therefore the spring bloom has been shown to be less intense than in other polynya systems [Tremblay et al., 2008]. There is also evidence that this area experiences a bloom in the fall season as storms entrain deeper nutrient-rich water to the surface [Arrigo and van Dijken, 2004; Brugel et al., 2009]. Mucci et al. [2010] observed $p\mathrm{CO}_{2sw}$ values close to equilibrium with the atmosphere in the summer and undersaturated $p\mathrm{CO}_{2sw}$ values in the previous fall.

The Banks Island Shelf is not as broad as the Mackenzie Shelf and, unlike the latter, is not host to significant river discharge. The areas sampled during this project were shallower than the Amundsen Gulf, with most depths less than 200 m. To our knowledge, this region has not been the subject of any major oceanographic studies. The large scale remote sensing study of primary productivity by Pabi et al. [2008] indicates that the region has similar productivity to Amundsen Gulf, but no data on $p\mathrm{CO}_{2sw}$ are available.

Combined, these areas make up a complex polynya/flaw lead region whose annual ice cycle has been described by Galley et al. [2008]. Ice formation begins in October with landfast ice developing around the coastal margins and mobile ice accumulating in the Beaufort Sea and Amundsen Gulf. The ice in Amundsen Gulf does become landfast in some years, but it typically remains dynamic throughout the winter with small, transient leads developing in response to wind–driven ice motion. Meanwhile, the ice in the Beaufort Sea is mobile all year, creating a shear zone along the coastal margins (along the Banks and Mackenzie shelves) where persistent winter flaw leads

exist. The motion of ice in the Beaufort Sea allows for dynamic ice export from Amundsen Gulf through the fall and winter [Kwok, 2006], eventually creating the spring open water feature known as the Cape Bathurst polynya. The Beaufort Sea mobile ice typically moves offshore at around the same time, creating early open water on the Mackenzie and Banks Island shelves.

3.3 Methods

3.3.1 Surface Water pCO_2 Sampling

Continuous pCO_{2sw} sampling was conducted using a shower-type equilibrator system composed of a sealed cylindrical tank (volume ∼15 L) with a shower head at the top and a drain at the bottom through which water was cycled at a rate of 1.5–2 L min^{-1}. The system was set up to maintain a water volume of about 2 L, while the headspace air (volume ∼13 L) was cycled through a LI-COR LI-7000 CO_2/H_2O gas analyzer at a rate of 3.5 L min^{-1}. Calibration of the LI-7000 was performed daily using ultra-high purity N_2 as a zero gas and a CO_2/air mixture (in the range of 380 ppm) traceable to WMO standards as a span gas. Atmospheric pCO_2 measurements were made using a separate LI–7000 (also calibrated daily with high–purity N_2 and a similar traceable span gas) which drew sample air from a meteorological tower on the foredeck of the ship at a height of ∼14 m above sea level.

The equilibrator system was located in the engine room of the ship, a short distance (< 5 m) downstream from a high volume scientific water intake at a nominal subsurface depth of 5 m. Despite the proximity to the intake, a thermocouple immersed in the equilibrator water registered a slight increase in water temperature relative to *in situ* conditions. To correct for this increase, a regression analysis was

performed by comparing equilibrator water temperature to coincident surface water temperature measurements obtained by the ship's CTD/Rosette system (see section 3.3.2). A total of 105 CTD casts were used in the analysis, which revealed a strong (R^2=0.97) and consistent linear relationship ($T_{sw} = 0.98T_{eq}$–1.7°C) between *in situ* surface water temperature (T_{sw}) and equilibrator water temperature (T_{eq}). That relationship was then used to correct pCO_{2sw} for thermodynamic effects following the procedure described by Takahashi et al. [1993].

Periodic interruptions of the pCO_{2sw} system occurred during icebreaking operations. During these operations, ice clogged the water intake at the ship's hull, stopping or severely restricting flow to the equilibrator. Data acquired during these instances were removed in post processing and represent the most significant cause of data loss.

3.3.2 Ancillary Data

To examine processes controlling pCO_{2sw} (section 3.3.3), we required ancillary data from collaborators who participated in the cruises (see Barber et al. [2010] for details on instruments and sampling strategies). Stations were sampled throughout the study area, as a network of transects during open water conditions, and opportunistically when the ship was drifting in floes during the winter. Whenever possible, stations were revisited seasonally. From CTD/Rosette casts (conducted at every station), we obtained salinity (S) and sea surface temperature (SST) from the shallowest possible depth; typically 1–5 m when deployed over the side of the ship (October 15 – November 5, 2007 & July 17 – August 5, 2008) and 10–15 m when deployed through the moon pool (November 5, 2007 - July 17, 2008). Uncertainty caused by sampling at these different depths depends on the season. In winter,

when the surface mixed layer was deep, we expect very little variation in SST or S; for example, during the fall side–of–ship deployments (when the mixed layer was >30 m deep) SST at 5 m was on average 0.1°C cooler and S was 0.1 lower than at 10 m. In spring and summer as the mixed layer shoaled this uncertainty likely became greater; during the summer side–of–ship deployments (when the mixed layer was sometimes as shallow as 10 m) SST at 5 m was on average 0.5°C warmer and S remained 0.1 lower than at 10 m. S measurements were also obtained from a thermosalinograph sensor installed on the same continuous water sample line as the pCO_{2sw} equilibrator. At several of the stations, we also obtained surface DIC, TA and Chl *a* measurements from discrete seawater samples collected by the rosette Niskin bottles. The analytical techniques for the DIC and TA samples are described in Shadwick et al. [2011], while the Chl *a* sampling protocol was similar to that described by Brugel et al. [2009].

Information on the extent of sea ice coverage (i.e., sea ice concentration) was obtained from Canadian Ice Service (CIS) charts (available online) which were created daily for the areas where the CCGS *Amundsen* was operating, and weekly for the broader western Arctic region. Hourly wind velocity data from Environment Canada weather stations at Sachs Harbour and Cape Parry (obtained online, see Figure 3.1 for locations) were used for bulk CO_2 flux calculations (section 3.3.3). MODIS SST imagery (500 m pixels, daytime 11 and 12 μm bands, obtained from the MODIS Rapid Response System) was used to locate the Mackenzie River plume and upwelling areas during the ice free seasons. The Mackenzie river plume can be identified visually on SST images as it is significantly warmer than shelf water (e.g. Vallières et al. [2008]), while upwelled water is significantly colder (e.g. Williams and Carmack [2008]).

3.3.3 Determination of Processes Controlling $p\mathrm{CO}_{2sw}$

Where possible, we calculated how various physical, chemical, and biological processes contributed to observed changes in $p\mathrm{CO}_{2sw}$. The processes that we identified as potentially important and the techniques used to quantify their relative influence on $p\mathrm{CO}_{2sw}$ are as follows:

1. **Gas exchange** reduces (increases) $p\mathrm{CO}_{2sw}$ when $p\mathrm{CO}_{2sw}$ is higher (lower) than atmospheric CO_2 ($p\mathrm{CO}_{2atm}$). We used a bulk flux approach to estimate CO_2 flux (F_{CO_2}):

$$F_{\mathrm{CO}_2} = k\alpha(p\mathrm{CO}_{2sw} - p\mathrm{CO}_{2atm})(1 - C_i) \tag{3.1}$$

   where k is the transfer velocity (computed as a function of wind velocity using Sweeney et al. [2007]), α is the solubility of CO_2 [Weiss, 1974] and C_i is the fractional ice coverage. We used hourly wind velocity measurements from the Cape Parry weather station for Amundsen Gulf, and from the Sachs Harbour station for the Banks Island and Mackenzie shelves. To compute change in DIC driven by gas exchange, F_{CO_2} was divided by the mixed layer depth (defined as the position of the vertical density gradient maximum as observed from CTD profiles) and multiplied by the length of time of interest. We then used the CO2calc program [Robbins et al., 2010] with the dissociation constants of Mehrbach et al. [1973] as refit by Dickson and Millero [1987] to calculate the resulting change in $p\mathrm{CO}_{2sw}$. To estimate a complete annual cycle of $p\mathrm{CO}_{2sw}$ in Amundsen Gulf for 2007–08, we performed a simple linear interpolation between measurements obtained at the start of August 2008 and the end of October 2007.

2. **Sea surface temperature** exerts a thermodynamic control on the seawater carbonate system and thus increases pCO_{2sw} by about 4% per °C [Takahashi et al., 1993]. For time periods of interest, we used the CO2calc program to calculate pCO_{2sw} from DIC, TA, S and SST measurements when a station was first visited, and then recalculated pCO_{2sw} at the SST measured when the station (or a station nearby) was revisited. The difference between these two calculated values reflects the change in pCO_{2sw} caused by the change in SST.

3. **Salinity** also affects the carbonate chemistry and hence pCO_{2sw}. If TA and DIC are held constant, an increase (decrease) in S would cause an increase (decrease) in pCO_{2sw} by reducing (increasing) the solubility of the gas. However, the processes that change S also typically modify TA and DIC concentrations, thus modifying the equilibrium state of the carbonate system and exerting a further control on pCO_{2sw}. Sea ice melt dilutes TA and DIC along with S, lowering pCO_{2sw}. Conversely, sea ice formation increases S along with TA and DIC of the residual water, raising pCO_{2sw}. For the Amundsen Gulf region, Shadwick et al. [2011] derived a series of equations to predict changes in surface water TA (dTA) and DIC (dDIC) concentrations as a function of change in S (dS):

$$\mathrm{dTA} = 49.38\mathrm{dS} + 0.42 \tag{3.2}$$

$$\mathrm{dDIC} = \mathrm{dTA}(\mathrm{DIC}/\mathrm{TA}) \tag{3.3}$$

This equation implicitly includes ice melt and river inputs, and is specific to Amundsen Gulf. Without as comprehensive a data set for the Mackenzie and Banks Island shelves, we were unable to carry out similar analyses. For

Amundsen Gulf, we calculated dTA and dDIC over a given time period using the change in S between two visits to the same or neighbouring stations. The effect on pCO_{2sw} was then determined as the difference between pCO_{2sw} computed from the surface water properties (TA, DIC) measured on the initial visit to the station and at the S measured on the subsequent visit combined with the calculated dTA/dDIC.

4. **Upwelling and vertical mixing** can have a significant impact on pCO_{2sw} by modifying the surface water properties and carbonate chemistry [Chierici et al., 2011]. Shadwick et al. [2011] and Lansard et al. [2012] showed that DIC, TA and pCO_2 in Amundsen Gulf are typically much higher below the mixed layer, and data from the Mackenzie and Banks Island shelves show similar profiles. Transport of this water into the surface layer thus typically increases pCO_{2sw}. For simple vertical mixing caused by mixed layer deepening, we calculated change in surface water DIC and TA (DIC_{sw}/TA_{sw}) following Gruber et al. [1998]:

$$\mathrm{dTA_{sw}} = \mathrm{dh(TA_{pyc} - TA_{sw})h^{-1}} \tag{3.4}$$

$$\mathrm{dDIC_{sw}} = \mathrm{dh(DIC_{pyc} - DIC_{sw})h^{-1}} \tag{3.5}$$

where h is the depth of the mixed layer on the first visit to a station, dh is the change in mixed layer depth between the initial station and subsequent visits to the same (or neighbouring) station, and the subscript "pyc" denotes the mean DIC and TA concentrations measured on the first visit to the station at a depth between the original and subsequent mixed layer depths. The effect of these changes in DIC_{sw} and TA_{sw} concentration on pCO_{2sw} were then

calculated in CO2calc. As per Gruber et al. [1998], we did not calculate any change in DIC or TA for time periods where the mixed layer shoaled.

5. **Biology** (excluding the biogenic $CaCO_3$ cycle) influences pCO_{2sw} by removing DIC and adding smaller amounts of TA during periods of net photosynthesis and adding DIC and removing TA during periods of net respiration. The biological controls on DIC and TA are often calculated from nutrient uptake, but such analyses are difficult in the Arctic due to the varied source waters of nutrients (e.g. Anderson et al. [2010]). In Amundsen Gulf, Shadwick et al. [2011] assumed that any residual change in DIC and TA not accounted for by changes in S, gas exchange or upwelling was due to biological activity. We adopted a similar approach, and assigned any residual changes in pCO_{2sw} not accounted for by other processes to biological processes. To add some understanding of the timing and magnitude of biological pCO_{2sw} reduction, we used surface water chlorophyll–a (Chl a) measurements as a proxy to identify periods of high photosynthetic activity.

6. **Horizontal advection** can modify pCO_{2sw} in regions where strong horizontal pCO_{2sw} gradients exist in conjunction with significant surface currents. Shadwick et al. [2011] showed that horizontal advection is negligible in Amundsen Gulf due to slow surface currents and minimal horizontal pCO_{2sw} gradients. We therefore ignored horizontal advection as a potentially important influence in that region. For the Mackenzie and Banks Island shelves, we used the daily sea ice motion vector product (averaged bi–monthly) provided by the National Snow and Ice Data Center [Fowler, 2010] to characterize surface currents. Where possible, we combined these surface current data with pCO_{2sw}

to derive qualitative estimates of the role of horizontal advection in modifying pCO_{2sw}.

3.4 Results and Discussion

3.4.1 Amundsen Gulf

Amundsen Gulf was the most frequently sampled area of the southeastern Beaufort Sea during this project, partly because the ship was confined to the area during the winter, and partly because transects were repeated there regularly during the open water seasons (Figure 3.2). This allowed us to create a detailed time series of pCO_{2sw} (Figure 3.3) within a box covering western Amundsen Gulf (see Figure 3.1), by averaging observations made within the box in weekly intervals. We also compiled a similar time series of Chl *a* (Figure 3.4). The long occupation of Amundsen Gulf also allowed us to evaluate the processes controlling pCO_{2sw} during each season. We did this by applying the methods outlined in section 3.3.3 between four dates that roughly represent the endpoints of fall, winter, spring and summer. The surface water data collected on these four dates are shown in Table 3.1, and the calculated change that each process imparted upon pCO_{2sw} between the dates are reported in Table 3.2.

Fall (November 2007)

The transects made shortly prior to freeze–up (Figure 3.2a), reveal that the surface mixed layer in Amundsen Gulf was consistently undersaturated, with a mean pCO_{2sw} of 302 μatm and a standard deviation of 10 μatm. To explain this undersaturation, we have to assume that the conditions observed the following summer (July 2008)

Table 3.1: Surface water conditions at four stations used to calculate the contribution of processes affecting pCO_{2sw} change in Amundsen Gulf. Station locations are shown in Figure 3.1. The subscript "*sw*" indicates a measurement made in the surface seawater (depth ~5 m), while the subscript "*pyc*" denotes a measurement made at a depth between the original and subsequent mixed layer depths (see section 3.3.3).

Date	SST (°C)	Sal	TA_s (μmol/kg)	DIC_s (μmol/kg)	TA_{pyc} (μmol/kg)	DIC_{pyc} (μmol/kg)	ML Depth (m)
05-11-07	-1.57	29.11	2077.8	1965.4	2204.3	2089.3	35
02-03-08	-1.72	31.64	2235.8	2127.3			37
31-05-08	-1.57	31.66	2224.5	2091.8			23
11-07-08	8.33	29.29	2077.0	1951.0	2195.4	2052.7	12.5

are representative of those in July 2007, prior to our arrival in the region (see for e.g. Shadwick et al. [2011]). If this is the case, a significant (94 μatm) decrease in pCO_{2sw} occurred between mid–July and early November (Table 3.2, Figure 3.3).

Table 3.2: Observed seasonal changes in pCO_{2sw} (μatm) in Amundsen Gulf, and calculated contributions of various processes to those changes. Section 3.3.3 describes how each term was calculated.

Change in pCO_{2sw}	Nov 5/07 – Mar 2/08	Mar 2/08 – May 31/08	May 31/08 – Jul 11/08	Jul 11/08 – Nov 5/07
SST	-2	2	162	-142
Air–Sea	1.5 (15)	0.8 (8)	22	114
Salinity	29	0	-10	-2
Vertical Mixing	2	0	0	-2
Biology	44	-77	-81	-63
Total	**74**	**-73**	**93**	**-94**

The cooling from peak summer SST (8.3°C) to near the freezing point accounts for a pCO_{2sw} reduction of 142 μatm, but our calculations of air–sea exchange show that this decrease would have been largely countered by CO_2 invasion from the

Figure 3.2: Measured pCO_{2sw} (μatm) during transects conducted in the study area. Coloured dots are pCO_{2sw}, the background image is ice concentration from the AMSR–E satellite [Spreen et al., 2008] and the white lines are bathymetric contours with a depth interval of 100m. The black line in the pCO_{2sw} scale indicates the approximate atmospheric pCO_2. Panel (a) shows transects conducted October 23 – November 2, 2007 overlain on an AMSR–E image from October 31. Panel (b) shows transects conducted May 21 – June 27, 2008 overlain on an AMSR–E image from May 25. Panel (c) shows transects conducted July 10 – July 27, 2008 overlain on an AMSR–E image from July 15

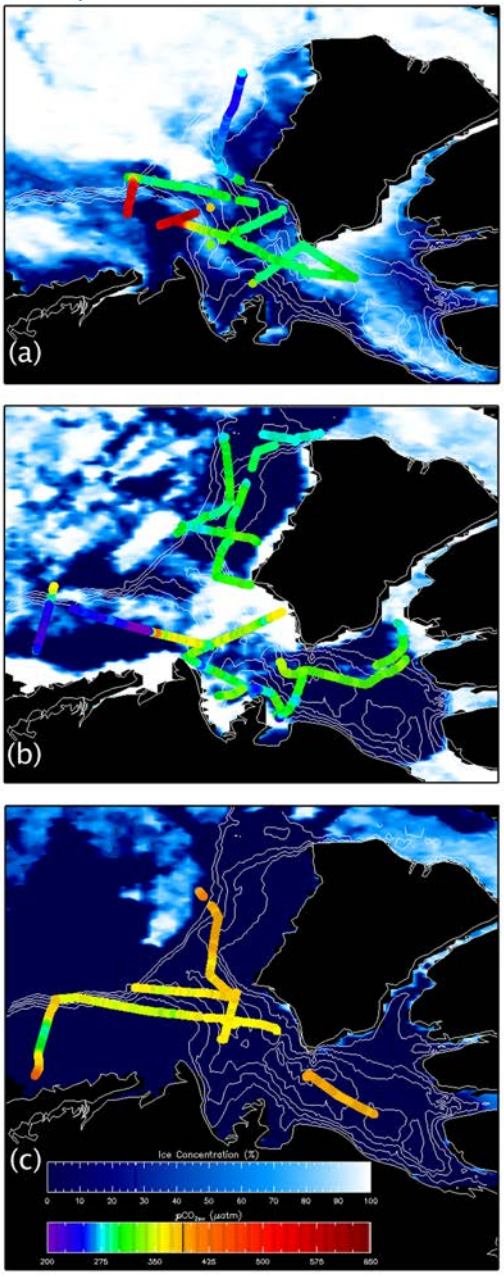

atmosphere (Table 3.2). An observed deepening of the mixed layer (Table 3.1; Shadwick et al. [2011]) may have also contributed slightly to the overall pCO_{2sw} decrease (Table 3.2) because the June profile of pCO_2 (derived from the DIC and TA profiles) contained a minimum within the pycnocline [Chierici et al., 2011], corresponding to a sub–surface chlorophyll maximum – a ubiquitous summer feature of seasonally ice–free Canadian Arctic waters [Martin et al., 2010]. To balance the budget, a biology–driven reduction of 63 μatm must have occurred (Table 3.2). This is consistent with past observations of significant fall phytoplankton blooms in Amundsen Gulf [Arrigo and van Dijken, 2004; Brugel et al., 2009] and with the high Chl a levels observed in October 2007 (Figure 3.4).

Figure 3.3: Weekly average pCO_{2sw} measurements in Amundsen Gulf (open circles), error bars are 1 standard deviation. Also shown is SST from the equilibration system (closed circles), atmospheric pCO_2 from the meteorological tower (grey dashed line) and sea ice concentration from weekly Canadian Ice Service charts (solid line).

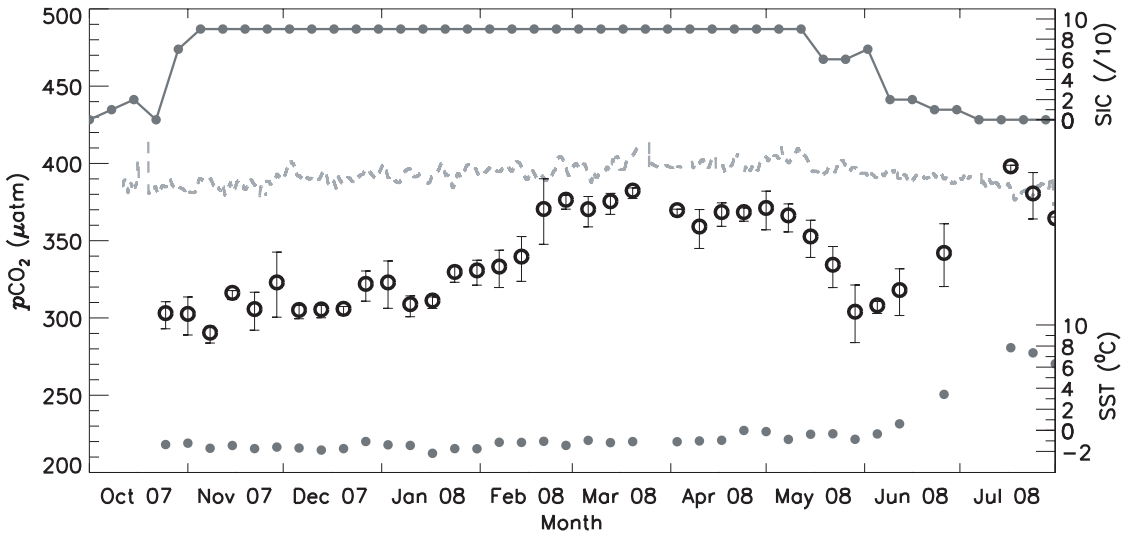

Winter (November 2007 - March 2008)

From late fall 2007 to early March 2008, we observed a gradual increase in pCO_{2sw} to a maximum near 380 μatm (Figure 3.3). During this period, surface S increased from 29.3 to 31.8, which Shadwick et al. [2011] attributed primarily to brine rejection by sea ice formation. Table 3.2 shows that this S increase (and the concomitant increase in DIC and TA) played an important role in the overall pCO_{2sw} increase (29 μatm of the observed 74 μatm increase). Vertical mixing and SST change imparted only minor impacts on pCO_{2sw}, suggesting that biology played a more important role by increasing pCO_{2sw} by 44 μatm (Table 3.2).

The change in pCO_{2sw} due to air–sea gas exchange (estimated using Equation 3.1) is small over this period (1.5 μatm). However, eddy covariance measurements that we made during the study (Else et al. [2011], Chapter 2) suggest that very rapid gas exchange may occur through open leads due to processes associated with new ice formation. Our measurements of CO_2 flux were typically one order of magnitude larger than fluxes estimated by the bulk flux approach, and we show the effect this enhanced flux would have on changes in pCO_{2sw} in parentheses in Table 3.2. If air–sea gas exchange was indeed as strong as our measurements suggest, the biological contribution to the pCO_{2sw} change must have been less. This in part shows that our budget–balancing approach yields a rather uncertain estimate of the impact of biological processes on pCO_{2sw} when certain processes cannot be accurately accounted.

Spring (March 2008 - May 2008)

In March, pCO_{2sw} began to decrease from the maximum of 380 μatm to 363 μatm in April, followed by a sharp decrease in May that bottomed out at $\sim$305 μatm

Figure 3.4: Timeseries of measured surface water Chl *a* in Amundsen Gulf. Sample depth is indicated by the different symbols.

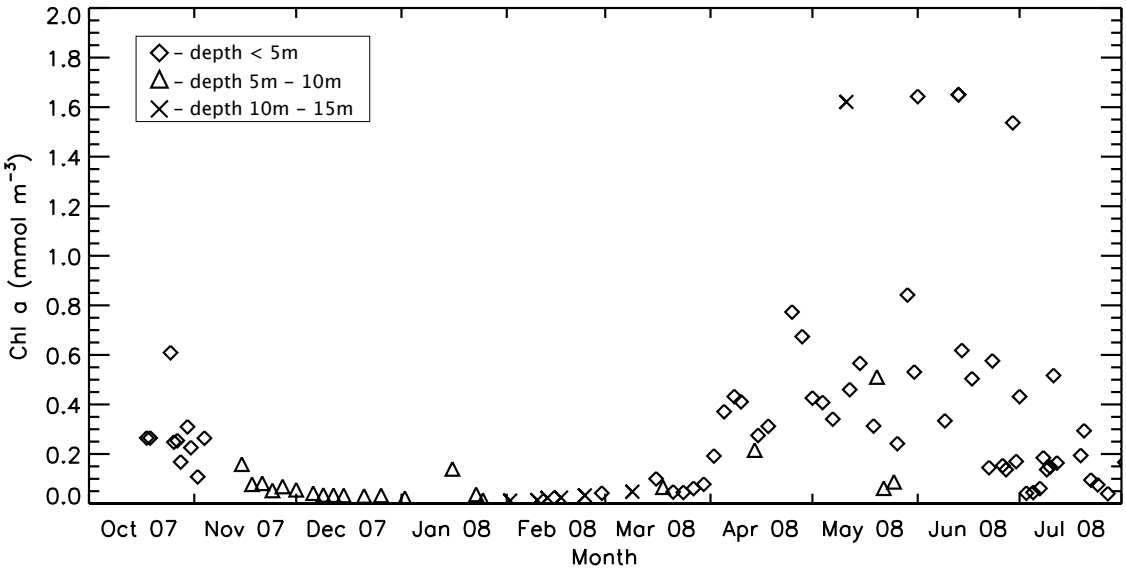

(Figures 3.2b, 3.3). As shown in Table 3.2, this decrease was driven almost entirely by biological production, and the decrease correlates well with an observed increase in Chl *a* (Figure 3.4). The March/April increase in Chl *a* was caused by an under–ice algae bloom [Shadwick et al., 2011] and was followed by a more intense open water bloom as ice cover decreased in mid–May (Figure 3.3). S and SST remained fairly constant over this time period, producing very little change in pCO_{2sw} (Table 3.2), and the mixed layer shoaled slightly (Table 3.1) preventing vertical mixing.

Summer (June – July 2008)

Figure 3.3 shows that pCO_{2sw} began to increase towards the end of June, reaching a maximum of about 400 μatm and creating a short–lived supersaturation in the second week of July. Transects in Amundsen Gulf (Figure 3.2c) confirmed that the near-saturation values extended throughout the region. Changes to the physical

characteristics of the surface mixed layer were responsible for most of this increase (Table 3.2). A warming from -1.6 to 8.3°C accounted for an increase of 162 μatm, while a decrease in S from 31.6 to 29.5 (and the accompanying dilution of DIC and TA) reduced pCO_{2sw} by 10 μatm. Results from Shadwick et al. [2011] show that the mixed layer became strongly stratified during this period due to warming and freshening, which must have suppressed vertical mixing. Biological pCO_{2sw} uptake was still significant during this period, but about a quarter of it was offset by air–sea gas exchange (Table 3.2).

3.4.2 Mackenzie Shelf

Fall (November 2007)

The Mackenzie Shelf showed very high (supersaturated) pCO_{2sw} (mean values of 553 μatm and a maximum value of 590 μatm) in fall 2007. This supersaturation was constrained shoreward of the shelf break, with sharp gradients observed along the shelf slope (Figure 3.2a). The surface S measurements collected in the region between October 21 and November 17 (Figure 3.5) show that S was much higher on the shelf (typically > 32) than beyond the shelf break (typically < 30). Figure 3.5 also shows that S was high along the southern margins of Amundsen Gulf. These high salinities were also associated with high pCO_{2sw} (not shown in Figure 3.2a), and are discussed in Chapter 4.

On the Mackenzie Shelf the polar mixed layer has a characteristic S of 31.6, while the upper–halocline waters (of Pacific origin) have a characteristic S of 33.1 [Macdonald et al., 1989]. This upper–halocline water is rich in nutrients and CO_2 and sits at depths corresponding to the shelf break [Carmack and Chapman, 2003]. When the edge of the Beaufort Sea mobile ice is beyond the shelf break, easterly

Figure 3.5: Surface salinity measurements made in the study region between October 21 – November 17, 2007.

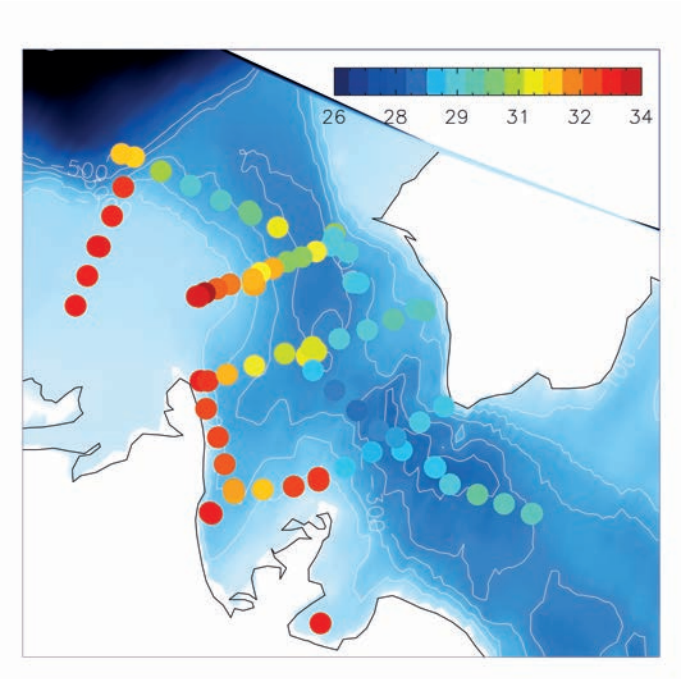

winds can drive an upwelling of upper–halocline water onto the shelf [Carmack and Chapman, 2003; Macdonald et al., 1987]. In fall 2007, the mobile ice was well beyond the shelf break, and strong easterly winds were frequent. Figure 3.6 shows that the high pCO_{2sw} measurements were strongly correlated with S, suggesting that shelf break upwelling of upper–halocline water is responsible for the elevated pCO_{2sw} (see also Tremblay et al. [2011] for a complete description of the 2007 upwelling events in this region). The formation of sea ice and subsequent rejection of CO_2–rich brine (e.g. Miller et al. [2011]; Rysgaard et al. [2007]) is another possible source of high pCO_{2sw}, but the amount of sea ice that had formed at this early point in the season could not have caused such a significant increase in S (see for example the winter evolution of S in Amundsen Gulf as described by Shadwick et al. [2011]).

Figure 3.6: Correlation plot of surface salinity vs. pCO_{2sw} measurements made between October 21 – November 17, 2007. The Figure includes pCO_{2sw} data from landfast ice margins of southern Amundsen Gulf not shown in Figure 3.2a.

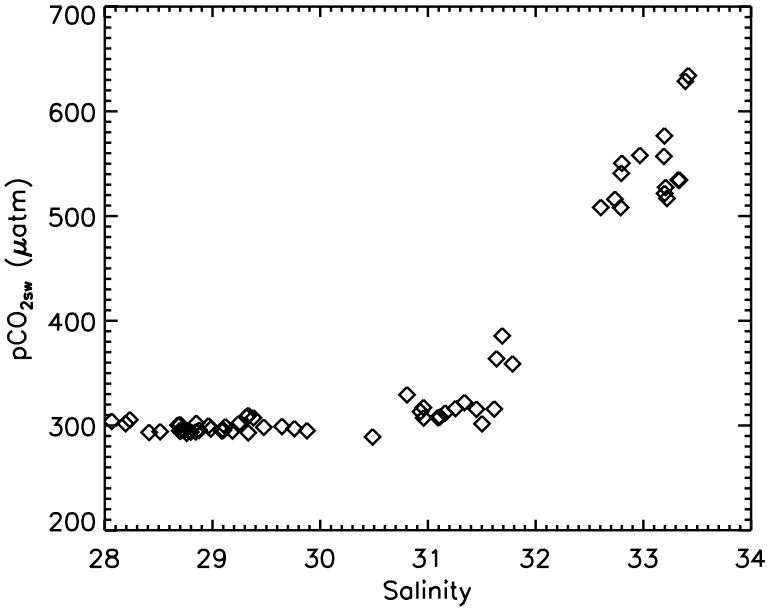

Figure 3.7 shows that ice (and hence surface water) circulation in this region is dominated by westward flow. During the fall, this would have moved the relatively low pCO_{2sw} water of Amundsen Gulf towards the Mackenzie Shelf. We expect that over the short period of time that the research vessel was in the region, this relatively slow (2–6 cm s^{-1}) transport would not have played an important role in determining the spatial distribution of pCO_{2sw} relative to the upwelling, which clearly dominated the pCO_{2sw} signal. However, since ice motion continued through the winter (Figure 3.7a), horizontal advection may have played an important role in eventually replacing this upwelled water with low–pCO_{2sw} water. With a current of $\sim$4 cm s^{-1}, surface water flowing from Cape Bathurst towards the Mackenzie River could have replaced the fall surface water in approximately 4 months.

Figure 3.7: Bi–monthly mean sea ice velocity and direction, from the NSIDC buoy/passive microwave sea ice motion vector product.

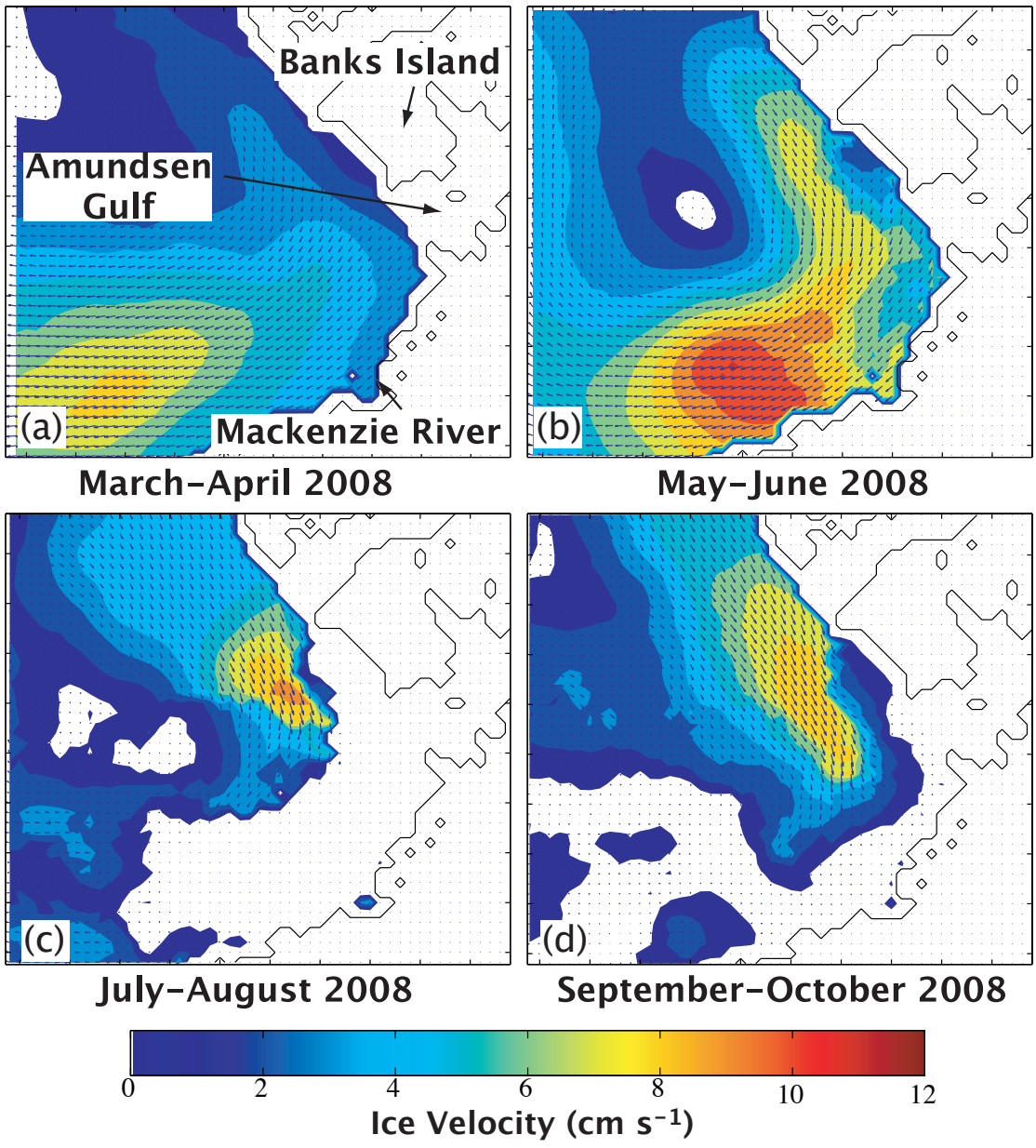

Spring (June 2008)

With no winter data for the Mackenzie Shelf, our next observation in the area was of strong undersaturation (pCO_{2sw} values from ~150–300 μatm, Figure 3.2b) in June 2008. Estimates of annual phytoplankton productivity indicate that the Mackenzie Shelf is more productive than Amundsen Gulf [Pabi et al., 2008], and that peak productivity occurs in June and July [Carmack et al., 2004]. We would therefore expect a more significant biological pCO_{2sw} reduction, which may be the cause of the lower pCO_{2sw} relative to Amundsen Gulf.

Processes on the Mackenzie Shelf are further complicated by the presence of the Mackenzie River plume [Carmack and Macdonald, 2002] and upwelling forced by the bathymetry of Cape Bathurst and other underwater features on the shelf [Williams and Carmack, 2008; Williams et al., 2008]. The impact of these features was evident in two transects conducted June 29–30 (Figure 3.8). The first transect started in western Amundsen Gulf where mean pCO_{2sw} was 356 μatm (Figure 3.8a, b). Slightly to the west of Cape Bathurst (at approximately 17:30 in Figure 3.8b), the ship encountered a small (~10 km wide) patch of water with high pCO_{2sw} (mean of 412 μatm). This patch of water was cold (0.6°C) and saline (32.1), and it was part of a larger cold water structure around Cape Bathurst (Figure 3.8a) that corresponds to the upwelling feature described by Williams and Carmack [2008]. After travelling through this upwelling patch, we encountered a larger patch (~30 km wide, 19:00–20:00 on Figure 3.8b) of very low pCO_{2sw} (minimum 152 μatm). This patch was also quite saline (S ~ 31–32), but was significantly warmer (~4°C) than the patch to the east. Williams and Carmack [2008] showed that the Cape Bathurst upwelling system can easily stretch as far west as this anomaly, and Tremblay et al. [2011] documented that upwelling events in this area bring nutrient-rich waters to the

surface that stimulate strong phytoplankton blooms. Therefore, nutrient enrichment by a previous upwelling event and a subsequent phytoplankton bloom (accompanied by surface warming) is a likely explanation for this feature. In June 2004 Mucci et al. [2010] observed nearly identical patches of high and low pCO_{2sw} in this region, and reached a similar conclusion regarding their genesis. Finally, the ship entered the Mackenzie River plume (shown by warm water in Figure 3.8a and the decrease in S in Figure 3.8b), where an across–shelf transect was conducted on June 30 (Figure 3.8c). This transect showed pCO_{2sw} in the plume was consistently low, with a mean and standard deviation of 237 $\pm$ 12 μatm (Figure 3.8c).

Figure 3.7b shows that ice motion in this region remained westerly during this period, increasing slightly from winter. The main impact of this surface current on the Mackenzie Shelf is to keep the Mackenzie River plume to the west. It may also import higher–pCO_{2sw} water onto the shelf from Amundsen Gulf, but the long timescale of this process probably keeps it from being important relative to the dominant processes of upwelling and river discharge.

Summer (July 2008)

A final visit to the Mackenzie Shelf was made in late July 2008 and consisted of two transects. The along–shelf transect was conducted further north than in June (Figure 3.2c), and SST imagery (not shown) showed no clear evidence of the influence of the Cape Bathurst upwelling or the Mackenzie River plume. On the shelf, pCO_{2sw} was lower (mean 350 μatm) than beyond the shelf break ($\sim$375 μatm), a pattern that was repeated in the across–shelf transect. The across–shelf transect was characterized by lower (mean 308 μatm) pCO_{2sw} than the along–shelf transect, and a rapid increase (to 434 μatm) near the coast (note that this transect went much closer to the coast than the June transect). The location of the transition from

Figure 3.8: Panel a shows pCO_{2sw} (coloured bar, in μatm) on the Mackenzie Shelf during transects conducted June 29–30, 2008, overlying a MODIS SST image obtained on June 30 (greyscale bar, in °C). Areas of high SST (7–15°C) are associated with the Mackenzie river plume, while low SST areas (-1–1°C) are associated with upwelling. Panels b & c show pCO_{2sw} (red line), S (blue line), SST (green line), and ship speed over ground (SOG, brown line) during the two transects. SOG is shown to highlight a problem with the second transect (panel c): during the transect the ship made several 30 minute stops (SOG = 0) for station sampling. At the stations, salinity increased rapidly while SST decreased, which was likely caused by ship maneuvers mixing the highly stratified surface water.

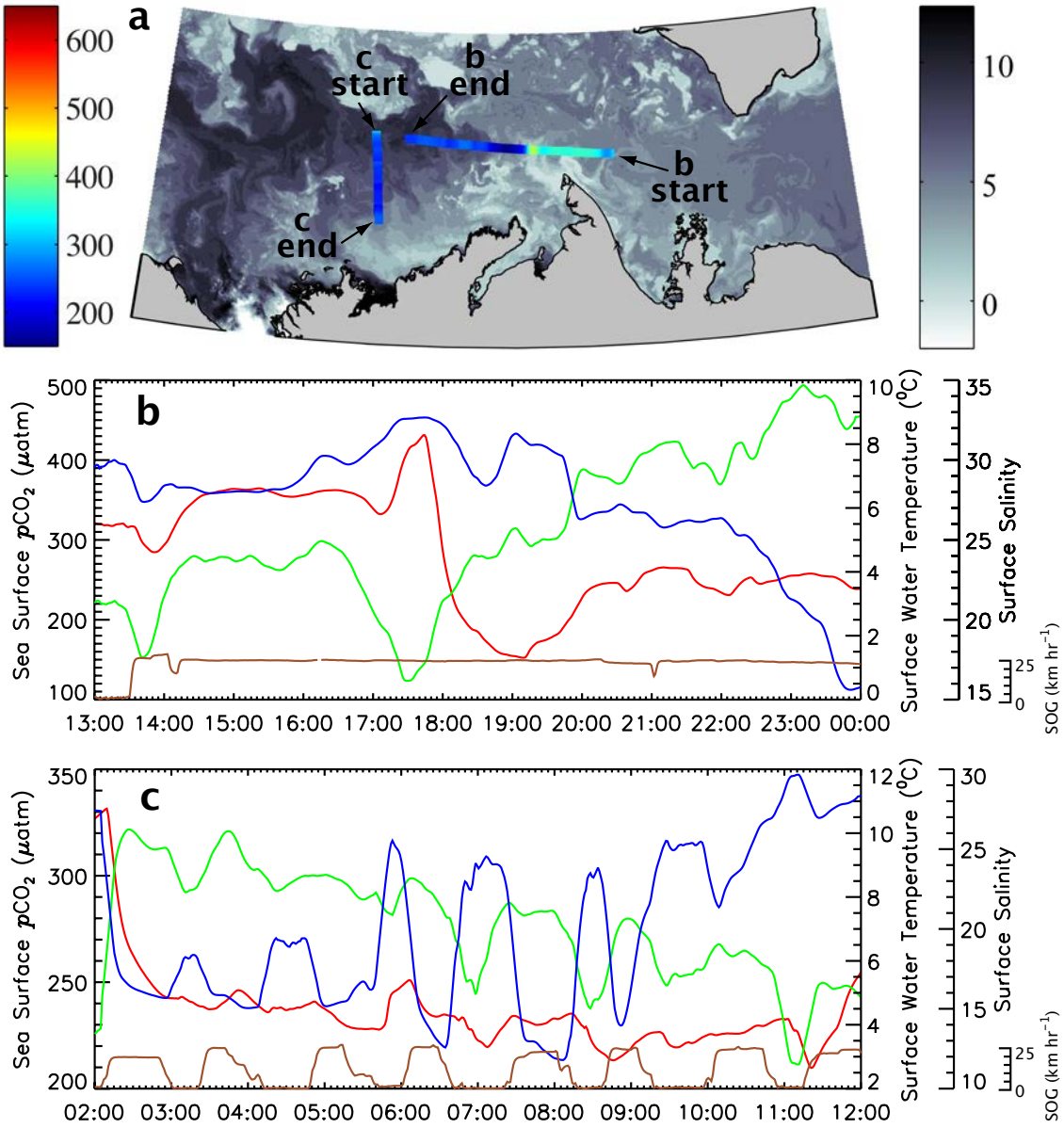

undersaturation to supersaturation occurred over the same depths that Vallières et al. [2008] identified as the transition from marine–dominated to river–dominated surface water. Vallières et al. [2008] showed that supersaturated Mackenzie River waters are the result of net heterotrophy fuelled by riverine dissolved (DOC) and particulate organic carbon (POC). In the marine zone, they found POC concentration to be much lower, DOC to be less labile, and higher primary productivity, resulting in a net–autotrophic system with undersaturated pCO_{2sw}. The Mackenzie River and adjoining shelf thus behave like many high–latitude shelves [Chen and Borges, 2009], but much differently than the western East Siberian and Laptev Seas where net heterotrophy dominates over broad expanses of the shelves [Anderson et al., 2009].

3.4.3 Banks Shelf

Fall (November 2007)

Unlike the Mackenzie Shelf, the Banks Island Shelf showed marked undersaturation (mean of 260 μatm) in the fall of 2007 (Figure 3.2a). Using the 2008 observations as an analogue for the conditions prior to fall, this region had similar summer pCO_{2sw} to Amundsen Gulf (Figure 3.2c). Assuming that the surface mixed layer cooled by a similar amount and experienced similar gas transfer, an additional reduction in pCO_{2sw} of $\sim$40 μatm occurred compared to Amundsen Gulf. Figure 3.7 shows that ice is typically funnelled from the north along the west coast of Banks Island. Although we lack pCO_{2sw} measurements north of our study area, observations from the Canada Basin (the source area for water advected along Banks Island) reveal that surface waters are typically undersaturated in summer, in the range of 150–350 μatm [Bates et al., 2011]. Thus, the additional reduction in pCO_{2sw} relative to

Amundsen Gulf may be due to horizontal advection. Another possibility is higher biological productivity. The nearby Sachs Harbour meteorological station recorded sustained northerly (i.e. upwelling–favourable) winds on four occasions in September 2007, and CIS charts showed that the mobile ice was seaward of the shelf break, which are both conditions conducive to effective shelf break upwelling [Carmack and Chapman, 2003]. This upwelling may have supplied a source of nutrients not available to Amundsen Gulf, producing a stronger or more sustained fall bloom.

Spring (May 2008)

Spring ice conditions on the Banks Island Shelf followed a similar to pattern to Amundsen Gulf, with significant open water occurring by mid-May. The spring transects (Figure 3.2b) were conducted May 25–29. With the exception of low pCO_{2sw} measurements of ~275 μatm on the western and northern edges of the transects, the mean pCO_{2sw} was 301 μatm, similar to observations in Amundsen Gulf (Figures 3.2b, 3.3). This suggests that spring on the Banks Island Shelf progressed similarly to Amundsen Gulf, probably with modest uptake by ice algae followed by a spring open water bloom.

The low pCO_{2sw} on the western and northern margins of the transects (pCO_{2sw} values ranging from 275 — 290 μatm, Figure 3.2b) correspond to the positions of the sea ice edges at the time of sampling. A key characteristic of Arctic marine ecosystems is the "ice edge bloom" – the rapid onset of photosynthesis promoted as light limitation is reduced by melting (or drifting) sea ice [Sakshaug, 2004]. The low pCO_{2sw} measurements may be a fingerprint of such ice edge blooms. The lower pCO_{2sw} observed during the northernmost transects also suggests that southerly flow of ice and surface water (Figure 3.7b) may have helped reduce pCO_{2sw} through horizontal advection.

Summer (July 2008)

We observed a mean pCO_{2sw} of 386 ± 12 μatm during the summer 2008 transect on the Banks Island Shelf (Figure 3.2c), an increase of 85 μatm from spring. Relative to the spring transects, SST increased from -1.0 to 7.0 °C and S decreased from 30.46 to 29.71, which we calculate to have caused changes in pCO_{2sw} of +119 and -17 μatm, respectively. Using the wind velocities from the Sachs Harbour weather station and assuming linear increases of pCO_{2sw} and SST, we calculate a change in pCO_{2sw} due to air–sea exchange of +20 μatm. This leaves a difference of -37 μatm between the calculated and observed changes in pCO_{2sw} that can be attributed to biological uptake. These perturbations to pCO_{2sw} are similar to those in Amundsen Gulf over the same time period (Table 3.2), reinforcing the idea that the two regions followed similar patterns in the spring and summer. Surface currents remained southerly during this period (Figure 3.7c), but we observed no gradients in pCO_{2sw} or SST along the northwards transect that would suggest an important role for horizontal advection. This may be partly due to the fact that the ice pack (and the associated low pCO_{2sw} water [Bates et al., 2011]) had retreated quite far north by this point in time (Figure 3.2c).

Extensive open water on the Banks Island Shelf and in Amundsen Gulf occurred about 3–4 weeks earlier than on the Mackenzie Shelf, which may explain why pCO_{2sw} in these regions was in equilibrium with the atmosphere by early July while the Mackenzie Shelf remained undersaturated (Figure 3.2c). In Amundsen Gulf, Tremblay et al. [2008] observed nutrient limitation in surface waters shortly after the ice cleared, whereas on the Mackenzie Shelf, Carmack et al. [2004] did not observe nutrient limitation until much later in the summer. If the Banks Island Shelf behaves similarly to Amundsen Gulf, it may become nutrient limited quickly,

allowing the surface waters to equilibrate with the atmosphere over the summer months.

3.5 Significance: Testing the Seasonal Rectification Hypothesis

A schematic of the seasonal cycle of pCO_{2sw} and air–sea gas exchange for polynya regions, as proposed by Yager et al. [1995] from their work on the NEW polynya, is shown in Figure 3.9. Schematics for the three regions examined in this study are shown in Figure 3.10. Differences between our observations and the seasonal rectification hypothesis (i.e. the Yager et al. [1995] model) are the result of processes that either did not occur in the NEW polynya (the NEW polynya apparently no longer forms, see note in Barber and Massom [2007]) or were not observed there. In the following discussion, we highlight these differences with the goal of improving our understanding of annual pCO_{2sw} cycles in Arctic environments. Broadly, Amundsen Gulf and the Banks Island Shelf followed similar cycles in 2007–08 (Figures 3.10 a & b) with persistent undersaturation, while the Mackenzie Shelf followed a different pattern of high fall/winter supersaturation followed by strong spring undersaturation (Figure 3.10c). Therefore, we have found it logical to split the discussion between these two groups.

It is worth noting that in contrast to Yager et al. [1995], we include the possibility of gas exchange through the ice–covered season. In most years the ice in Amundsen Gulf remains mobile, producing an icescape composed of drifting floes and leads. The fractional area of open water can thus at times be quite high; between November 2007 – January 2008 we estimated the lead fraction to vary from $\sim$ 0.1 – 10%

Figure 3.9: Schematic summarizing the seasonal cycles of pCO_{2sw} and potential for air–sea exchange in the NEW polynya, as suggested by Yager et al. [1995]. The solid dot represents observed pCO_{2sw}, and the dashed line is a rough extrapolation that we propose based on the discussion in Yager et al. [1995]. The boxes at the top of the panels denote the time series of sea ice concentration in the region. Black arrows at the top indicate the potential for air–sea exchange, with down arrows indicating potential invasion, up arrows indicating potential evasion, and the relative size of the arrows denoting the expected magnitude based on the air–sea pCO_2 gradient and wind velocities. The annotations below the pCO_{2sw} curve indicate the processes believed to be important in controlling pCO_{2sw} during the various seasons. The processes are abbreviated as: Bio – biology, SST – sea surface temperature, Sal – salinity, F_{CO_2} – air–sea gas exchange. Upward arrows indicate a process that increases pCO_{2sw}, downward arrows indicate a process that decreases pCO_{2sw}, and the size of the arrows indicates the relative importance of each process.

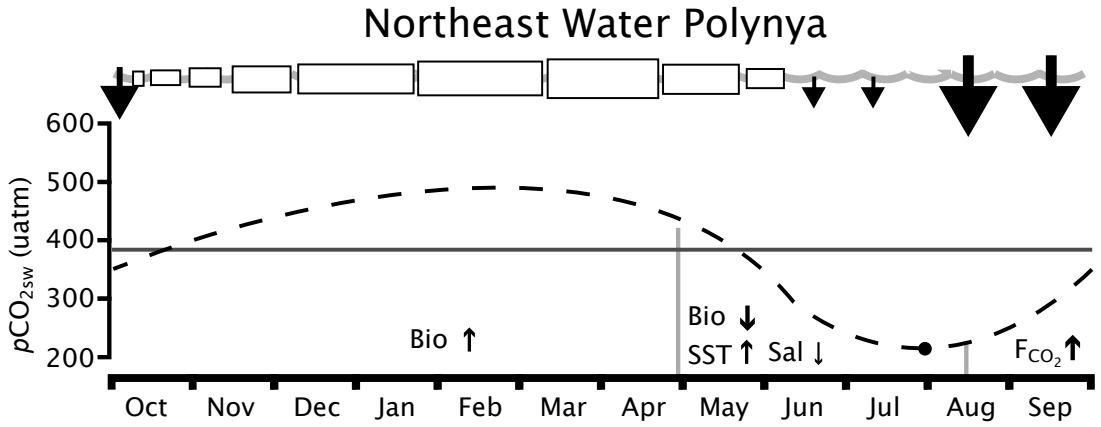

(Else et al. [2011], Chapter 2). Open water may be even more important on the Banks Island and Mackenzie Shelves, where motion of the Beaufort Sea ice away from the coast can create extensive winter shore–lead polynyas. Given recent water column [Anderson et al., 2004], laboratory [Loose et al., 2009] and micrometeorology (Else et al. [2011], Chapter 2) studies showing enhanced gas exchange through such icescapes, we feel it is important to consider that significant air–sea CO_2 flux may occur even in the winter.

3.5.1 Amundsen Gulf and the Banks Island Shelf

Yager et al. [1995] predicted that as long as wind velocities are sufficient, fall gas exchange will bring pCO_{2sw} to equilibrium with the atmosphere. Despite very strong winds, we found Amundsen Gulf and the Banks Island Shelf to be significantly undersaturated at freeze–up in 2007. Our analyses and past investigations [Arrigo and van Dijken, 2004; Brugel et al., 2009] indicate that fall phytoplankton blooms and surface water cooling may be responsible for this undersaturation. The potential for fall blooms was not discussed by Yager et al. [1995], but should perhaps be revisited for the NEW region.

The seasonal rectification hypothesis also states that for polynya regions to act as net CO_2 sinks, a sea ice cover is necessary to prevent outgassing during the winter. Our results show that Amundsen Gulf remained undersaturated throughout the winter, and it is likely that the Banks Island Shelf behaved similarly. pCO_{2sw} did increase under the ice cover, but it did so slowly, such that saturation was not reached until early March when algae production began to reduce pCO_{2sw}. This winter cycle is similar to many mid– and high–latitude shelves where the continental shelf pump prevents the recycling of organic matter in the surface layer (see for e.g. Anderson

Figure 3.10: Schematic summarizing the seasonal cycles of pCO_{2sw} and potential for air–sea exchange in the three southeastern Beaufort Sea study regions, with annotations as per Figure 3.9. The solid line in panel (a) and the solid dots in (b-c) indicates observations, while the dashed lines are extrapolations based on the processes known to be occurring. Additional annotations for the processes are: HA – horizontal advection, Up – upwelling, VM – vertical mixing, River – riverine input. Question marks denote significant uncertainty in the magnitude of the corresponding arrows.

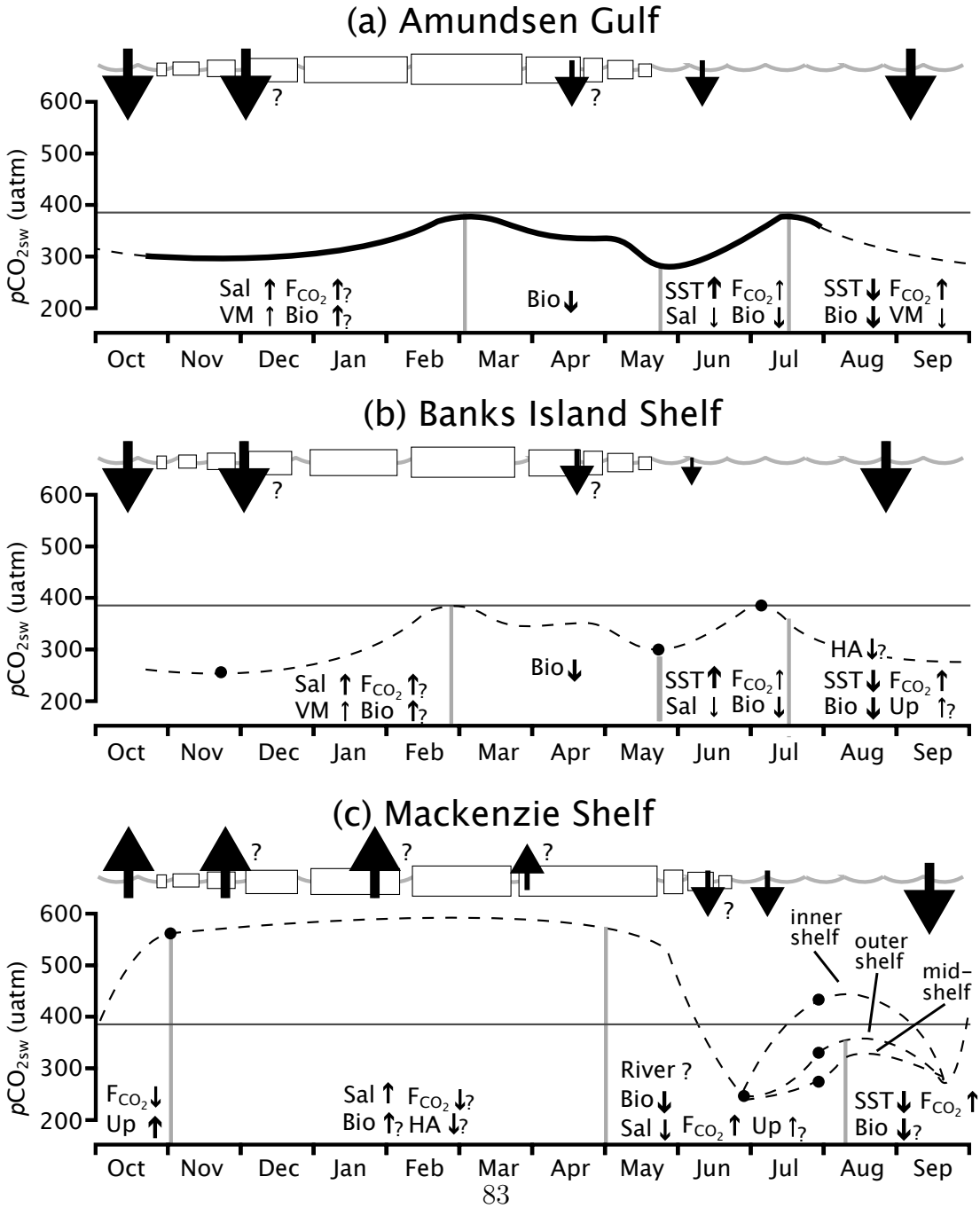

et al. [2010]; Tsunogai et al. [1999]). The persistent undersaturation may also be driven by the relatively low DIC to TA ratio typically observed in the polar mixed layer [Bates et al., 2009], which should buffer respiration–driven pCO_{2sw} increases. Amundsen Gulf and the Banks Island Shelf thus did not require a winter ice cover to act as net sinks of CO_2 in 2007–08.

We also observed significant deviation from the Yager et al. [1995] model in Amundsen Gulf and the Banks Island Shelf in the spring. The spring pCO_{2sw} in both regions ($\sim$275–300 μatm) was considerably higher than observed in the NEW polynya (mean 218 μatm). This is consistent with the observations of Tremblay et al. [2008] that spring phytoplankton blooms are less intense in the southeastern Beaufort Sea, due mostly to the limited nutrient supply caused by strong surface water stratification. We were, however, able to confirm the hypothesis that under–ice algae blooms play a significant role in lowering pCO_{2sw} prior to break up (as was also shown in Shadwick et al. [2011]). This was important to the Yager et al. [1995] model in order to prevent a release of built–up CO_2 when the polynya first forms.

Finally, the surface water of both regions experienced a rise towards near–atmospheric pCO_{2sw} levels in the summer that is not included in the seasonal rectification hypothesis. Significant warming of the sea surface (to 7–8°C) was primarily responsible for this pCO_{2sw} increase (Table 3.2). In contrast, the maximum surface temperature recorded during the NEW Polynya study was 3°C [Wallace et al., 1995]. The lower temperatures in the NEW polynya may reflect the horizontal advection of cold water from the adjoining ice covered areas, as is the case in the Northwater Polynya [Melling et al., 2001]. The apparent lack of significant horizontal advection in Amundsen Gulf and the Banks Island Shelf during our study, combined with strongly stratified surface waters and a lower latitude location probably all

contributed to the high summer SST. The combination of a limited phytoplankton bloom and summer warming make the potential for open water season CO_2 uptake less dramatic in our observations than in the Yager et al. [1995] model.

3.5.2 Mackenzie Shelf

The Mackenzie Shelf (Figure 3.10c) more closely followed the proposed pCO_{2sw} pattern for the NEW region (Figure 3.9), but the timing of the fall pCO_{2sw} supersaturation was very different. In contrast to a gradual increase in pCO_{2sw} over the winter driven by respiration in the surface water, we found a rapid increase to high supersaturation due to shelf break upwelling. Our results show that this upwelling is limited to certain coastal regions and weather conditions in the southeastern Beaufort Sea. Since many polynyas exist on continental shelves and along coastlines, fall upwelling is potentially significant across the Arctic, particularly in polynyas that that are partially maintained by the warm water associated with such upwelling. In these upwelling regions, the ability (or inability) of the sea ice cover to prevent outgassing is very important if the region is to act as a net annual CO_2 sink.

This region was also more similar to Figure 3.9 in its spring/summer biological reduction of pCO_{2sw} than the Banks Island Shelf or Amundsen Gulf. Although not as strong as in the NEW or NOW polynyas, we did observe high spring undersaturations, particularly in regions where nutrients were supplied by episodic upwelling [Tremblay et al., 2011]. This undersaturation was maintained through the summer on the mid–shelf, although we did observe higher pCO_{2sw} where the influence of river discharge was greatest. Again, this is consistent with current understandings of continental shelves affected by river inflow; outgassing can be significant along a narrow coastal band, but undersaturation is typically prevalent across a much larger area

of the offshore shelf [Chen and Borges, 2009]. Given that river–influenced shelves are very common in the Arctic, we expect this to be an important consideration for many seasonally ice–free regions.

3.6 Summary and Conclusions

This study is perhaps the most comprehensive observation of pCO_{2sw} in an Arctic marine environment. The complex nature of our study area allowed us to examine an annual cycle of pCO_{2sw} and the processes controlling it in three distinct environments: the Amundsen Gulf, a spring–opening polynya region that typically experiences ice motion and fracturing throughout the winter; the Banks Island Shelf, a flaw–lead polynya region that opens in the spring similar to Amundsen Gulf and can also experience extensive open water during the winter; and the Mackenzie Shelf, which is heavily influenced by riverine inputs and where the ice opens slightly later in the spring.

Our results show that in 2007–08, none of these systems precisely followed the simple model of annual pCO_{2sw} suggested for the NEW polynya region by Yager et al. [1995]. Amundsen Gulf and the Banks Island Shelf showed undersaturation at freeze–up due to fall phytoplankton blooms, and gradual increases in under–ice pCO_{2sw} that never exceeded atmospheric levels. Biological uptake of CO_2 and reduction of pCO_{2sw} began in early spring in these regions, but was never as intense as observed in more northerly polynyas. Summer warming increased pCO_{2sw} and surface layer stratification restricted photosynthetic CO_2 uptake, limiting the potential open–water sink of CO_2. On the Mackenzie Shelf, fall upwelling of CO_2–charged upper–halocline waters created rapid supersaturation prior to ice formation. We were unable to measure winter pCO_{2sw} in this region, but the spring undersatura-

tion was more intense than in Amundsen Gulf or on the Banks Island Shelf. Spring and summer pCO_{2sw} distributions on the Mackenzie Shelf were complicated by the Mackenzie River plume and bathymetrically–induced upwelling.

Given these results, we propose that the following processes need to be considered when assessing the annual pCO_{2sw} cycle of polynya regions.

1. **Fall surface cooling** may play an important role in lowering pCO_{2sw} prior to freeze–up, particularly if the cooling happens rapidly (or over a large range) such that the resulting pCO_{2sw} drop cannot be effectively countered by air–sea gas exchange.

2. **Fall phytoplankton blooms** may be initiated by nutrient replenishment from strong wind mixing or episodic upwelling, producing undersaturated pCO_{2sw} at freeze–up.

3. **Fall upwelling** can create high pCO_{2sw} prior to freeze–up, if it occurs late enough in the season that light limitation prohibits photosynthetic CO_2 drawdown despite the availability of nutrients. Vertical mixing at any time in the year will likely bring high–pCO_2 water into the surface, and may be particularly important during brine rejection–driven mixing associated with sea ice formation, and stormy open water seasons.

4. **Winter under–ice respiration in surface water** needs to be better constrained to understand the potential magnitude of winter pCO_{2sw} increase.

5. **The continental shelf–pump** may play an important role in suppressing winter pCO_{2sw} increase by preventing the recycling of organic matter in the surface mixed layer.

6. **Winter air–sea gas exchange** needs to be included in the annual air–sea CO_2 flux and seasonal pCO_{2sw} evolution for polynyas regions whose ice cover is not continuous through the winter.

7. **Spring/summer nutrient supply** needs to be considered when determining the magnitude of biological pCO_{2sw} reduction.

8. **Summer warming** of the surface layer may counteract some of the biological pCO_{2sw} reduction, reducing the open–water uptake potential.

9. **River input** may play a complicating role in seasonal pCO_{2sw} patterns in coastal regions where runoff is significant. Remineralization of riverine DOC/POC will cause elevated pCO_{2sw}, which is normally constrained close to shore (e.g. Chen and Borges [2009], this study), but can extend well onto the shelves in some Arctic regions (e.g. Anderson et al. [2009]).

10. **Horizontal advection** can modify pCO_{2sw} if significant surface currents and strong horizontal gradients of pCO_{2sw} exist. This may play an important role in keeping pCO_{2sw} low when water is transported into a polynya region from surrounding ice covered areas.

By better accounting for these processes, we can improve our ability to predict air–sea CO_2 exchange budgets for the Arctic, particularly in polynya regions and other regions with variable ice conditions. In identifying these processes, we also hope to instruct future efforts to model the potential impacts of climate change on air–sea CO_2 exchange in polynyas. Fall shelf break upwelling is likely to become more important as the perennial ice retreats further beyond the shelf break [Carmack and Chapman, 2003] and remains there later into the fall [Tremblay et al., 2011]. Later fall freeze–up, increased winter ice motion [Hakkinen et al., 2008] and earlier spring

break–up will promote air–sea gas exchange. The biological system is expected to experience significant changes, with longer growing seasons [Arrigo et al., 2008] but possibly reduced nutrient supply due to increasing surface stratification [Tremblay et al., 2008]. The effectiveness of the continental shelf pump may be affected by changes in the biological system as well; for example Forest et al. [2010] found lower vertical carbon export in Amundsen Gulf associated with longer open water seasons. Increases in SST [Steele et al., 2008] may limit the potential for summer CO_2 uptake by increasing pCO_{2sw}. Perhaps most significantly, the transition of broad reaches of the Arctic Ocean to seasonal ice as the summer sea ice extent declines [Perovich and Richter-Menge, 2008; Stroeve et al., 2007] means that a progressively larger area of the Arctic will undergo ice cycles similar to our study region. Ultimately, the new understandings presented in this paper will help predict how the Arctic's current role as a sink for atmospheric CO_2 [Bates and Mathis, 2009] will change in the future.

Chapter 4

Sea Surface pCO_2 Cycles and CO_2 Fluxes at Landfast Sea Ice Edges in Amundsen Gulf, Canada

Accepted to *Journal of Geophysical Research – Oceans*,

doi:10.1029/2012JC007901

Brent G.T. Else*[1], Ryan J. Galley[1], Tim N. Papakyriakou[1], Lisa A. Miller[2], Al Mucci[3], David G. Barber[1]

[1]Centre for Earth Observation Science, Department of Environment and Geography, University of Manitoba, Winnipeg, Manitoba, Canada

[2]Centre for Ocean Climate Chemistry, Institute of Ocean Sciences, Fisheries and Oceans Canada, Sidney, British Columbia, Canada

[3]GEOTOP, Department of Earth and Planetary Science, McGill University, Montreal, Québec, Canada.

Abstract

In late fall, spring, and early summer, we measured the surface ocean and atmospheric partial pressures of CO_2 (pCO_{2sw} and pCO_{2atm}, respectively) to calculate CO_2 gradients ($\Delta pCO_2 = pCO_{2sw} - pCO_{2atm}$) and resulting fluxes along the landfast ice regions of southern Amundsen Gulf, Canada. In both the fall and spring seasons we observed positive ΔpCO_2 caused by wind–driven upwelling. The presence of a landfast ice edge appeared to be an important factor in promoting this upwelling in some instances. Despite the potential for significant CO_2 evasion, we calculated small fluxes during these periods due to high sea ice concentration. In summer, ΔpCO_2 became strongly negative across the entire study area. Primary production no doubt played a role in the pCO_{2sw} drawdown, but we also found evidence that melting sea ice was important via dilution and the likely release of alkalinity from calcium carbonate crystals. The seasonal ΔpCO_2 cycle suggests a net annual sink of atmospheric CO_2 for these landfast ice regions, since calculated summer uptake by the ocean was much stronger than fall/spring outgassing and occurred over a longer time period. However, we hypothesize that this balance is highly dependent on the strength of upwelling and the timing of ice formation and decay, and therefore may be influenced by interannual variability and the effects of climate change.

4.1 Introduction

Landfast sea ice is essentially motionless ice that is either anchored to the coast or seabed, or is constrained by narrow channels. Unlike a mobile ice cover, which is typically composed of some fraction of open water, landfast ice is usually characterized by a complete ice coverage (i.e. ice concentration of $10/10^{ths}$ [Galley et al., 2012]). Cracks may occur due to tidal heaving (particularly near the coast) and the ice may decay to the point where thaw holes melt through the ice in late summer [Jacobs et al., 1975], but for most of its temporal and spatial extent landfast ice acts as a separation between ocean and atmosphere.

Across this separation, significant air–sea gradients of CO_2 (defined as $\Delta pCO_2 = pCO_{2sw} - pCO_{2atm}$, where sw and atm denote the partial pressure of CO_2 in the surface seawater and atmosphere, respectively) can develop. In Prydz Bay, Antarctica, Gibson and Trull [1999] observed strongly negative ΔpCO_2 under landfast ice in the spring and fall, and a gradual increase in pCO_{2sw} over the winter that approached equilibrium with the atmosphere (i.e. ΔpCO_2=0). Fransson et al. [2009] found strongly negative ΔpCO_2 associated with summer landfast ice in the Canadian Arctic Archipelago, while Sejr et al. [2011] found persistent negative gradients under landfast ice in a Greenland Fjord.

These under–ice CO_2 gradients are formed by biogeochemical and physical processes that are heavily influenced by the sea ice itself. During the winter, low incoming solar radiation is further attenuated by sea ice and the overlying snowpack, limiting photosynthesis. Under these conditions, respiration is expected to dominate over photsynthesis, explaining in part observed under–ice increases of pCO_{2sw} in the winter [Else et al., 2012b; Gibson and Trull, 1999; Miller et al., 2002; Shadwick et al.,

2011]. Part of the increase can also be explained by the addition of brines to the mixed layer, which have typically have high pCO_{2sw} in winter due to the rejection of impurities by ice formation and the retention of alkalinity by calcium carbonate crystals within the ice volume [Dieckmann et al., 2008; Rysgaard et al., 2007]. With the advent of spring, sufficient light begins to penetrate to the base of the sea ice, ice algae communities begin to draw down pCO_{2sw} [Else et al., 2012b; Gibson and Trull, 1999; Shadwick et al., 2011], and ice melt further lowers pCO_{2sw} by dilution and the dissolution of calcium carbonate crystals [Rysgaard et al., 2009, 2007]. Eventually, the ice cover is removed and spring open water phytoplankton blooms (potentially seeded by ice algae) have the potential to further lower pCO_{2sw}.

These processes suggest that landfast ice areas should in general absorb atmospheric CO_2 once the ice cover is removed (e.g. Gibson and Trull [1999]), but there is an emerging debate about whether or not air–sea CO_2 exchange can occur across the sea ice boundary. Both Gosink et al. [1976] and Loose et al. [2010] have shown that gases can diffuse through sea ice, but their observed exchange rates were several orders of magnitude lower than even the most modest exchange through open water. Accordingly, Loose et al. [2010] proposed that transfer through leads and other open water portions of the icescape is the dominant pathway for air–sea gas exchange in seasonal ice environments.

In this paper, we focus on understanding the air–sea exchange of CO_2 in the landfast ice regions of Amundsen Gulf, Canada. Since regions affected by landfast sea ice contain no open water during the winter, we adopt the working hypothesis that the net air–sea exchange of CO_2 is determined by the exchange of CO_2 during the ice–free or partially ice–free seasons. This approach limits us from understanding the total surface exchange of CO_2 (which in certain seasons could include exchanges

between the ice surface and the atmosphere, e.g. Nomura et al. [2010]; Papakyriakou and Miller [2011]; Semiletov et al. [2004]), but it does allow us to investigate an important component of the Arctic marine carbon cycle. The objectives of this work are: (1) to examine how the landfast ice interacts with biogeochemical cycles to form pCO_{2sw} gradients, and (2) to estimate the air–sea exchange of CO_2 arising from those gradients, focusing on the role of sea ice in modulating gas exchange.

4.2 Methods

4.2.1 Study Area

This study was conducted in the landfast ice surrounding Amundsen Gulf, a relatively deep coastal channel connecting the Canadian Arctic Archipelago (CAA) to the southeastern Beaufort Sea (Figure 4.1). Sea ice in the middle of Amundsen Gulf is usually mobile throughout the winter, while ice on the periphery becomes landfast as early as the first week of November [Galley et al., 2012]. The region is best known to the scientific community as the site of the Cape Bathurst polynya, which typically forms in the first week of June with the dynamic export of sea ice out of Amundsen Gulf [Galley et al., 2008]. Ice on the periphery, however, typically remains landfast until early July [Galley et al., 2012] before a combination of dynamic and thermodynamic forcings removes the ice cover.

During the 2007–08 International Polar Year, the research icebreaker CCGS *Amundsen* spent nearly 10 months in this area conducting ArcticNet projects [ArcticNet, 2010] and the Circumpolar Flaw Lead System Study [Barber et al., 2010]. On several occasions, the research vessel sailed into the landfast ice along the southern margin of Amundsen Gulf. Fast ice sites in Franklin Bay, Darnley Bay, Cape

Bathurst and Cape Parry (Figure 4.1) were visited in early November 2007, and then studied extensively in June 2008 as the ice edges decayed.

Figure 4.1: Map of the study area. Black polygons/points indicate areas where land-fast ice sampling occurred. The bathymetric contour interval is 100 m; in Amundsen Gulf depth contours range from 100 m to 500 m.

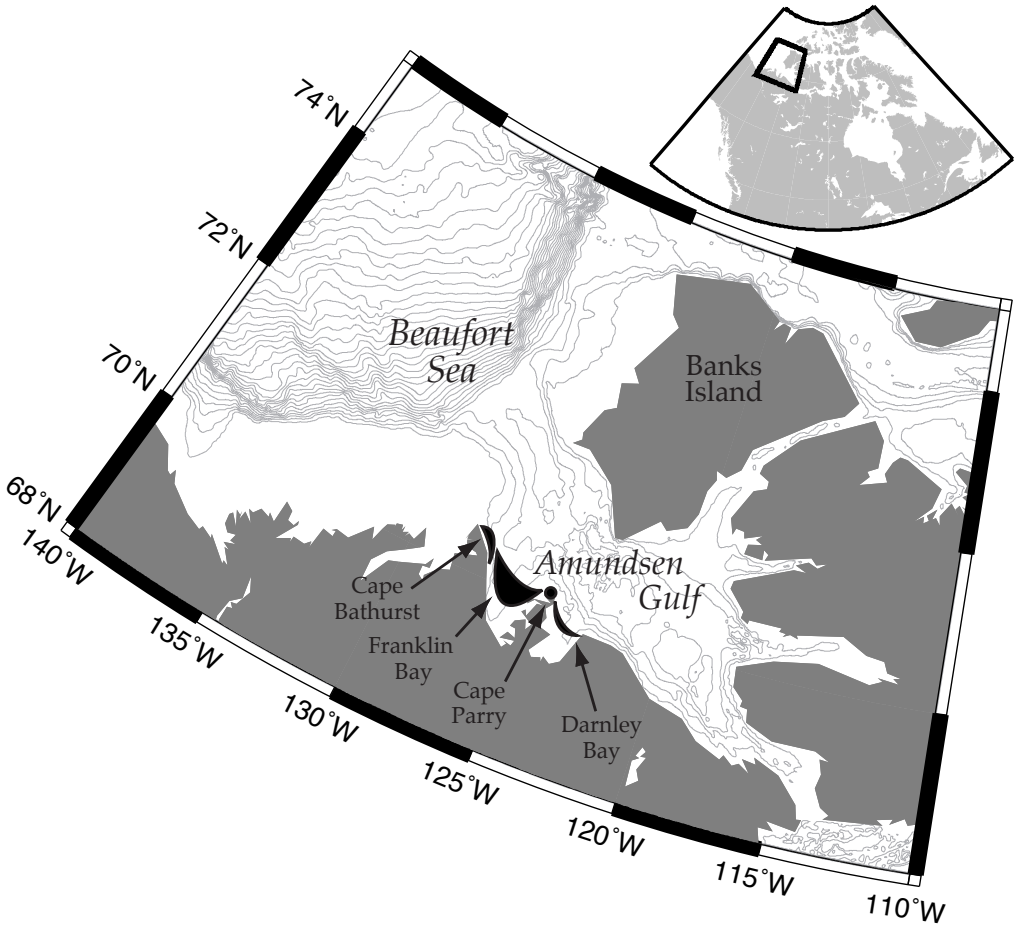

4.2.2 Sampling

To measure pCO_{2sw} we used a custom built equilibrator, which sampled at one minute intervals. The system was composed of a cylindrical tank with a shower inlet supplied by water diverted water from a high–volume scientific intake located at ∼5 m depth. Headspace air in the tank was cycled through a desiccant column

and a LI-7000 gas analyzer which measured the dry air mixing ratio of CO_2 (xCO_2). A continuous stream of ultra–high purity N_2 was passed through the reference cell of the LI-7000 to reduce sensor drift, and the instrument was calibrated daily using a certified gas standard. The mean rate of sensor drift during the experiment was 0.03 ppm hr^{-1}, resulting in calibration–to–calibration drift typically on the order of 0.7 ppm. We calculated pCO_{2sw} from xCO_2 as follows:

$$pCO_{2sw} = xCO_2 \times (P - pH_2O) \tag{4.1}$$

where P is the atmospheric pressure, and pH_2O is the saturation vapor pressure of air in the equilibration chamber (determined empirically from water temperature and salinity using the equations of Weiss and Price [1980]). Although the intake was fairly close to the equilibrator, a correction was required to correct the pCO_{2sw} measurements for warming of the seawater relative to *in situ* conditions [Takahashi et al., 1993]. The warming was typically on the order of ∼1.5°C, and after correction the system showed good correspondence with independent estimates of pCO_{2sw} obtained from station measurements of carbonate system chemistry (see Else et al. [2012b, 2011] for further details).

Based on examination of the pCO_{2sw} sensor output in comparison to a thermosalinograph sampling the same inlet stream, the system appeared to experience a lag time on the order of 5–10 minutes. For stationary applications this was not a significant problem, but when the ship was under power we lagged sample times by 7 minutes to allow better comparisons with thermosalinograph data. The thermosalinograph sensor also sampled at one minute intervals, and was used as the primary source of sea surface salinity and temperature measurements for equation

4.1, and for interpretation of the pCO_{2sw} data. When the thermosalinograph data was unavailable (due to sensor malfunction), we used data from CTD casts.

Atmospheric CO_2 measurements were obtained with a separate LI-7000 connected to a gas sampling system that drew air from an inlet located on a meteorological tower ~14 m above the water surface. This system was also calibrated daily with a certified standard (mean drift < 0.01 ppm hr^{-1}) and utilized a continuous N_2 stream through the reference cell. Mixing ratio measurements were converted to saturated pCO_{2atm} using a similar approach to equation 4.1, and data were filtered to remove instances where measurements may have been contaminated by emissions from the ship's smokestack [Else et al., 2011].

4.2.3 CO_2 Flux Calculations

For ice affected seas, air–sea CO_2 flux (F_{CO_2}) is commonly estimated using a standard form of the bulk flux equation, scaled by the ice concentration (C_i, measured in tenths):

$$F_{CO_2} = k\alpha(pCO_{2sw} - pCO_{2atm})(1 - C_i/10) \tag{4.2}$$

where k is the gas transfer velocity, α is the solubility of CO_2 in seawater and pCO_{2atm} is the partial pressure of CO_2 in the overlying atmosphere. This approach is fundamentally sound (assuming that sea ice does not act as a conduit for air–sea exchange), but only if the choice of k parameterization is appropriate. When C_i is greater than 0 (but less than 10), the open water patches are fetch–limited, which is expected to reduce k relative to open water conditions (e.g. Woolf [2005]). Unfortunately, useful parameterizations that account for this effect do not exist, forcing the use of parameterizations developed for ice free oceans. Although this approach

has become common, we stress that it should be used with the understanding that F_{CO_2} will likely be overestimated to some degree. In this study, we used the k parameterization of Sweeney et al. [2007]:

$$k = 0.27U^2(Sc/660)^{(-1/2)} \tag{4.3}$$

where Sc is the Schmidt number (a function of sea surface temperature (SST) as per Jähne et al. [92]), and U is the wind velocity at 10 m height.

We used this approach to estimate air–sea CO_2 flux in our study area during ice formation, breakup, and the open water season. When a location became landfast ($C_i = 10$), we assumed that the air–sea flux was negligible [Loose et al., 2010]. The calculations were made using the one minute measurements of pCO_{2sw} and pCO_{2atm} for the periods during which the research vessel was in the vicinity of Franklin Bay, Darnley Bay, Cape Parry and Cape Bathurst. Ice concentration was obtained from digital ice charts prepared by the Canadian Ice Service (CIS), which were typically available every 2–5 days during our study. For wind velocity, we used one minute data recorded on the ship's meteorological tower at a height of ∼14 m, scaled to a height of 10 m assuming a logarithmic wind profile (see Else et al. [2011] for instrument details and quality control information).

Since the research vessel was not always in the study area, we also used wind velocity measurements from the Cape Parry Environment Canada station (Figure 4.1) to assist with understanding seasonal wind conditions in the area. This station is located at a height of ∼90 m on a small spit of land which extends into Amundsen Gulf. When wind velocities are scaled to 10 m height they are in reasonable agreement with ship–based velocities and directions (mean differences in x/y wind components <3 m s^{-1}).

4.3 Results

4.3.1 pCO_{2sw} and Landfast Ice Cycles

Fall/Winter (October–November 2007))

Observations made at the landfast ice sites in autmun 2007 are summarized in Figure 4.2. In late October (Figure 4.2a), Franklin and Darnley Bays were not yet covered by landfast ice, but were mostly covered by newly forming ice. At that time, pCO_{2sw} was fairly low (mean 320 μatm, standard deviation $\pm$13 μatm) in offshore Amundsen Gulf (see also Else et al. [2012b]), but was much higher in the landfast ice forming areas (Figure 4.2a); pCO_{2sw} was 363 $\pm$ 9 μatm in Franklin Bay, 493 $\pm$ 25 μatm near Cape Bathurst and 508 $\pm$ 4 μatm near Cape Parry.

This elevated pCO_{2sw} relative to the offshore measurements can be linked to fall upwelling events that occurred in the region [Else et al., 2012b; Tremblay et al., 2011]. The vertical distribution of water masses in this area is fairly typical for the Arctic Ocean [Shadwick et al., 2011]; a relatively fresh polar mixed layer (PML) overlies a steep halocline that is characterized by salinity in the range of 32–35. Between October 8–20, several storms occurred with sustained easterly (along–shore) winds in excess of 15 m s^{-1} (Figure 4.3a) that provided the necessary conditions for upwelling of saline halocline waters to the surface. In late October, surface salinity in offshore Amundsen Gulf ranged from 28.0 to 29.6, while salinity near the coast ranged from 31.5 to 33.2. Salinity was particularly high ($\sim$32.7) along Cape Bathurst, an area known for bathymetry–induced upwelling [Williams and Carmack, 2008] and Cape Parry (31.7), an area with similar bathymetric features. Since pCO_{2sw} in Amundsen Gulf increases rapidly with depth [Lansard et al., 2012; Shadwick et al., 2011], this

Figure 4.2: Measured pCO_{2sw} (μatm) during transects conducted in October–November 2007. Transects are overlain on RADARSAT-1 SAR imagery, with the image dates noted in the top left corner. The dashed lines (white or black) denote the landfast ice edges, as identified by the Canadian Ice Service (CIS).

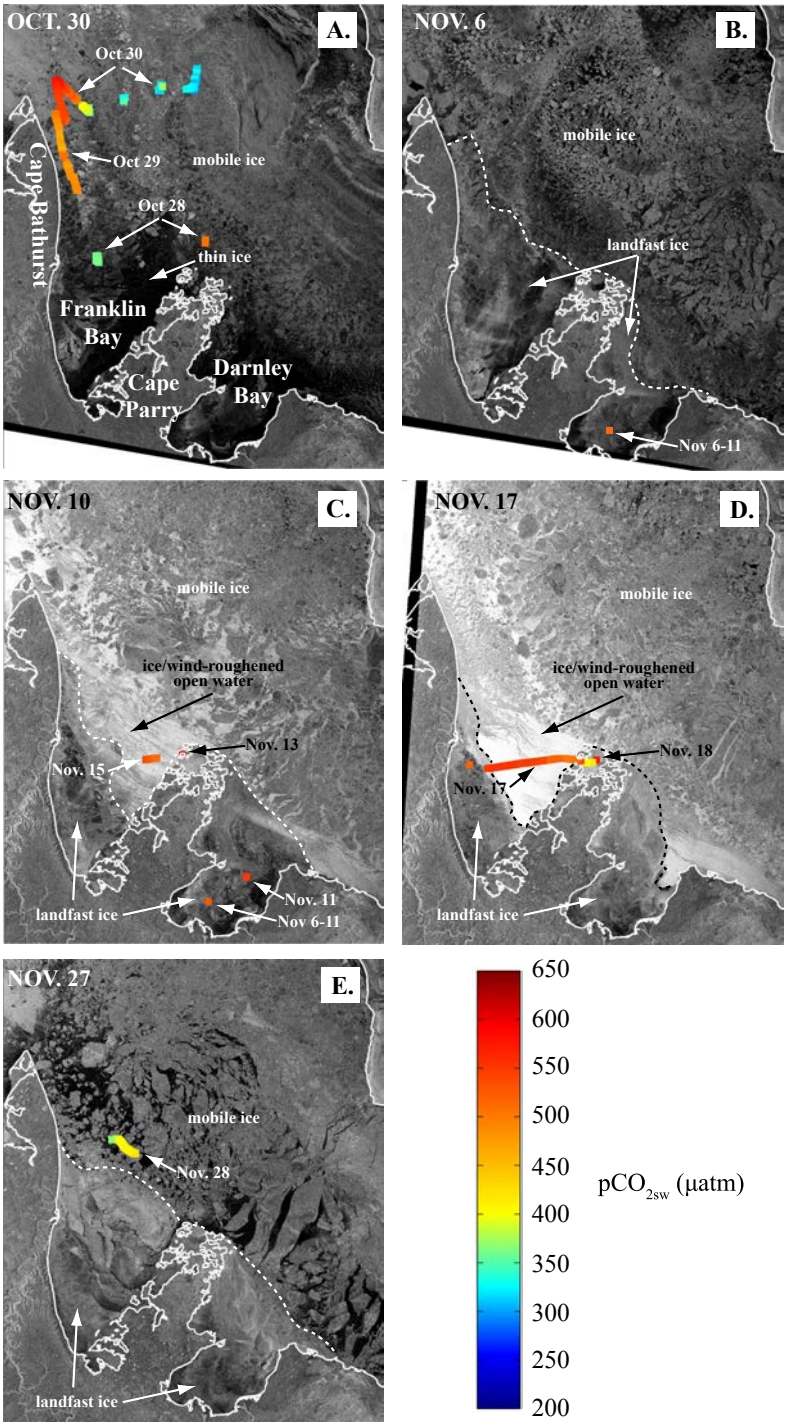

upwelling brought with it CO_2–rich water to the surface, contributing to the high near–shore pCO_{2sw} reported in Figure 4.2a.

Measurements made about two weeks later (Figure 4.2c) show that similar upwelling also occurred in Darnley Bay. According to CIS charts, the ice in Darnley Bay was landfast by November 6 (Figure 4.2b) when the CCGS *Amundsen* entered the Bay. A station in the southern half of the Bay was occupied until November 11, where we measured pCO_{2sw} of 530 $\pm$ 14 μatm and salinity of 33.2. From there, the ship travelled to a small bay near Cape Parry (Figure 4.2b), where pCO_{2sw} had increased by approximately 100 μatm (to 598 $\pm$ 5 μatm) since the previous measurement in the area (Figure 4.2a), suggesting that upwelling intensified as the season progressed (unfortunately no salinity samples were available at that station). The intensifying upwelling was no doubt driven by strong easterly winds that persisted throughout early November (Figure 4.3a), and the upwelling eventually had a pronounced effect in Franklin Bay where we measured pCO_{2sw} ranging from 500 – 560 μatm (Figure 4.2d) and salinity of 33.2 between November 16 – 18.

The timing of fall landfast ice formation varied throughout the study area. The first ice charts to show landfast ice in Franklin and Darnley Bays were dated November 6 (Figure 4.2b), although subsequent strong winds mobilized the ice (Figure 4.2c–d). After winds died down around November 18, the landfast ice in the bays re–established itself and persisted throughout most of the winter (Figure 4.2e). The ice around Cape Parry became landfast at around the same time, while Cape Bathurst did not become landfast until January. At its maximum extent, landfast ice stretched across the mouth of Franklin Bay from Cape Bathurst to Cape Parry, and across the mouth of Darnley Bay from Cape Parry eastwards.

Figure 4.3: Wind velocity measurements from the Cape Parry weather station for the three time periods discussed in the text. The dark black lines indicate winds from an upwelling–favourable (easterly) direction.

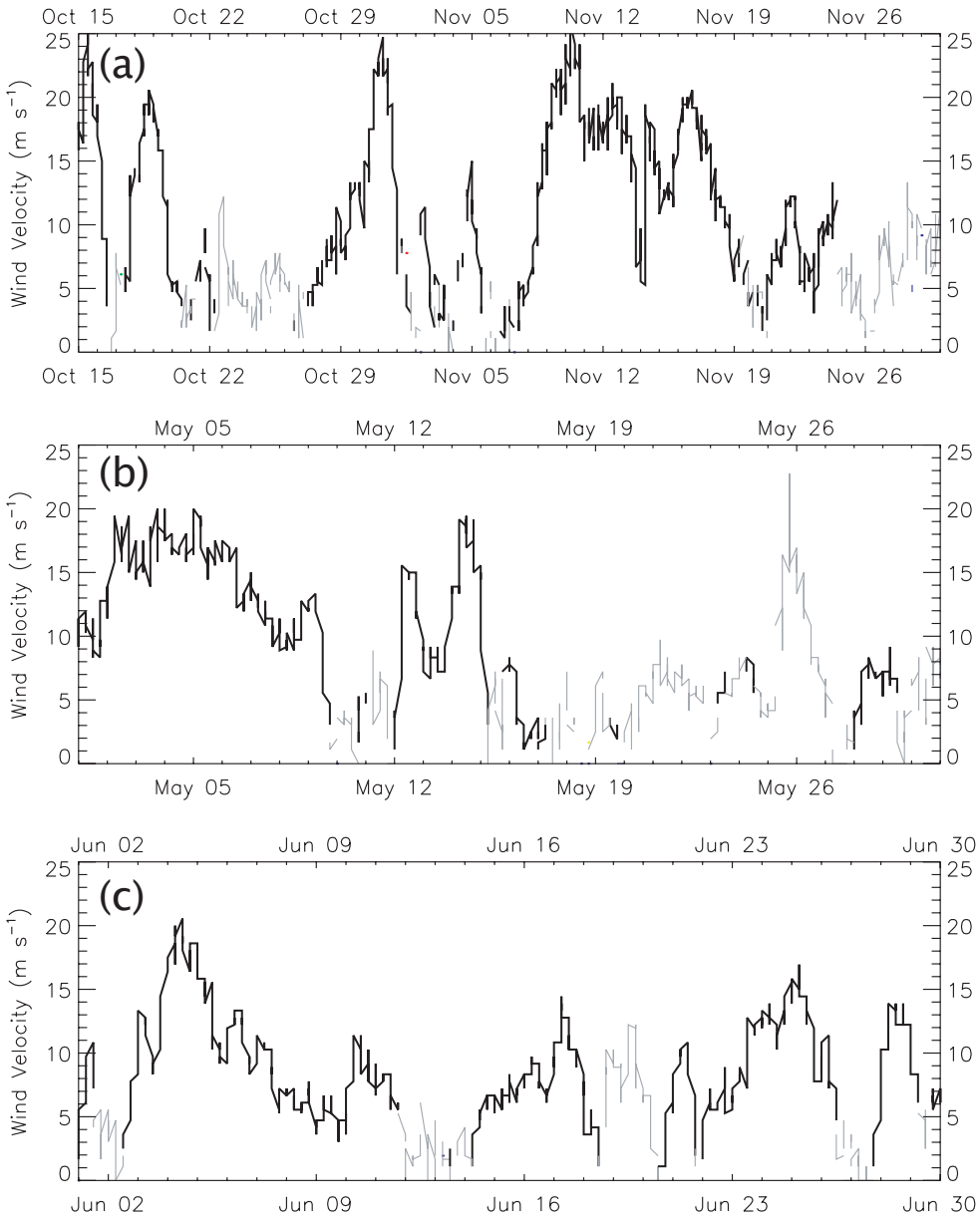

Early Spring (May 2008)

This maximum landfast ice extent was not sustained throughout the winter; CIS charts show the landfast edge in Franklin Bay migrating southwards as early as February 17, eventually culminating in a significant fracture of the northern quarter of the landfast ice around April 15. This fracture allowed the CCGS *Amundsen* to travel along the margin between the new landfast ice edge and the fractured ice in early May (Figure 4.4). As Figure 4.4a shows, pCO_{2sw} was still high (430–500 μatm) in Franklin Bay, and near Cape Parry (531 $\pm$ 16 μatm) in mid–May.

Lacking a complete time series, it is difficult to know how pCO_{2sw} was modified through the winter to produce the levels that we observed in May (Figure 4.4a). In both Franklin Bay and Cape Parry, pCO_{2sw} decreased by ~60–70 μatm relative to November 2007 measurements, and surface salinity decreased to 32.9 (from 33.2 in Franklin Bay). The decreased salinity indicates that advective mixing must have taken place, replacing to some extent the PML water that was displaced by the fall upwelling. Without such mixing we would have expected salinity to increase over the winter due to brine rejection as was observed in Amundsen Gulf [Shadwick et al., 2011] and in Franklin Bay during the 2003–04 winter [Miller et al., 2011]. The lower pCO_{2sw} (maximum 382 μatm, Else et al. [2012b]) and fresher (maximum salinity ~31.5, Shadwick et al. [2011]) surface waters of Amundsen Gulf are the likely source water for this mixing. Under ice biological activity may also have played a role in lowering pCO_{2sw} from its fall maximum; in Amundsen Gulf we observed a biological reduction in pCO_{2sw} on the order of ~15 μatm by early May [Else et al., 2012b], and the ice algae biomass was 4–8 times higher under the landfast ice in Franklin Bay [Tremblay et al., 2011].

Figure 4.4: Measured pCO_{2sw} (μatm) during transects conducted in May 2008. Transects are overlain on true–colour MODIS imagery. Note that no pCO_{2sw} are plotted in b & c – they have been included to show the evolution of the landfast ice during the month of May.

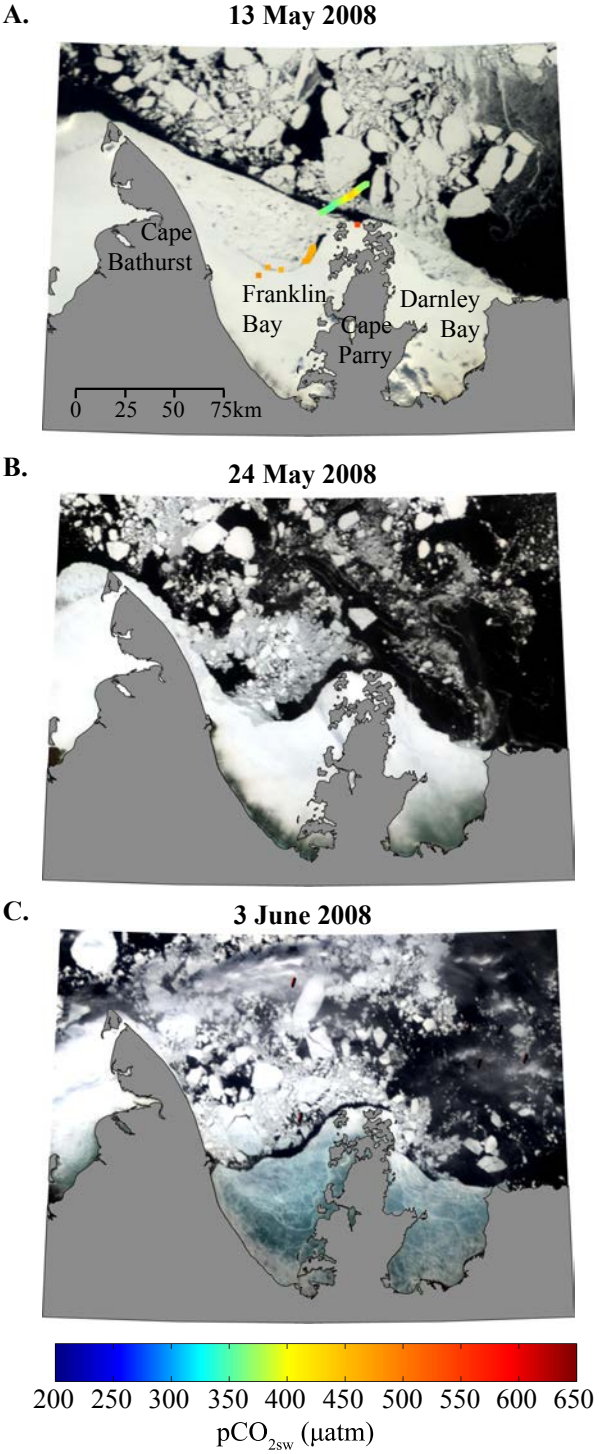

Late Spring/Summer (June 2008)

The ship's initial return to the area in June corresponded with the final departure of ice from the northern quarter of Franklin Bay (compare Figures 4.4c, 4.5a & b). Patches of very low (250–275 μatm) pCO_{2sw} were observed just seaward of the Darnley Bay ice edge (Figure 4.5a), and a mean pCO_{2sw} of 293 $\pm$ 11 μatm was observed approximately 1 km into the ice. Assuming that conditions in May were similar to Cape Parry and Franklin Bay, pCO_{2sw} decreased by $\sim$200 μatm, and salinity by $\sim$1.8 over 4 weeks. We estimate the contribution of ice melt to pCO_{2sw} decrease to be $\sim$16 μatm per unit of salinity, assuming conservative mixing between measurements of the carbonate system in meltwater [Lansard et al., 2012] and the PML for this region in June [Shadwick et al., 2011]. Therefore, ice melt was responsible for only $\sim$30 μatm of the decrease from early May. Sea surface temperature stayed near the freezing point during this time period and stratification due to ice melt would have limited vertical mixing, leaving biological production as the likely cause of the majority of the pCO_{2sw} change. This is consistent with the results of Tremblay et al. [2011] who calculated new phytoplankton production at remarkably high rates (i.e. 6 times the rate observed in 2004) in Franklin Bay, and Mundy et al. [2009] who calculated similar production rates in Darnley Bay.

Transects conducted the following week (Figure 4.5b) showed a very different pattern; patches of pCO_{2sw} up to 456 μatm were observed, with the highest values just offshore of Cape Parry. The June 6 transect from Cape Parry to the Darnley Bay ice edge is detailed in Figure 4.6, and it reveals coherent patterns of pCO_{2sw} and salinity, suggesting the influence of upwelling. Particularly high pCO_{2sw} was observed after occupying a station just inside the Darnley Bay ice edge on June 6 (Figure 4.7), in association with an upwelling event that has been described in

Figure 4.5: Measured pCO_{2sw} (μatm) during transects conducted in June 2008. Transects are overlain on true–colour MODIS imagery.

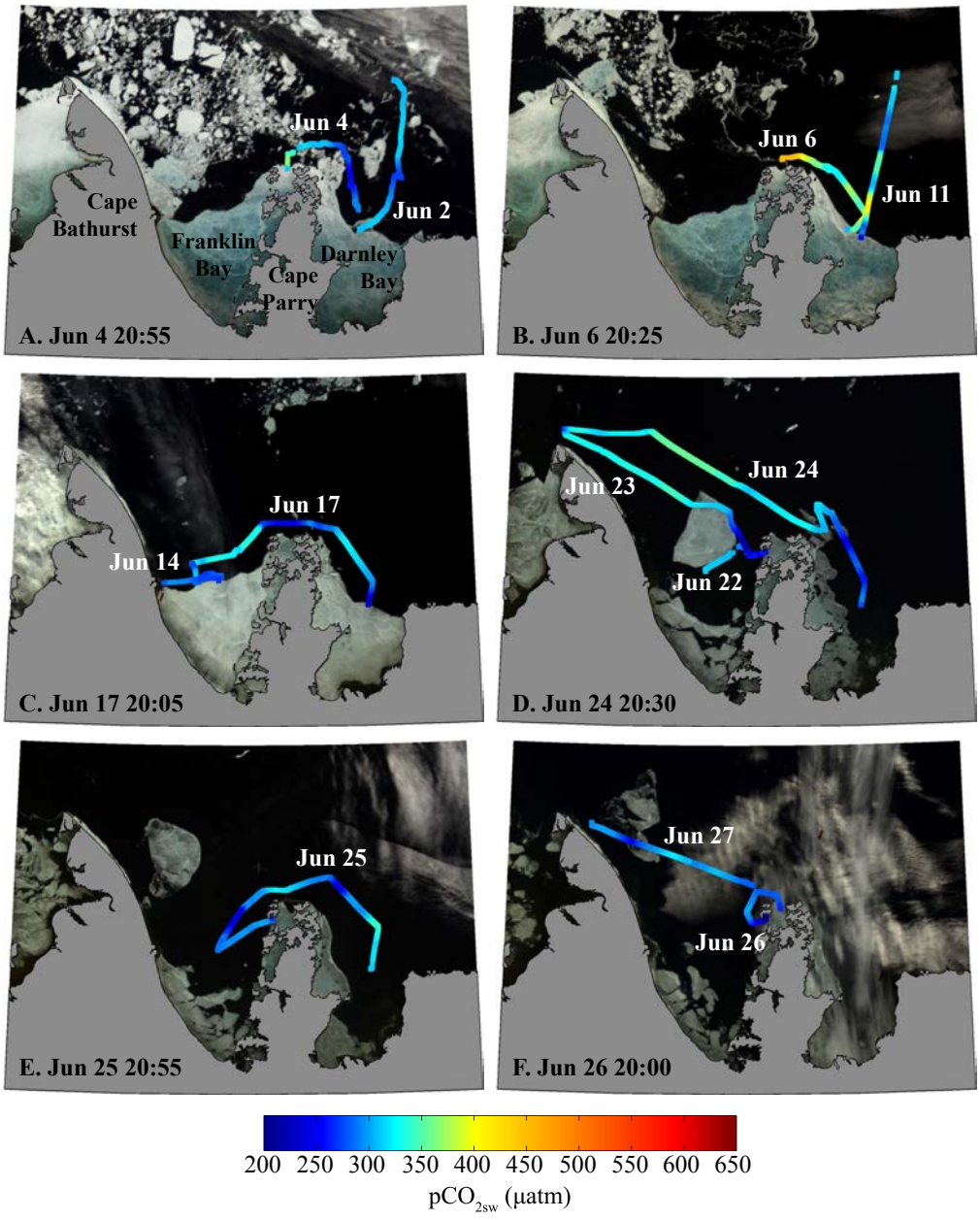

Figure 4.6: Measured pCO_{2sw} (μatm, red line), surface salinity (blue line) and sea surface temperature (green line) during the June 6 transect from Cape Parry to Darnley Bay (Figure 4.5b).

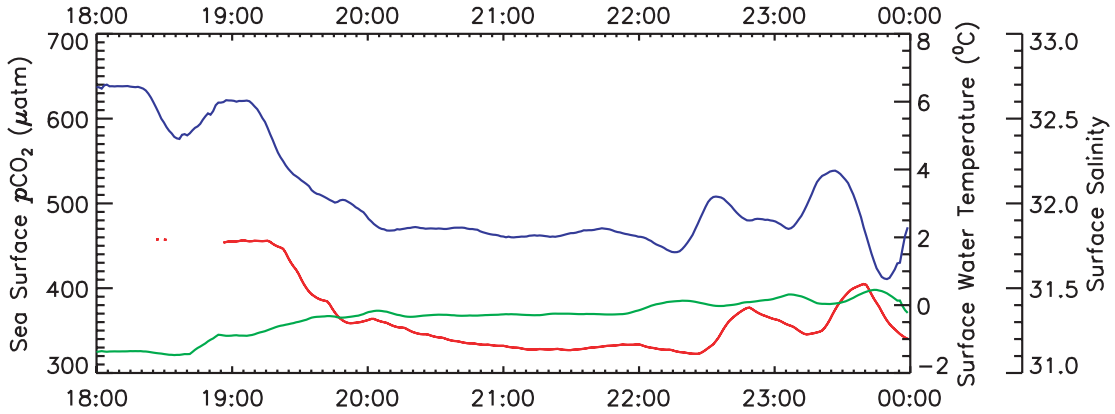

detail by Mundy et al. [2009]. From its peak on June 7, pCO_{2sw} decreased to ~300 μatm along with salinity as PML water returned while the upwelling–favourable winds relaxed. Mundy et al. [2009] also detected a near–surface phytoplankton bloom triggered by this upwelling, which persisted for several days even though the nutrient maximum quickly retreated to below the surface. The continued decrease in pCO_{2sw} evident in Figure 4.7 was likely a result of that bloom.

After the upwelling, strongly negative ΔpCO_2 was prevalent across the region for the rest of June (Figures 4.5c–f). We measured pCO_{2sw} minima of 232 μatm on June 18 in Darnley Bay, 212 μatm on June 23 in Franklin Bay, and 226 μatm on June 26 near Cape Parry. This continued reduction in pCO_{2sw} no doubt reflected the strong biological productivity that continued through the month [Mundy et al., 2009; Tremblay et al., 2011], but sea ice melt played a significant role as well. As an example of this effect, Figure 4.8 shows pCO_{2sw} in relation to salinity and SST during the June 23 transect in Franklin Bay (Figure 4.5d). On this transect, the ship left a station near Cape Parry and navigated around a large floe of formerly landfast

Figure 4.7: Measured pCO_{2sw} (μatm, red line), surface salinity (blue line) and sea surface temperature (green line) at the Darnley Bay landfast ice edge station (Figure 4.5b) occupied from June 7–10.

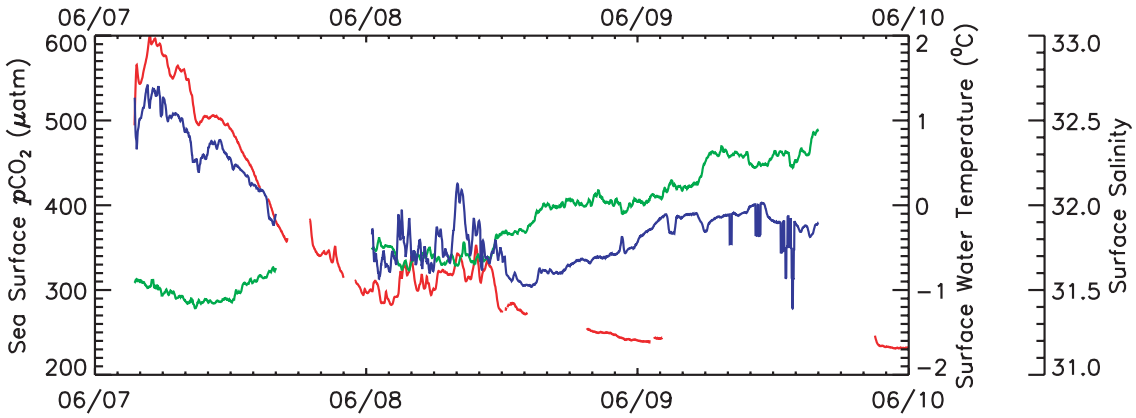

ice that had recently fractured and was drifting northwest. Near the southeast edge of the floe, we encountered a patch of water that was fresher (by 8 units) and had lower pCO_{2sw} (by 100μatm) than water near Cape Parry or towards Cape Bathurst. Given the location of this patch at the trailing edge of the drifting floe, the low salinity must have been caused by ice melt. Measurements in Franklin and Darnley Bays showed that pCO_2 in the brine of decaying ice was very low (0–188 μatm, Geilfus et al. [2012]), confirming the link between low salinity and low pCO_2. The effect of ice melt associated with this particular drifting ice floe was also captured in two transects towards Cape Bathurst. On June 24 (before the floe drifted across the region), the transect yielded a constant pCO_{2sw} measurement of ~335 μatm (Figure 4.5d) and salinity of ~31, whereas the transect following the floe on June 27 (Figures 4.5f) revealed lower "ambient" pCO_{2sw} (315 μatm) and salinity (29.5) with patches of pCO_{2sw} as low as 240 μatm. These results show that the breakup and decay of landfast ice affected pCO_{2sw} over a large spatial domain.

Figure 4.8: Measured pCO_{2sw} (μatm, red line), surface salinity (blue line) and sea surface temperature (green line) during the June 23 transit around the decaying ice floe in Franklin Bay (Figure 4.5d).

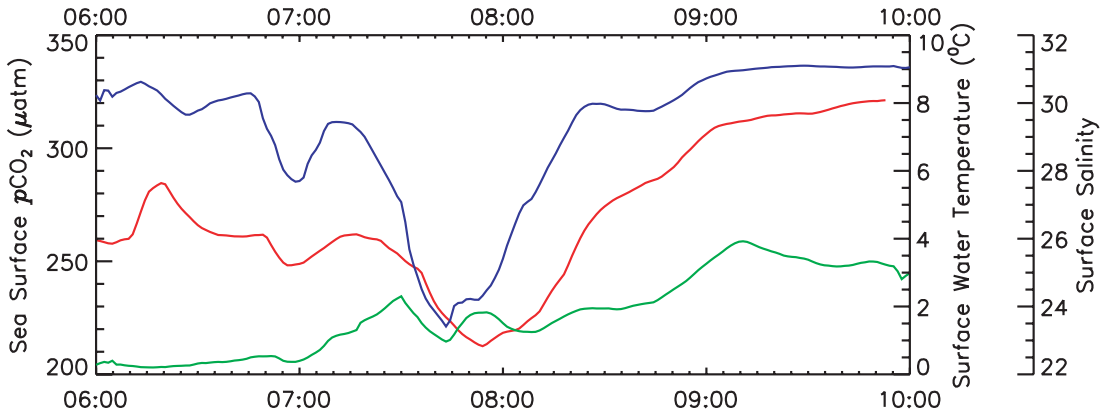

4.3.2 CO_2 Fluxes

Franklin Bay

Estimated CO_2 fluxes across the air–sea interface in Franklin Bay are shown in Table 4.1, along with the key parameters used in the flux calculation. During the ship's initial visit to Franklin Bay (October 28), ΔpCO_2 was -20 μatm, and we calculated a weak uptake of atmospheric CO_2 due largely to the high ($9/10^{ths}$) ice concentration. On our subsequent fall trips to the region ΔpCO_2 had become significantly positive, and we calculated a strong outgassing (46 mmol m^{-2} d^{-1}) on November 17 associated with a significant reduction in ice concentration (to $5/10^{ths}$, see Figure 4.2d). The switch from a weak uptake to a strong outgassing confounds whether Franklin Bay acted as a source or sink of CO_2 during the fall. From October 30–November 12 there were strong easterly winds (Figure 4.3a), which means that upwelling may have resulted in positive ΔpCO_2 well before the ship returned to the area in mid–November. This suggests that outgassing towards the end of the freeze–up season

dominated, and that Franklin Bay was probably a source of CO_2 to the atmosphere until exchange was limited by the formation of landfast ice.

Table 4.1: Flux estimates and associated parameters for the Franklin Bay region. Data were obtained on transects and station occupations depicted in Figures 4.2, 4.4 and 4.5.

Date	mean pCO_{2sw} (μatm)	stddev pCO_{2sw} (μatm)	pCO_{2atm} (μatm)	ΔpCO_2 (μatm)	U (m/s)	C_i ($/10^{ths}$)	F_{CO_2} (mmol/m^{2}d)
Oct 28	363	9	383	-22	6.9	9	**-0.4**
Nov 15	549	10	384	165		9.7	
Nov 17	510	8	389	121	15	5	**46**
May 11-18	486	17	400	86	6	9.7	**0.32**
Jun 14-18	287	14	390	-103	3.0	0	**-3.2**
Jun 20-22	301	10	391	-90	7.4	0	**-15.9**
Jun 25	287	12	393	-106	8	0	**-15.7**
Jun 26	253	21	391	-138	8.7	0	**-26.0**

The flux calculations for the May trip to Franklin Bay are shown in Table 4.1 for the portion of the bay that had fractured in mid–April (section 4.3.1, Figure 4.4). Our calculations show outgassing of CO_2 at this time, but at very low rates (< 0.5 mmol m^{-2} d^{-1}) due to the high ice concentrations. When ice was finally exported out of the northern portion of the bay in June (Figure 4.5), we calculated fairly strong (mean values of -3 – -26 mmol m^{-2} d^{-1}) CO_2 uptake as ΔpCO_2 became negative due to biological production and ice melt (Table 4.1). The eventual loss of ice from the southern portions of Franklin Bay (Figure 4.5e–f) allowed this uptake to occur over a large spatial extent, and the observed decrease in pCO_{2sw} through the month of June suggests that uptake likely persisted beyond the end of our study

(June 25). It therefore seems likely that Franklin Bay acted as a fairly strong sink of atmospheric CO_2 through the spring and early summer periods.

Darnley Bay

On our first trip to Darnley Bay (November 6 – 11), we measured strongly positive ΔpCO_2 (Table 4.2), similar to the November measurements in Franklin Bay. However, due to the complete landfast ice cover that existed at that time, we estimate that no outgassing from the seawater occurred. A subsequent storm created limited open water between November 7–18 in the northern half of Darnley Bay (Figure 4.2d) which may have allowed some outgassing, but the generally higher ice concentration probably resulted in less total outgassing than in Franklin Bay.

Table 4.2: Flux estimates and associated parameters for the Darnley Bay region. Data were obtained on transects and station occupations depicted in Figures 4.2 and 4.5.

Date	mean pCO_{2sw} (μatm)	stddev pCO_{2sw} (μatm)	pCO_{2atm} (μatm)	ΔpCO_2 (μatm)	U (m/s)	C_i ($/10^{ths}$)	F_{CO_2} (mmol/m^{2}d)
Nov 6	530	14	390	140	5.6	10	**0.0**
Nov 11	570	10				10	
Jun 2-4	293	10	392	-99	5.2	10	**0.0**
Jun 7-10	388	98	395	-7	5.4	10	**0.0**
Jun 11-14	243	12	390	-147	1.5	10	**0.0**
Jun 18-19	383	23	393	-10	4.2	10	**0.0**
Jun 24-25	303	13	396	-93	10.6	2	**-21.7**
Jun 27	313	14	392	-79	3.9	0	**-2.9**

In spring, Darnley Bay remained completely landfast until late June. For the most part, this prevented CO_2 exchange with the atmosphere, including potential outgassing associated with the early–June upwelling event (Figure 4.7). The ice

finally broke up in Darnley Bay around June 21, permitting fluxes of CO_2 that reached $\sim$ -22 mmol m^{-2} d^{-1} (Table 4.2). Darnley Bay therefore likely acted as a sink of atmospheric CO_2 through the spring and early summer, but the uptake was probably not as significant as in Franklin Bay due to the later ice–out date.

Cape Parry & Cape Bathurst

Tables 4.3 & 4.4 show that Cape Parry and Cape Bathurst followed a similar pattern to Franklin and Darnley Bays. We calculated modest outgassing ($\sim$ 1 mmol m^{-2} d^{-1}) near the end of October at Cape Bathurst, followed by increasing ice concentration at both locations that would have limited further exchange. This shut–off was more dramatic at Cape Parry, where ice became landfast earlier and remained fast until the end of June. Ice stayed more mobile at Cape Bathurst, which would have allowed a more significant outgassing to occur through the fall until the ice became landfast in late December.

Table 4.3: Flux estimates and associated parameters for the Cape Parry region. Data were obtained on transects and station occupations depicted in Figures 4.2, 4.4 and 4.5.

Date	mean pCO_{2sw} (μatm)	stddev pCO_{2sw} (μatm)	pCO_{2atm} (μatm)	ΔpCO_2 (μatm)	U (m/s)	C_i ($/10^{ths}$)	F_{CO_2} (mmol/m^2d)
Oct 28	508	4	384	124		9.7	
Nov 13	598	5	375	223		10	
Nov 18	575	3	384	191	12.7	10	**0.0**
May 8	525	4	403	122		10	**0.0**
May 10	555	13	408	147	1.9	10	**0.0**
Jun 4-6	445	38	394	51		10	**0.0**
Jun 22-23	270	7	390	-20	0.9	10	**0.0**

In May, the landfast ice around Cape Parry prevented a potentially strong outgassing driven by the high (∼125 μatm) ΔpCO_2. No pCO_{2sw} measurements were made in May in the Cape Bathurst region and therefore no flux calculations are available, but it is clear from Figure 4.4 that the area was covered by very high concentrations of landfast ice, and was probably not involved in significant air–sea gas exchange.

Table 4.4: Flux estimates and associated parameters for the Cape Bathurst region. Data were obtained on transects and station occupations depicted in Figures 4.2 and 4.5.

Date	mean pCO_{2sw} (μatm)	stddev pCO_{2sw} (μatm)	pCO_{2atm} (μatm)	ΔpCO_2 (μatm)	U (m/s)	C_i ($/10^{ths}$)	F_{CO_2} (mmol/m^{2}d)
Oct 29	493	25	385	108	9.0	9.7	**0.8**
Oct 30	557	14	385	172	9.8	9.7	**1.2**
Jun 23-24	324	4	391	-67	5.5	0	**-4.9**

At Cape Bathurst the landfast ice began to break up in early June, and was completely exported by mid month. We calculated a weak uptake of CO_2 in late June due to low wind velocities (Table 4.4), but we expect that the ice free conditions would have allowed significant uptake through the month. At Cape Parry ΔpCO_2 was strongly negative through June, but the ice remained landfast, resulting in no calculated CO_2 uptake for the entire month. According to CIS charts the ice broke up in the first week of July, which likely would have permitted significant CO_2 uptake given the strongly negative ΔpCO_2 observed at the end of June (Table 4.3). For both the Cape Bathurst and Cape Parry regions it is likely that significant uptake occurred through the rest of the open water season.

4.4 Discussion

4.4.1 Annual Air–Sea CO_2 Budgets

Without a more complete time series of pCO_{2sw} measurements and flux calculations, it is not possible to precisely assign an annual budget of air–sea CO_2 exchange to any of the landfast ice regions examined in this study. Nevertheless, it appears that outgassing periods were limited by the presence of sea ice, whereas uptake was able to proceed freely once the landfast ice had broken up and been exported. This seasonal cycle would result in net annual uptake of CO_2, and is very similar to the "seasonal rectification" cycle described by Yager et al. [1995] for the Northeast Water polynya.

A key aspect of this cycle in landfast ice regions is the lack of potential for air–sea gas exchange through winter open water. In offshore Amundsen Gulf, we observed episodes of CO_2 exchange 1–2 orders of magnitude higher than expected through open water associated with rapidly re–freezing leads [Else et al., 2011]. In Else et al. [2012b], we made the argument that the seasonal rectification hypothesis does not hold in offshore Amundsen Gulf because the frequent leads that occur in the area may permit significant air–sea gas exchange. This study shows that the seasonal rectification hypothesis is more applicable in the nearby landfast ice regions where the lack of leads likely prevents winter outgassing.

One exception to this idea is the brief period of time in mid–November when the landfast ice in Franklin and Darnley Bays was mobilized by strong winds (Figure 4.2c–d), resulting in the high CO_2 outgassing that we calculated in Franklin Bay on November 17 (Table 4.1). This event probably drove conditions very similar to the leads we observed in offshore Amundsen Gulf, and therefore the outgassing may

have been even stronger than we calculated. Since this event was fairly short lived (less than 10 days) it probably does not change our theory that the regions acted as a net sink for CO_2 in 2007–08, but it does suggest that the net annual exchange may be vulnerable to changes in winter ice conditions.

4.4.2 Upwelling Events in 2007–08

A review of past studies conducted in landfast ice regions show that our observations of positive ΔpCO_2 episodes are unique; persistently negative ΔpCO_2 has been observed under landfast ice in Antarctica [Gibson and Trull, 1999] and Greenland [Sejr et al., 2011], and Miller et al. [2011] observed no supersaturation during the 2003–04 CASES overwintering project in Franklin Bay. The key difference for the landfast ice of southern Amundsen Gulf in 2007–08 therefore appears to be the fall/spring upwelling, which raises the question of whether such events are typical for the region.

The first requirement for upwelling in this region is strong easterly winds. In comparison to the long–term (1979–2009) records, wind speeds recorded at the Cape Parry weather station were approximately 35% stronger than average in the fall of 2007, and 25% stronger than average in the spring of 2008. Furthermore, the mean easterly component of wind velocity was about 5 times stronger than average in the fall, and nearly 2 times stronger in the spring. As Figure 4.9 shows, these strong easterlies were driven by a very steep pressure gradient caused by anomalously high pressure to the north of the study area and low pressure to the south. This structure is part of the "Arctic Dipole" pattern, which is strongly correlated with increasing fall open water in the western sector of the Arctic Ocean [Overland and Wang, 2010], a dominant feature in 2007 [Perovich et al., 2008] and 2008.

Figure 4.9: Seasonal pressure anomalies relative to the decadal (1999-2009) mean. Data are from the NCEP/NARR reanalysis [Kalnay and co authors, 1996], plotted using the web-based plotting tools of the NOAA/ESRL Physical Sciences Division (Boulder, Colorado).

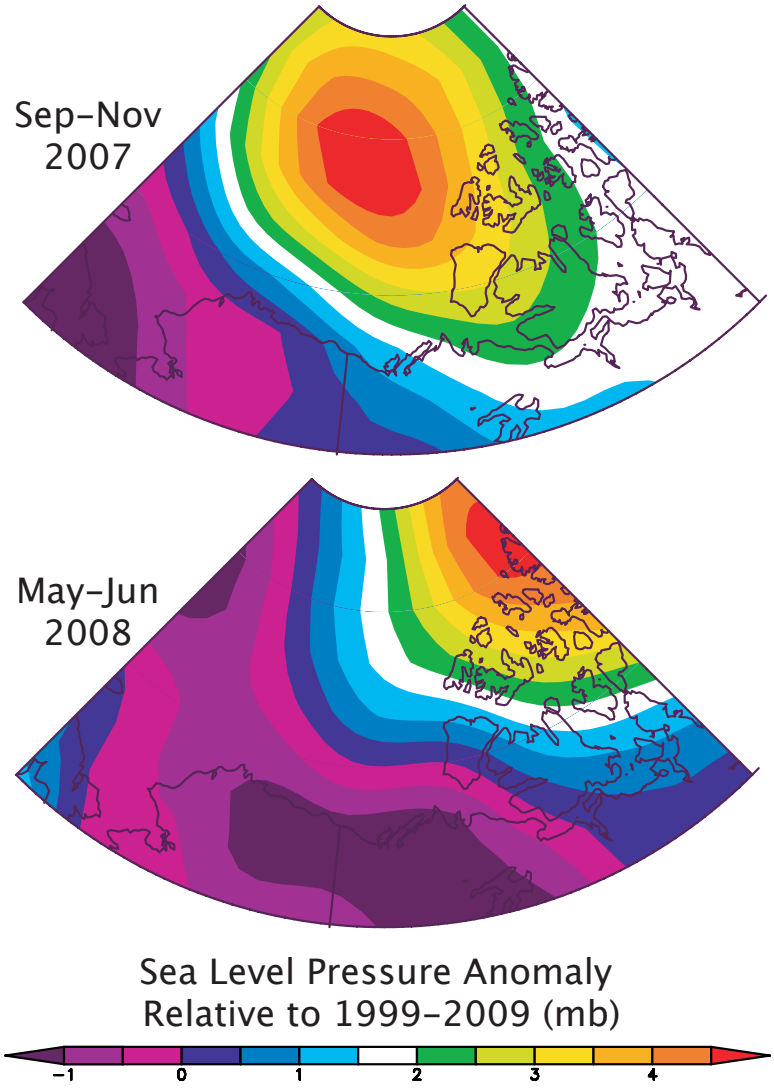

The second requirement for upwelling is the correct coastline or ice edge geometry. The area around Cape Bathurst is well known to produce significant upwelling in the presence of easterly winds [Mucci et al., 2010; Tremblay et al., 2011; Williams and Carmack, 2008] and Figure 4.2a shows that Cape Parry may act in a similar manner. In contrast, significant fall upwelling did not occur in Franklin Bay (Figure 4.2b) until an ice edge was established (Figure 4.2b–d), despite upwelling–favourable winds earlier in the season (Figure 4.3b). Similarly, Mundy et al. [2009] hypothesized that the presence of an ice edge was necessary to force the early June upwelling event in Darnley Bay (Figure 4.5b. Although the spring break–up of landfast ice edges in 2008 was fairly typical for the region, they first formed in the fall around November 6, a condition that only occurs in about 25% of years [Galley et al., 2008]. This suggests that there may have been a unique combination of strong winds and ice conditions that that made the fall of 2007 very conducive to upwelling.

If the upwelling in this region is indeed controlled by wind and ice conditions, then the air–sea CO_2 exchange cycle that we observed could be subject to significant interannual variability. For example, in years where upwelling does not occur (as appeared to be the case in 2004 [Miller et al., 2011; Tremblay et al., 2011]) the presence or absence of landfast ice in the fall and spring may not be important in preventing outgassing and maintaining a net annual sink. However, given observations of the Arctic Dipole pattern beginning to dominate circulation in the Arctic [Maslanik et al., 2007; Overland and Wang, 2010], it seems possible that upwelling favourable winds may become a more common occurrence in this region. If that is the case, then the maintenance of a net sink for atmospheric CO_2 may lie with the fate of the landfast ice. Presently, no trends in landfast ice duration, break–up date, or freeze–up date have been identified for this region, but other areas of the Cana-

dian Arctic are showing signs of a transition to a shorter landfast ice season [Galley et al., 2012]. If this region does begin to experience a shorter landfast ice season in conjunction with increased upwelling (keeping in mind that upwelling at the Capes can occur without a landfast ice edge), then the net annual sink of atmospheric CO_2 that we have proposed for 2007–08 may not be maintained.

4.5 Conclusions

The landfast ice regions of southern Amundsen Gulf likely acted as net annual sinks for atmospheric CO_2 in 2007–08. Upwelling episodes created positive ΔpCO_2 in late fall and early spring, but we calculated that high ice concentrations prevented significant outgassing. In contrast, primary production and ice melt caused negative ΔpCO_2 in late spring and early summer, which allowed significant CO_2 uptake once the landfast ice broke up and was exported. This cycle of inhibited outgassing in the fall/spring and free uptake in the summer is similar to the cycle proposed by Yager et al. [1995] for Arctic polynya regions, but is different from recent observations in other landfast ice regions [Gibson and Trull, 1999; Miller et al., 2011; Sejr et al., 2011]. The main difference in our region was the occurrence of upwelling events, which appear to have been caused by abnormally strong easterly winds. In some areas, the presence or absence of a landfast ice edge seemed to be an additional requirement for strong upwelling. The importance of these two variables (easterly winds and ice edge position) on our observations suggests that air–sea CO_2 exchange in the region may be subject to significant interannual variability. It also suggests a vulnerability to climate change, particularly if observed changes in Arctic atmospheric circulation (e.g. Maslanik et al. [2007]; Overland and Wang [2010]) and landfast ice conditions (e.g. Galley et al. [2012]) continue on their current trajectory.

Chapter 5

An Annual Air–Sea CO_2 Flux Budget for the Cape Bathurst Polynya Region

Brent G.T. Else*[1], Tim N. Papakyriakou[1], M.G. Asplin[1], David G. Barber[1], Ryan J. Galley[1], Lisa A. Miller[2], Al Mucci[3]

[1]Centre for Earth Observation Science, Department of Environment and Geography, University of Manitoba, Winnipeg, Manitoba, Canada

[2]GEOTOP, Department of Earth and Planetary Science, McGill University, Montreal, Québec, Canada.

[3]Centre for Ocean Climate Chemistry, Institute of Ocean Sciences, Fisheries and Oceans Canada, Sidney, British Columbia, Canada

Abstract

During the Canadian International Polar Year projects in the Cape Bathurst polynya region, we measured a near–complete annual cycle of sea surface CO_2 (pCO_{2sw}), atmospheric CO_2 (pCO_{2atm}), sea surface temperature (SST), salinity (S), and wind velocity (U). In this paper, we combine these data with ancillary measurements of sea ice concentration (C_i) to estimate the mean annual (September 2007–September 2008) air–sea CO_2 exchange for the region. For the non–freezing seasons the exchange was calculated using a standard bulk aerodynamic approach, whereas during the freezing seasons we extrapolated eddy covariance measurements of CO_2 exchange. Our results show that in 2007–08 the region served as a net sink of atmospheric CO_2 at a mean rate of -10.1 $\pm$ 6.5 mmol m^{-2} d^{-1}. The strongest calculated uptake occurred in the fall when wind velocities were highest, pCO_{2sw} was significantly lower than pCO_{2atm}, and ice was beginning to form. Atmospheric CO_2 uptake was calculated to occur (at lower rates) throughout the rest of the year, except for a brief period of outgassing during late July. Using archival U, C_i, and pCO_{2sw} data for the region, we found that winds in 2007–08 were 25–35 % stronger than normal and were predominately easterly, which appears to have driven a relatively late freeze–up (by $\sim$3 weeks relative to mean conditions) and an early polynya opening (by $\sim$4 weeks). These conditions may have permitted a high CO_2 uptake relative to mean conditions. Estimated winter CO_2 exchange through leads and small polynya openings made up more than 50% of the total CO_2 uptake, consistent with recent observations of enhanced CO_2 exchange associated with open water components of the winter icescape. Our calculations for the Cape Bathurst polynya region are con-

sistent with past studies that estimate the total winter CO_2 uptake in Arctic coastal polynyas to be on the order of 10^{12} g C yr^{-1}.

5.1 Introduction

Polynyas (areas of recurring open water that exist when a complete ice cover would be expected) are wide spread across the Arctic and Antarctic but only account for a small portion of the total area of polar seas [Barber and Massom, 2007]. Despite their limited extent, at times they provide the only direct connection between the atmosphere and the underlying ocean, making them important sites for air–sea interactions. The air–sea exchange of CO_2 during time periods when polynyas occur has received considerable interest (e.g. Miller and DiTullio [2007]), but significant exchange has also been observed during other seasons [Else et al., 2011]. By understanding air–sea CO_2 transfer through an entire annual cycle in geographic areas that host polynyas (areas we term "polynya regions") we can better understand their role in global and regional atmospheric carbon budgets.

The potential for CO_2 exchange at the air–sea interface is determined by the CO_2 gradient across the interface, $\Delta pCO_2 = pCO_{2sw} - pCO_{2atm}$, where pCO_{2sw} and pCO_{2atm} are the sea surface and atmospheric partial pressures of CO_2, respectively. To date, almost all observations of ΔpCO_2 in polynya regions have been made in spring, summer, and fall, forcing annual budgets of CO_2 exchange to rely on assumptions about the winter season. For instance, in the Northeast Water (NEW) polyna, Yager et al. [1995] observed low mid–summer pCO_{2sw} caused by strong primary production earlier in the spring. They hypothesized that the region acted as a CO_2 sink during the open water season with strong fall winds exploiting the negative ΔpCO_2 gradient. They also predicted that ΔpCO_2 would become positive

in winter due to excess respiration, but that the winter ice cover would prevent any outgassing. Support for this hypothesized cycle was provided by Miller et al. [2002] who observed a brief positive ΔpCO_2 before the spring opening of the Northwater polynya, followed by strongly negative ΔpCO_2 as the ice cleared. Likewise, modelling [Sweeney, 2003] and summer pCO_{2sw} measurements [Sweeney et al., 2000] in the Ross Sea polynya regions (Antarctica) have revealed a similar cycle (see also the review by Miller and DiTullio [2007]).

Although the cycle described in Yager et al. [1995] has played an important role in shaping our understandings of air–sea CO_2 exchange in seasonal sea ice areas, recent observations have shown some important deviations. In winter, ice remains mobile in many such regions, allowing open water to exist in the form of leads and winter polynya openings. If such regions follow the pCO_{2sw} cycles described above, winter outgassing should occur, possibly at a rate that would balance the summer/fall uptake. Instead, Anderson et al. [2004] reported water column evidence from the Storfjorden polynya (Svalbard, Norway) indicating a strong winter uptake of atmospheric CO_2. Also using water column data, Omar et al. [2005] calculated the rate of winter uptake in that region to be about 10 times larger than the surrounding non–polynya areas. In the Cape Bathurst polynya region (southeastern Beaufort Sea, Canada), we recently observed episodes of strong winter uptake using micrometeorological techniques (i.e., eddy covariance) [Else et al., 2011], and we were able to show that ΔpCO_2 remained negative through the entire winter [Else et al., 2012b].

In this paper, we use the pCO_{2sw} data set described in Else et al. [2012b], combined with our direct observations of winter fluxes [Else et al., 2011] to calculate a full–year (2007–08) air–sea CO_2 flux budget for the Cape Bathurst polynya region.

In doing so, we create one of the most complete estimates of annual air–sea CO_2 exchange available for any polar sea, allowing greater insight into the role of polynya regions in atmospheric carbon cycling. Our approach updates a preliminary estimate of CO_2 exchange created for the region by Shadwick et al. [2011]. We also examine whether the conditions experienced in 2007–08 (ice, ocean, atmosphere) represent a "typical" annual cycle for this region, and we discuss the implications of our results at the circumpolar scale.

5.2 Methods

5.2.1 Data Sources

The majority of the data required for this study were collected during the International Polar Year ArcticNet and Circumpolar Flaw Lead System Study projects. The projects were conducted onboard the research icebreaker CCGS *Amundsen*, and are summarized by ArcticNet [2010] and Barber et al. [2010]. The objective of the projects was to conduct multidisciplinary sampling while remaining mobile in the Cape Bathurst polynya region for most of an annual cycle (Figure 5.1). In this paper, we used data that were collected from October 22, 2007 to August 2, 2008 in western Amundsen Gulf, the primary location of ship activities (Figure 5.1). To create CO_2 flux estimates spanning a complete annual cycle, we defined a study period of September 15, 2007 to September 14, 2008, necessitating an extension of the data by ∼6 weeks on either side of the field program. Various ancillary data sets were required to facilitate this extension, and fill other gaps in the field data.

Wind velocity was measured by a propeller anemometer installed on an open–lattice meteorological tower located at the bow of the research vessel (see Else et al.

Figure 5.1: The study area. The dashed line outlines the approximate location of the Cape Bathurst polynya (and also outlines Amundsen Gulf). The solid polygon denotes the area in which field data were collected.

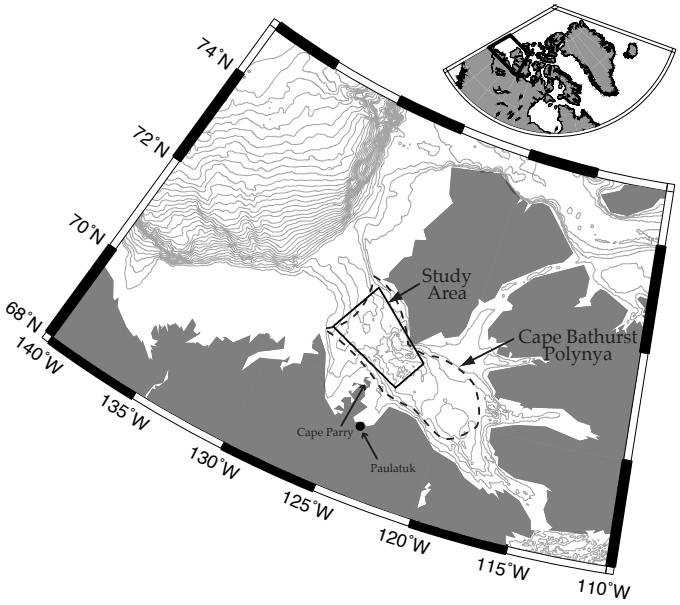

[2011] for instrument details, including data quality control). We used hourly averages, and when ship based data were not available (usually due to ship orientation) we used hourly data collected at the Cape Parry (preferably) or the Paulatuk Environment Canada weather stations (see Figure 5.1). All wind velocity data were scaled to a height of 10 m above sea level, and the different data sources showed reasonable agreement when compared during periods of overlap (root mean square differences of velocity on the order of 4–5 m s^{-1}).

Ice concentration was obtained at daily intervals from the University of Bremen AMSR-E passive microwave satellite imagery products [Spreen et al., 2008]. This data product reports ice concentration on a ratio scale from 0 (ice free) to 1 (complete ice cover) at a spatial resolution of 6.25 km.

Sea surface temperature (SST) was measured during the field experiment using a ship–based CTD (SeaBird 911+). The CTD was deployed over the side

of the ship during the open water seasons, providing samples at a minimum water depth of ∼2 m. During the winter the CTD was deployed through a moon pool, and the minimum sampling depth was ∼10 m (as per Else et al. [2012b], the error associated with these different depth measurements is small). To extend the SST data set beyond the duration of the field program, we used daily L3 MODIS-Aqua daytime 11μ SST satellite imagery.

Salinity was also measured using the Rosette/CTD. No supplemental measurements were available beyond the dates of the sampling program, so we used a simple interpolation based on a polynomial fit to the field data.

$p\mathbf{CO}_{2atm}$ was measured on the meteorological tower at the bow of the ship, using a near–infrared gas analyzer (LiCor model LI-7000) system which drew sample air from an inlet located ∼14 m above sea level. The instrument was calibrated regularly [Else et al., 2012a, 2011], and instances where the sample air may have been contaminated by ship emissions were removed in post–processing. For the time period when the ship was not in the area, we used data from the Scripps CO_2 Program sampling station at Barrow, Alaska (approximately 1000 km west of our study area) [Keeling et al., 2001]. Those data were available approximately bi–weekly during the winter and weekly through the rest of the year, and showed good agreement with our ship–based samples (root mean square error 4.1 ppm, based on 14 dates when coincident measurements were made at Barrow and on the CCGS *Amundsen*).

$p\mathbf{CO}_{2sw}$ was measured using a shower–type equilibrator connected to a short (∼ 5m) intake line with an inlet at ∼5m depth. The equilibrator's headspace air was continuously cycled through an infrared gas analyzer (LI-7000) calibrated daily with ultra–pure nitrogen (to set the instrument's zero reading) and a CO_2–air mixture

traceable to WMO standards (to set the span reading). A detailed description of this instrument, its components, and the reproducibility of the measurements can be found Else et al. [2012b] and Else et al. [2012a]. To extend these data beyond the field study time period, we assumed that changes in pCO_{2sw} between August and October are best described by changes in water temperature. We used measurements of pCO_{2sw} and SST from the start of the field season to define an initial state, and then calculated pCO_{2sw} for the 6 weeks prior to sampling using the thermodynamic equations of Takahashi et al. [1993] and the MODIS SST data. We did likewise for the 6 weeks after the end of the field sampling program. This is of course a simplification, but the results of this approach (shown in Figure 5.2c & e, discussed below) yield a reconstruction very similar to what might be achieved by simple interpolation between summer 2008 and fall 2007 data (i.e., the approach used by Shadwick et al. [2011]).

5.2.2 Flux Calculation

For any ice–affected sea it is useful to partition the net surface CO_2 flux ($F_{CO_{2total}}$) into a component that describes the exchange between open seawater and the atmosphere (which we denote $F_{CO_{2as}}$) and one that describes exchange between the ice surface and the atmosphere ($F_{CO_{2ai}}$):

$$F_{CO_{2total}} = F_{CO_{2as}} + F_{CO_{2ai}} \tag{5.1}$$

Although not often considered, observations of significant $F_{CO_{2ai}}$ have been reported using micrometeorological techniques [Miller et al., 2011; Papakyriakou and Miller, 2011; Semiletov et al., 2004; Zemmelink et al., 2006], chamber techniques [Nomura et al., 2010; Semiletov et al., 2004], and laboratory experiments [Nomura et al.,

2006]. While the community is approaching consensus on the expected direction of these exchanges (CO_2 outgassing during winter, CO_2 uptake in the spring/summer), the observed fluxes vary by 1–2 orders of magnitude. Therefore, in this paper we limit ourselves to deriving only $F_{CO_{2as}}$, with the understanding that $F_{CO_{2ai}}$ could be added to create a more complete budget as the state of the science evolves.

To calculate $F_{CO_{2as}}$, we used a standard form of the bulk flux equation, scaled by the ice concentration (C_i, reported as a fraction of the areal coverage):

$$F_{CO_{2as}} = k\alpha\Delta pCO_2(1 - C_i) \tag{5.2}$$

where k is the gas transfer velocity, and α is the solubility of CO_2 in seawater (a function of SST and salinity). During the non–freezing season, we used the parameterization of Sweeney et al. [2007] to calculate k:

$$k = 0.27U^2(Sc/660)^{(-1/2)} \tag{5.3}$$

where U is the wind velocity at 10 m height, and Sc is the Schmidt number (a function of SST). The time period that we applied this k parameterization to was September 15 – November 14, 2007 and May 16 – September 14, 2008 (see below for explanation), and we denote those fluxes $F_{CO_{2as:norm}}$.

Unfortunately, the Sweeney et al. [2007] k parameterization cannot account for observations of enhanced winter fluxes (e.g. Anderson et al. [2004]; Else et al. [2011]; Loose et al. [2009]). These enhanced fluxes (which we denote as $F_{CO_{2as:enh}}$) appear to be associated with the formation of new sea ice in open water [Else et al., 2011], which in the Cape Bathurst polynya region typically occurs in leads throughout the entire winter. To provide a rough estimate of how strong this enhanced winter flux might be, we calculated the mean winter transfer velocity from measurements made

in the Cape Bathurst polynya ($\overline{k}_{enh}$ = 458 ± 334 cm hr^{-1}, [Else et al., 2011]) and used that value in equation 5.2. The $\overline{k}_{enh}$ value was derived from 32 half–hour eddy covariance samples, which span a large range of mean wind velocity (4 – 18 m s^{-1}), air temperature (-5 – -23°C), sensible heat flux (-15 – 150 W m^{-2}) and ΔpCO_2 (-80 – -38 μatm) conditions. For this study, we calculated $F_{CO_{2as:enh}}$ from November 15 2007 – May 15 2008, which corresponds to the time period when SST was at the freezing point (see section 5.3.1), surface air temperatures were consistently lower than SST, and conditions were typically within the bounds of those experienced when collecting the k_{enh} data.

It is worth noting that we did observe significant non–linear relationships between observations of k_{enh} and wind velocity ($\ln(k_{enh}) = 0.16U + 3.97$, r^2=0.55) and k_{enh} and air temperature ($\ln(k_{enh}) = -0.09T_{air} + 4.49$, r^2=0.33). Both of these relationships might be expected from our hypothesis that the flux enhancement is partly driven by wind and high sensible heat fluxes producing a very turbulent sea surface [Else et al., 2011]. However, we decided that it was imprudent to use parameterizations based on these variables at this time given how limited the data set is, and given that causal links between these variables and k_{enh} have not yet been proven. Instead, using the mean k_{enh} value (and incorporating the considerable variability around that mean) gives us a first–order estimate of how strong the flux may have been through the winter.

5.2.3 Data Integration

A key challenge for the flux calculations was the discontinuous sampling intervals inherent in some of the variables. The field data set (SST, salinity, pCO_{2sw}, pCO_{2atm}) was discontinuous because the ship would often leave the study area for several days

to sample in other locations. The Scripps CO_2 data sampling interval was also discontinuous (sampling occurred weekly through most of the year, and was less frequent during the winter), and SST was only retrievable from MODIS imagery on cloud–free days. On the other had, the wind velocity and AMSR–E ice concentration data were very continuous. To deal with this issue, we fit polynomials to the pCO_{2sw}, pCO_{2atm}, SST, and salinity data to allow interpolation over periods of missing data. Such an approach gives a generalized view of the annual cycle of these variables and eliminates high–frequency (e.g. diurnal) variability, which has been observed to play an important role in CO_2 exchange at low latitudes (e.g. McGillis et al. [2004]). However, we did not observe significant high–frequency variability in pCO_{2sw} in this region [Else et al., 2012b], and we do not expect high–frequency variability in pCO_{2atm}, SST, or salinity to play a strong role in influencing CO_2 flux calculations. The variability that did occur in these parameters was characterized by calculating standard deviations around the polynomial fits, and the standard deviations were used in error evaluation of the resulting CO_2 flux calculations.

5.3 Results

5.3.1 Observed Conditions

Time series of the variables required for the flux calculations are shown in Figure 5.2. Wind velocities (Figure 5.2a) were highest between October and November 2007, with a mean velocity (and standard deviation) of 7.2 $\pm$ 4.8 m s^{-1} and storm episodes with sustained winds in excess of 15 m s^{-1}. Over the winter (December to March) winds were somewhat weaker, with mean velocities of 6.2 $\pm$ 3.7 m s^{-1} and storms that rarely sustained winds in excess of 15 m s^{-1}. Spring (April to June)

saw a slight increase in mean winds (6.5 ± 4.0 m s^{-1}) and similar storm activity. Winds were weakest through the open water season (July to September 2008) with mean velocities of 5.4 ± 3.0 m s^{-1} and limited storm activity.

The time series of C_i is shown in Figure 5.2b. Ice began forming in the region around October 25, and reached 0.99 on December 10. Throughout the winter season the ice cover remained mobile, resulting in leads and small polynyas that kept C_i fluctuating between 0.95 and 0.99. Ice concentration first dropped below 0.9 in mid–April, followed by a rapid decrease that started on May 10 and resulted in ice–free conditions by June 22.

The observed annual pCO_{2sw} cycle is displayed in Figure 5.2c. To briefly summarize the findings of Else et al. [2012b], pCO_{2sw} was low (∼300 μatm) upon arrival in October 2007, likely due to SST cooling from a summer maximum and fall phytoplankton blooms. After ice formation, pCO_{2sw} slowly increased due to brine rejection, respiration, and gas exchange, reaching a maximum of ∼380 μatm in late March. This was followed by a gradual decrease in spring caused by an ice algae bloom, and then an accelerated decrease due to open water phytoplankton blooms that reduced pCO_{2sw} to ∼300 μatm in early June. In mid-July pCO_{2sw} increased rapidly to ∼410 μatm as a result of gas exchange and surface warming, and then began to decrease as the sea surface cooled.

Atmospheric pCO_2 (Figure 5.2d) varied from ∼375 μatm in the fall to ∼395 μatm in mid-winter, following the expected global seasonal CO_2 pattern. These pCO_{2atm} values kept ΔpCO_2 negative for most of the annual cycle, except for a brief positive excursion in mid–July.

Sea surface temperature through the study period is shown in Figure 5.2e. In the fall, SST reached the freezing point in mid–November, and then decreased slightly

Figure 5.2: Observations of (a) wind velocity, (b) ice concentration, (c) pCO_{2sw} (x symbols are observed daily means, open diamonds are extrapolated data as per section 5.2.1), (d) pCO_{2atm} (x symbols were observed on the research vessel, open diamonds are from Barrow, Alaska), (e) sea surface temperature (x symbols were observed on the research vessel, open diamonds were obtained from the MODIS instrument), and (f) salinity (measured onboard the research vessel). For panels b-f, the solid lines are the fitted polynomials that were used for resampling the data to one–hour intervals.

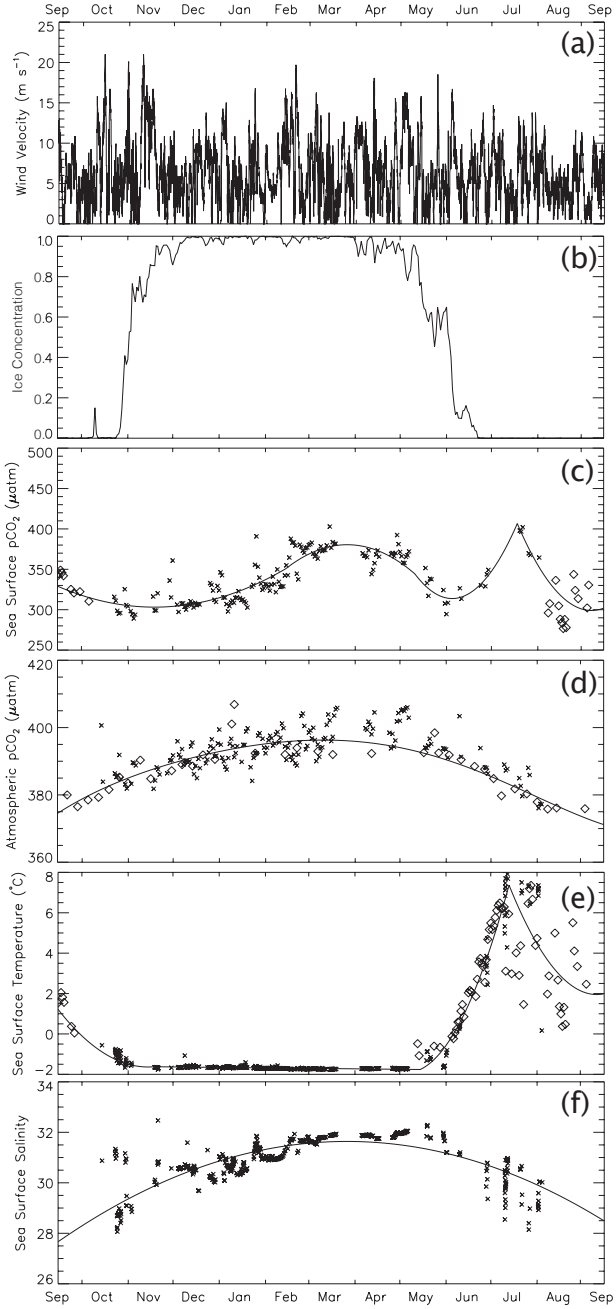

through the winter as the freezing point was lowered by increasing salinity (Figure 5.2f). A rapid increase in SST then started in mid–May as C_i decreased (Figure 5.2b), reaching a maximum near 8°C in mid–July. This was followed by a more gradual decrease in SST as waters cooled in the fall.

Salinity followed a distinct cycle, which has been described thoroughly in Shadwick et al. [2011] (Figure 5.2f). At the beginning of the study period salinity was low (28–29), and then gradually increased to a maximum near 32 in April due largely to brine rejection by the growing ice cover. As the ice began to melt in May, salinity decreased back towards fall values.

5.3.2 Calculated Fluxes

The time series of calculated fluxes during the non–freezing season ($F_{CO_{2as:norm}}$) is shown in Figure 5.3. The strongest fluxes (up to -40 mmol m^{-2} d^{-1}) occurred in October 2007, when winds were highest (Figure 5.2a) and ΔpCO_2 was strongly negative (Figures 5.2c & d). Significant CO_2 uptake by the ocean continued through most of November, but $F_{CO_{2as:norm}}$ was essentially cut off towards the end of the month when C_i began to consistently exceed 0.95 (Figure 5.2b). In early May, $F_{CO_{2as:norm}}$ resumed with small episodes of uptake, and then proceeded in earnest in late May and June as the ice cover was removed by wind forcing. Despite negative ΔpCO_2 similar to the fall of 2007, maximum uptake rates during the spring were around -30 mmol m^{-2} d^{-1} because of weaker winds. In July, a short period of outgassing (maximum ~5 mmol m^{-2} d^{-1}) occurred due to the mid-summer pCO_{2sw} peak (Figure 5.2c). This was followed by modest uptake in August and September (maximum ~-15 mmol m^{-2} d^{-1}) due to the light wind conditions and moderately

negative ΔpCO_2. Overall, we calculated a mean $F_{CO_{2as:norm}}$ of -5.2 ± 2.0 mmol m^{-2} d^{-1} over the non–freezing period (184 days).

Figure 5.3: Calculated $F_{CO_{2as:norm}}$ (black line) and $F_{CO_{2as:enh}}$ (red line) for the study area.

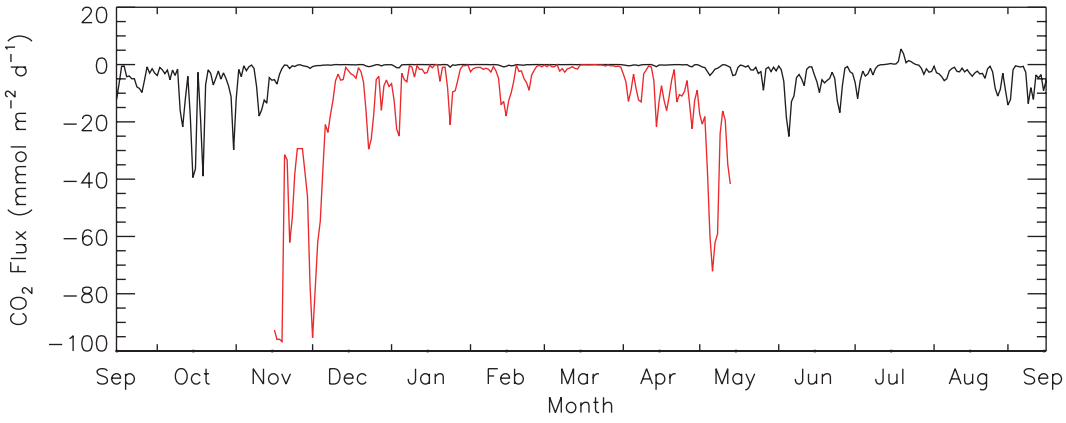

Also shown in Figure 5.3 is our rough estimate of the winter enhanced flux ($F_{CO_{2as:enh}}$). These results show two key features: high–magnitude fluxes in the fall and spring, and weaker but still significant fluxes throughout the winter. The high flux estimates in the fall were a result of the large amounts of open water present as the ice began to form while ΔpCO_2 was strongly negative (Figures 5.2b, c & d). This initial pulse of rapid uptake is consistent with the findings of Anderson et al. [2004], but to our knowledge the potential for a spring uptake as polynyas form in the spring has not been previously identified. The high spring flux estimates occurred because under–ice primary production began to reduce pCO_{2sw} in March and April [Else et al., 2012b; Shadwick et al., 2011] and when dynamic processes began to break up the ice in early May, the atmospheric conditions were still conducive to new ice formation and thus enhanced flux.

The mean $F_{CO_{2as:enh}}$ calculated for the freezing period (182 days) was -15.0 ± 10.0 mmol m^{-2} d^{-1}. If this estimate is reasonable, then the amount of carbon transferred

to the mixed layer by this exchange should at least fit within dissolved inorganic carbon (DIC) budgets for the region. In the same study area, Shadwick et al. [2011] observed a mixed layer DIC increase over the 2007-08 winter period (which they defined as November 15 – March 15) of nearly 200 μmol kg^{-1}. Assuming a 50 m mixed layer depth, the DIC increase resulting from $F_{CO_{2as:enh}}$ over that time period would only be $\sim$37 μmol kg^{-1}, or 19% of the total winter DIC increase, showing that our estimate of $F_{CO_{2as:enh}}$ is reasonable.

Since the freezing period is essentially equal in length to the non–freezing period, this estimated flux enhancement greatly increases the annual $F_{CO_{2as}}$ relative to simply computing $F_{CO_{2as:norm}}$ for the entire year. By combining the non–freezing and freezing season fluxes, we obtain a total annual average $F_{CO_{2as}}$ of -10.1 $\pm$ 6.5 mmol m^{-2} d^{-1} for the Cape Bathurst polynya region.

5.4 Discussion

5.4.1 How "Typical" Was 2007–08?

Mean annual fluxes for a given region are often compiled in papers that attempt to budget air–sea gas exchange on larger scales (e.g. Bates and Mathis [2009]; Borges et al. [2005]; Cai et al. [2006]; Chen and Borges [2009]). This approach is most effective when the compiled studies provide some analysis of interannual variability. We do not have the data set necessary to calculate a complete annual budget for our study area over several years, but in this section we use other data sets to discuss the long–term variability in many of the parameters that directly affect CO_2 flux. The goal of this analysis is to determine if our mean annual flux estimate is typical of the

mean state of the Cape Bathurst polynya, or if it represents a somewhat anomalous year.

pCO_{2sw} Conditions

To examine interannual variability in pCO_{2sw}, we collected data from other cruises during which pCO_{2sw} measurements were carried out in the study region between 2003–2009. The first available data are from Mucci et al. [2010], who calculated pCO_{2sw} from surface DIC, pH, and total alkalinity (TA) measurements during fall 2003 and spring/summer 2004. In 2006, our research group made direct pCO_{2sw} measurements on the CCGS *Amundsen* using an underway instrument composed of a membrane contactor (Liqui-Cel SuperPhobic x50) and an LI-7000 gas analyzer, similar to a system described in Else et al. [2008a]. In 2009, we returned to the area, this time with a commercially built underway pCO_{2sw} system (General Oceanics model 8050), which has an expected accuracy of 2 μatm [Pierrot et al., 2009].

The pCO_{2sw} measurements made during these cruises are shown in Figure 5.4 in comparison to the generalized cycle and variability observed in 2007–08. Despite the diversity in measurement techniques, there is remarkable consistency in pCO_{2sw} observations made between September and November, with most falling within ± 1 standard deviation of the 2007–08 measurements. This suggests that negative ΔpCO_2 and a decreasing trend in pCO_{2sw} as the sea surface cools is typical for the region in autumn, at least over the past decade.

The only other time period where we can make interannual comparisons is in the summer open water season. As Figure 5.4 shows, 2004 appeared to follow a similar pattern to 2008, with pCO_{2sw} increasing to a peak near 400 μatm in mid–July and then decreasing through August. It is worth noting that spring/summer ice cycles in 2004 followed a very similar pattern to 2008, with break–up occurring at essentially

Figure 5.4: pCO_{2sw} observations made in the Cape Bathurst polynya region during other cruises in comparison to the polynomial fit of the 2007–08 pCO_{2sw} data. The dashed lines show ± one standard deviation around the polynomial fit.

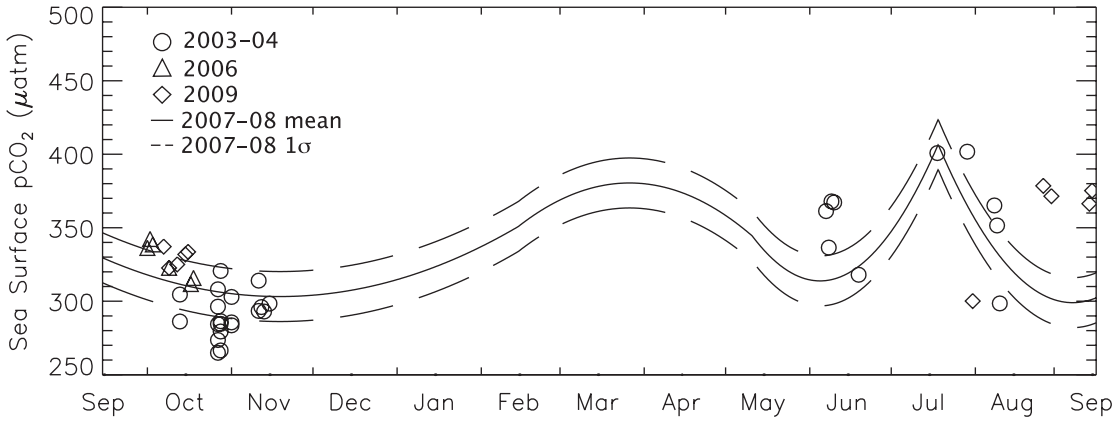

the same time. In 2009, pCO_{2sw} appeared to experience a similar summer pattern to 2008, but perhaps with a delayed increase (starting at the end of July) and a smaller peak value (∼375 μatm in August). Ice break–up in 2009 occurred nearly one month later than in 2008, and the region did not become completely ice free until mid–August. This apparently delayed and reduced the summer pCO_{2sw} increase, possibly by limiting air–sea gas exchange and keeping SST low (SST reached a maximum of ∼5°C in 2009 compared to ∼8°C in 2008). These results suggests that variations in the annual pCO_{2sw} cycle may be linked to sea ice cycles, which raises the question of how typical the ice conditions were in 2007–08.

Ice Conditions

We compared the 2007–08 ice conditions to a regional climatology based on the AMSR-E C_i data from 2002–2010 (Figure 5.5). In 2007, ice formation began about three weeks later than average, but reached a concentration of 0.80 only one week later than average. The winter leads and small polynyas generated by ice motion in

2007–08 are typical for the region, as evidenced by the long–term mean winter C_i below 1 and variability (standard deviation ∼0.02) around that mean. The significant decline in C_i in mid-May 2008 was also typical, although the region became ice–free more than 4 weeks earlier than average. Overall, there were very few instances when C_i in 2007–08 fell outside of one standard deviation of the 2002–2010 mean. Therefore, the 2007–08 ice cycle could be described as a "light" ice year with late freeze–up and rapid spring break–up, but not anomalously light within the context of the last decade.

Figure 5.5: 2007–08 ice concentration in the Cape Bathurst polynya region (red line) compared to the 2002–10 mean (black line). The grey shaded area represents ± one standard deviation around the 2002–10 mean.

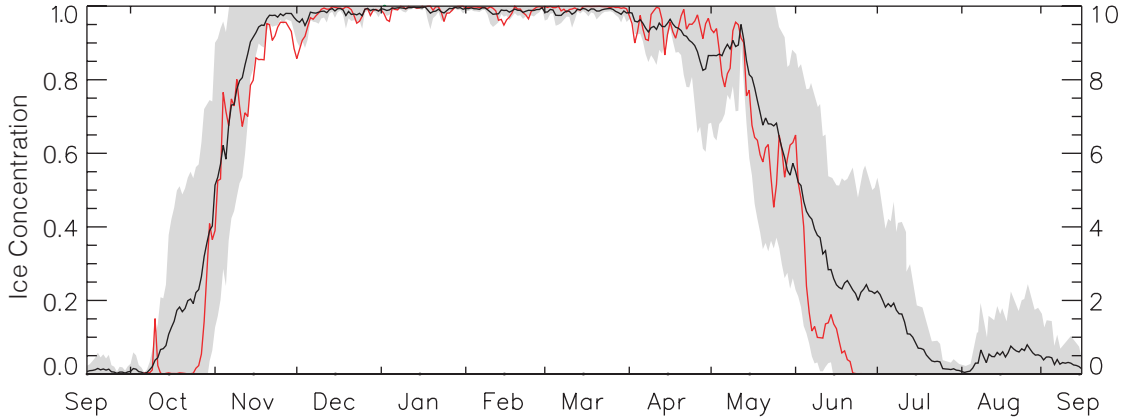

Wind Conditions

Wind velocity and direction in 2007–08 was grouped by season and compared to wind data collected at the Cape Parry weather station between 2000–2010. Figure 5.6 shows that fall 2007 wind velocities were significantly higher than average, but adhered to the usual easterly direction. Winter and spring 2007–08 also displayed a typically easterly direction with stronger than average velocities. Summer 2008 wind

velocities were substantially higher than the long–term mean and were even more easterly than usual. One–way analysis of variance (ANOVA) testing confirmed that mean wind velocities during all four seasons were significantly higher than the 2000-2010 seasonal averages. We can thus conclude that 2007–08 was an anomalously windy year, with winds predominantly from the east.

Effects of Variability in Wind and Ice Conditions on Calculated Flux

Although we cannot perform a complete analysis of interannual variability in $F_{CO_{2as}}$, we can examine the impact that interannual variability in wind velocity (U) and C_i has on $F_{CO_{2as}}$ by using the 2007–08 cycles of pCO_{2sw}, SST, and salinity as a baseline. For the years 2002–2010 (when both C_i and U data are available) we used the 2007–08 pCO_{2sw}, SST, and salinity data to calculate $F_{CO_{2as}}$ while allowing C_i and U to vary, both independently and in combination (Table 5.1). We used the estimated enhanced gas transfer velocity when C_i exceeded 0.80 in the fall and fell below 0.80 in the spring.

By introducing interannual variability in both U and C_i using data from 2002–2010, the calculated mean annual $F_{CO_{2as}}$ ranges from -6.0 to -12.4 mmol m^{-2} d^{-1} (Table 5.1), with an average difference from 2007–08 of $\pm$1.7 mmol m^{-2} d^{-1}. Allowing only wind velocity to vary produces a weaker sink of CO_2 by 0.2–0.8 mmol m^{-2} d^{-1} with a mean of 0.6 mmol m^{-2} d^{-1}, showing that the abnormally strong winds in 2007–08 enhanced CO_2 uptake relative to average conditions over the past decade. In contrast, by allowing only C_i to vary, $F_{CO_{2as}}$ ranges from a 3.3 mmol m^{-2} d^{-1} stronger sink to a 2.9 mmol m^{-2} d^{-1} weaker sink, indicating that C_i is likely the more important factor in controlling interannual variability in $F_{CO_{2as}}$. Much of this variability arises from our estimation of $F_{CO_{2as:enh}}$, both in terms of the length of the season to which the estimation is applied (which ranges from 179–233 days), and

Figure 5.6: Wind rose plots comparing the frequency of hourly wind velocities and directions by season observed in 2007–08 (left column) to the 2001–10 mean (right column). SON = September, October, November; DJF = December, January, February; MAM = March, April, May; JJA = June, July, August. Data are from the Cape Parry Environment Canada weather station.

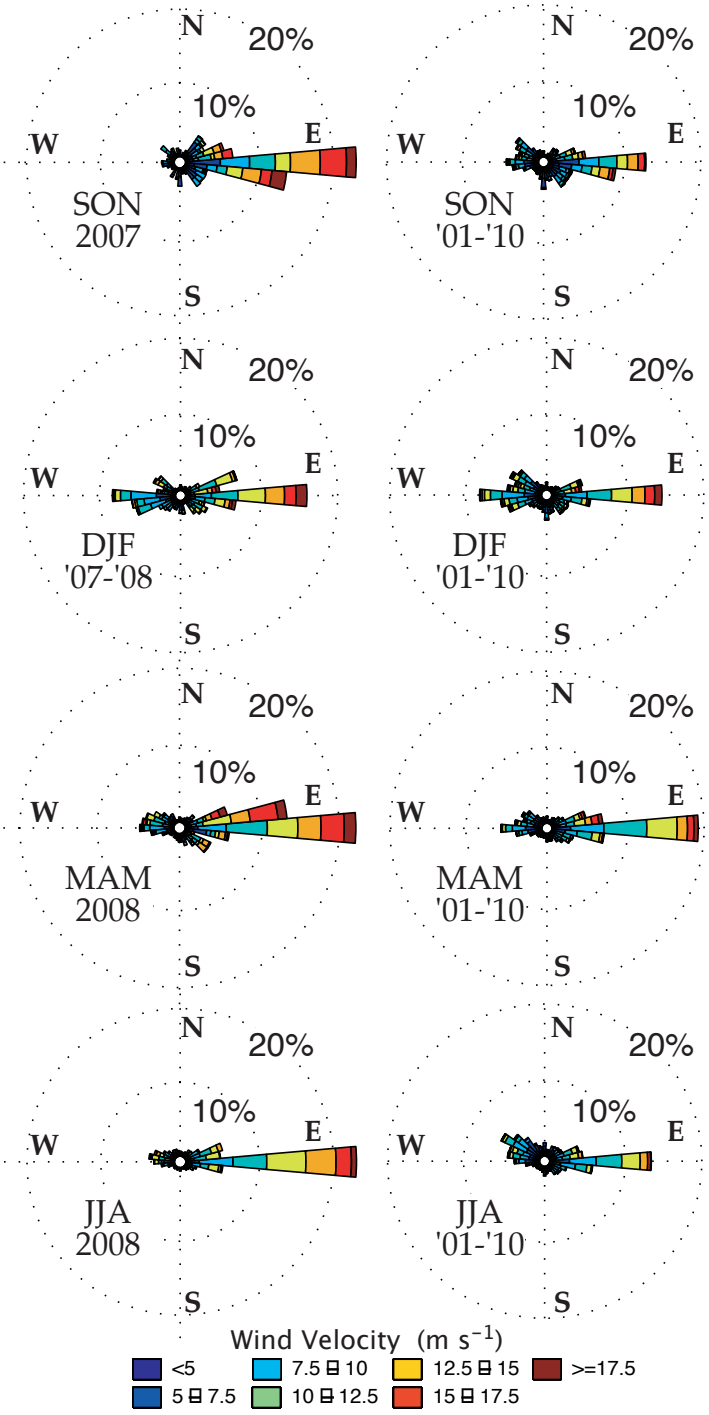

Table 5.1: Estimated impacts of interannual variability in sea ice concentration and wind velocity on air-sea CO_2 flux. Columns 2-5 give seasonal (SON = September, October, November, DJF = December, January February, MAM = March, April May, JJA = June, July, August) mean/standard deviation wind velocities for each year. Columns 6-8 present sea ice concentration data for each year. Columns 9-10 show the total (including the enhanced fluxes in winter) and winter flux (respectively). Columns 11–12 show the difference in total flux relative to 2007–08 if only one of ice or wind is allowed to vary.

Year	SON U mean (std)	DJF U mean (std)	MAM U mean (std)	JJA U mean (std)	Freeze Up Date	Break Up Date	Winter C_i mean (std)	$F_{CO_{2as}}$ Both Vary	$F_{CO_{2enh}}$ Both Vary	$F_{CO_{2as}}$ Ice Vary	$F_{CO_{2as}}$ Wind Vary
2000–01	5.2 (2.9)	5.6 (3.7)	5.2 (2.8)	4.6 (2.8)							0.73
2001–02	5.6 (3.7)	5.1 (3.4)	4.9 (3.1)	4.3 (2.6)							0.76
2002–03	6.1 (3.9)	5.2 (3.3)	4.5 (3.3)	3.9 (2.6)	15-Oct	17-Apr	0.962 (0.064)	-12.2	-21.2	-3.2	0.6
2003–04	5.6 (3.5)	6.1 (3.6)	5.7 (3.8)	4.2 (3.1)	01-Nov	25-May	0.980 (0.038)	-6.0	-7.6	2.9	0.7
2004–05	5.2 (3.6)	6.4 (3.8)	6.0 (3.7)	4.6 (2.8)	26-Oct	10-May	0.957 (0.060)	-9.5	-14.0	-0.3	0.6
2005–06	6.4 (3.7)	6.1 (3.6)	5.1 (2.9)	4.4 (2.4)	02-Nov	23-Jun	0.974 (0.041)	-8.9	-11.6	0.2	0.5
2006–07	5.9 (3.5)	6.0 (3.8)	5.4 (3.4)	4.1 (2.5)	12-Nov	04-Jun	0.970 (0.044)	-9.2	-13.4	-0.5	0.7
2007–08	**6.9 (4.6)**	**6.4 (3.6)**	**6.6 (3.9)**	**5.8 (3.2)**	**16-Nov**	**13-May**	**0.967 (0.043)**	**-10.1**	**-15.0**		
2008–09	5.5 (3.2)	5.5 (2.8)	5.1 (2.7)	5.1 (3.1)	08-Nov	10-Jun	0.961 (0.060)	-12.4	-18.1	-3.3	0.4
2009–10	6.1 (3.9)	5.8 (3.3)	6.1 (3.5)	5.4 (2.8)	09-Nov	17-May	0.973 (0.032)	-7.8	-10.8	1.4	0.20

the strength of the enhancement (which ranges from a mean of -7.6 – -21.2 mmol m^{-2} d^{-1}). Obviously, these numbers are somewhat speculative given the nature of our estimation of $F_{CO_{2as:enh}}$. Nevertheless, given the multiple influences that variability in C_i has on $F_{CO_{2as}}$ (including its potential role in contributing to variability in pCO_{2sw}), it is safe to say that interannual variability in C_i plays a dominant role in interannual variability of air–sea CO_2 exchange in the Cape Bathurst polynya region.

5.4.2 Large Scale Atmosphere/Ocean Circulation and CO_2 Fluxes in the Cape Bathurst Polynya

Given the critical role of sea ice, it is interesting to consider the two remarkable events that bookended the 2007–08 year: the record low Arctic sea ice extent in September 2007, and the second–lowest recorded sea ice extent in September 2008 (since eclipsed by the September 2011 minimum). Those events raise the question of whether some of the conditions we observed in the Cape Bathurst polynya were influenced by the same factors that drove hemispheric–scale reductions in sea ice extent.

In Figure 5.7, we show the seasonal sea level pressure in the Arctic during 2007–08, which reveals high pressure on the North American side of the Arctic for most of the year. Intense high–pressure was particularly obvious over the Beaufort Sea in fall 2007 and spring 2008. A strong Beaufort high drives anti–cyclonic circulation, explaining the strong easterly winds that we experienced during these seasons (Figures 5.2, 5.6). It also may explain some of the ice conditions we experienced, in particular the late fall freeze–up and the early spring break–up.

Figure 5.7: Mean seasonal sea level pressure (in mbar) for the Arctic in 2007–08. SON = September, October, November; DJF = December, January, February; MAM = March, April, May; JJA = June, July, August. Data are from the NCEP/NAR reanalysis [Kalnay and co authors, 1996], plotted using the web-based plotting tools of the NOAA/ESRL Physical Sciences Division (Boulder, Colorado).

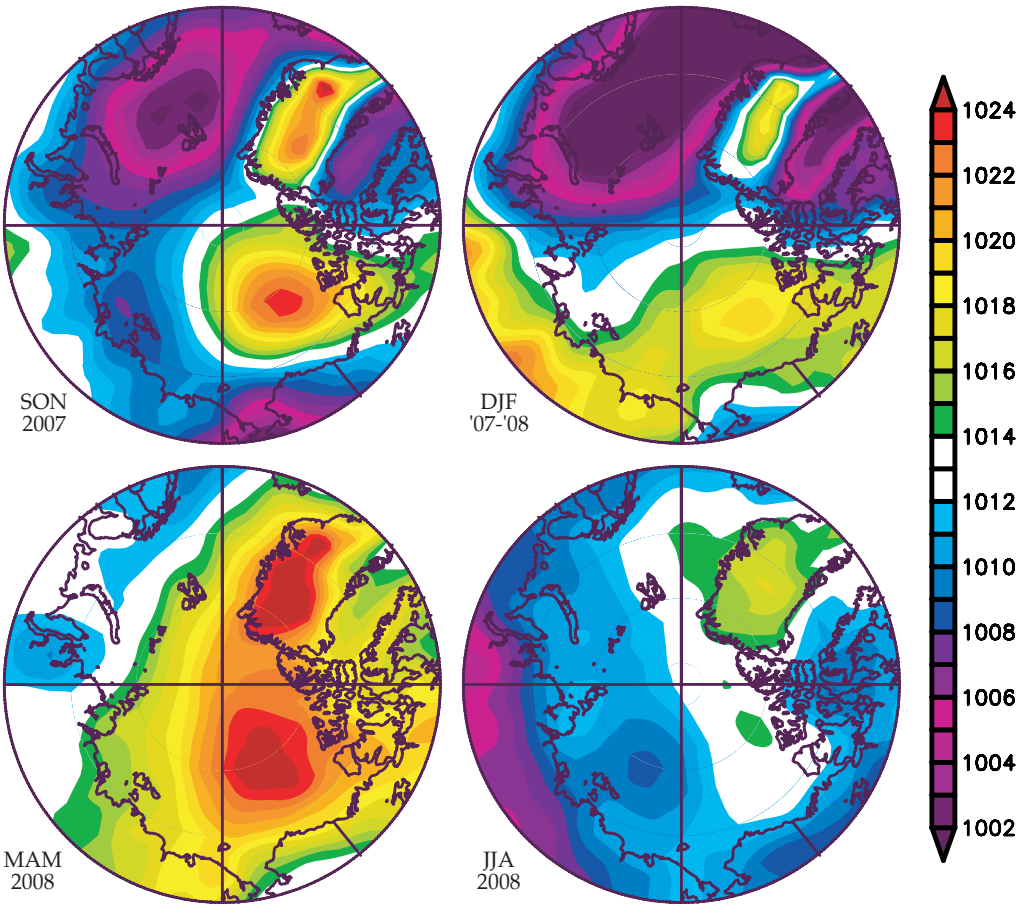

Galley et al. [2009] hypothesized that the spring opening of the Cape Bathurst polynya is largely driven by easterly winds. We investigated this hypothesis using the ice–out dates between 1980–2004 reported by Galley et al. [2008], and found that easterly winds in March–April–May are indeed significantly correlated ($p < 0.01$) with earlier polynya opening dates (r=0.59). It seems likely, therefore, that the early ice free conditions experienced in the spring of 2008 were driven to some extent by winds associated with the high pressure anomaly in the Beaufort Sea.

Although easterly winds in June–July–August are likewise significantly correlated (r=-0.50, $p<0.01$) with later freeze–up dates, the linkage between freeze–up date and large scale pressure variability is more complex. One important control which may drive earlier freeze–up in Amundsen Gulf is the intrusion of an "ice tongue" from the Beaufort pack ice. Galley et al. [2008] show that this ice tongue existed in about 40% of years between 1980–2004, and Galley et al. [2009] proposed that its presence seeds ice formation in Amundsen Gulf, potentially leading to earlier freeze–up. A strong Beaufort high (such as we observed in fall 2007) drives anticyclonic ice motion in the Beaufort Gyre, which moves ice away from the archipelago [Kwok, 2006; Lukovich and Barber, 2006], likely inhibiting the intrusion of this ice tongue. Certainly, archived data from the Canadian Ice Service show there was no ice tongue present in Amundsen Gulf in fall 2007, which may account for the late freeze–up.

Based on this discussion, the timing of open water in the Cape Bathurst polynya was likely linked to pressure patterns in the Beaufort Sea, both through controls on wind forcing in Amundsen Gulf, and through behaviour of sea ice in the Beaufort Gyre. One of the major causes of the anomalous basin–wide conditions in 2007 and 2008 was the persistence of a strong "Dipole Anomaly" (DA), a statistical

description of sea level pressure variability in the Arctic [Overland and Wang, 2010; Wang et al., 2009]. The phase of the DA that persisted for all of 2007 and 2008 is associated with anomalously high pressure on the North American side of the Arctic [Wang et al., 2009], as is apparent in Figure 5.7. Given the important role that this pressure pattern played in influencing our observations in 2007–08, the DA may be useful in explaining conditions in the Cape Bathurst polynya.

If this hypothesis of a link between strong easterly winds, light ice conditions, and a dominant DA is sound, our presence in the Cape Bathurst polynya in 2007–08 was particularly fortuitous. The Arctic ocean appears to have transitioned from a period where the positive phase of the Arctic Oscillation dominates circulation patterns, to one in which the DA is dominant [Maslanik et al., 2007; Overland and Wang, 2005]. Therefore, the 2007–08 CO_2 flux budget that we have calculated for the Cape Bathurst polynya may be representative of the region under contemporary circulation patterns. Although the emergence of the DA is difficult to explain (and thus difficult to predict), it may in part be due climate warming as a result of anthropogenic forcings [Zhang et al., 2008]. If the pattern were to intensify as those forcings intensify, we might predict higher easterly winds, earlier break–up, later freeze–up, and more winter ice motion in the Cape Bathurst polynya, all of which would tend towards an increasing atmospheric CO_2 sink.

5.4.3 Implications at the Circumpolar Scale

Our study area is an example of the many coastal polynyas distributed around the circumpolar Arctic (e.g. Barber and Massom [2007]). If the rates of atmospheric CO_2 uptake that we estimated are similar in other Arctic polynyas, then the Arctic–wide uptake of CO_2 through these features may be significant. Of particular interest

is the winter CO_2 uptake. In the Storfjorden polynya, Omar et al. [2005] estimated a mean winter CO_2 flux of -14.8 mmol m^{-2} d^{-1}, and performed a simple extrapolation to calculate a total winter uptake for all Arctic coastal polynyas of 2.3×10^{12} gC yr^{-1}. Such an uptake is on the same order of magnitude as that observed in many mid– and high–latitude shelf seas [Cai et al., 2006], despite the total area of coastal polynyas being relatively small. The finding is particularly significant, because at least some of the carbon absorbed by this processes is expected to be removed from further exchange with the atmosphere via the formation of deep and intermediate water by brine rejection [Omar et al., 2005].

Our estimated rate of winter uptake for the Cape Bathurst polynya region (-15.1 $\pm$ 10.0 mmol m^{-2} d^{-1}) is remarkably similar to the rates found by Omar et al. [2005], lending support to their theory that polynyas play a significant role in CO_2 sequestration. If we extrapolate our mean winter flux to the same area that Omar et al. [2005] used for coastal polynyas (3.5×10^{10} m^2) and assume a 184–day freezing season (section 5.3.2), we calculate a slightly smaller uptake for Arctic coastal polynyas of 1.2×10^{12} gC yr^{-1}. Even the lower rate of exchange that we estimated can be partly explained by differences between the two regions; the Storfjorden polynya opens periodically through the winter, keeping the mean open water fraction relatively high (7–13%, Skogseth et al. [2005]), while the Cape Bathurst polynya does not experience a large–scale opening until spring, with a lower open water fraction in winter (2–4%, Table 5.1). This illustrates that upscaling will result in an estimate biased by the peculiarities of the model polynya, but our results support Omar et al. [2005]'s conclusion that their estimate is of the right order of magnitude.

We caution, however, that further investigations are required to confirm if negative ΔpCO_2 throughout the winter is a typical state for Arctic polynya regions. Along the southern margins of Amundsen Gulf and on the Mackenzie Shelf, we observed episodes of strongly positive ΔpCO_2 associated with wind–driven upwelling events in the late fall [Else et al., 2012a,b]. It is unknown at this time if that upwelling persisted through the winter, but it is quite plausible that certain polynyas may be sustained by upwelling–favourable winds, or that ice motion in a polynya may drive winter upwelling (e.g. McPhee et al. [2005]). Furthermore, evidence of winter supersaturation has been presented for the Northwater polynya [Miller et al., 2002] and in landfast ice near the re–occurring flaw lead north of Point Barrow, Alaska [Semiletov et al., 2007]. If polynya or flaw lead regions with supersaturated winter pCO_{2sw} are in fact widespread, then the CO_2 uptake estimate of Omar et al. [2005] must be offset to some degree by such regions.

During the non–freezing seasons, Arctic shelf seas typically absorb CO_2 at rates between -1.0 to -15 mmol m^{-2} d^{-1} (see for example Table 3 in Else et al. [2008b]). The mean CO_2 uptake rate that we observed (-5.2 $\pm$ 2.0 mmol m^{-2} d^{-1}) is median to that range, although considerable variability in both the magnitude and direction occurred over the ice–free season (Figure 5.3). Our results thus reinforce the paradigm that, with a few notable exceptions (e.g. Anderson et al. [2009]), Arctic shelf seas generally absorb atmospheric CO_2 during non–freezing seasons [Bates and Mathis, 2009].

5.5 Summary and Conclusions

The potential role of polynya regions as atmospheric CO_2 sinks has long been acknowledged [Yager et al., 1995], but opportunities for thorough investigation have

been rare. This study shows that the Cape Bathurst polynya region does indeed act as a strong CO_2 sink, but not entirely for the reasons that Yager et al. [1995] suggested. They hypothesized that in spring–opening polynya regions, potential winter outgassing would be prevented by a sea ice cover. In contrast, we found that in the presences of a broken and mobile ice cover, a persistently negative ΔpCO_2 coupled with an enhanced rate of gas exchange allowed CO_2 uptake through the winter at a mean rate in excess of the open water seasons. When combined with the exchange that occurred through the other seasons, our calculated mean annual rate of CO_2 uptake for this region was approximately 3 times higher than the preliminary estimate of Shadwick et al. [2011].

An investigation into interannual variability of the conditions responsible for CO_2 exchange revealed that anomalously strong winds during 2007–08 likely enhanced CO_2 uptake relative to the decadal mean. Further adding to the strong uptake were light ice conditions, characterized by a late freeze–up (by ∼3 weeks) and early breakup (by ∼4 weeks). The light ice conditions may have been caused in part by the strong easterly winds, and in turn appeared to influence the pCO_{2sw} cycle. Both the wind and ice conditions that we observed in 2007-08 were likely controlled by a strong north–south pressure gradient, a characteristic of the Arctic Dipole phase that was particularly strong through the study period. If that phase of the Arctic Dipole pattern becomes the norm for the Arctic (as recent observations suggest), then the mean annual CO_2 flux we estimated for 2007–08 may be quite representative of current and future air–sea CO_2 exchange in the region.

Net annual uptake of atmospheric CO_2 by the Cape Bathurst polynya region agrees with the paradigm that most Arctic shelf seas act as sinks for atmospheric CO_2. Bates and Mathis [2009] estimated that the Arctic Ocean absorbs 0.6–1.9

$\times 10^{14}$gC yr^{-1} during the open water seasons, and our estimated open water CO_2 fluxes are within the range of observations used to arrive at that conclusion. More interestingly, our study also supports an emerging school of thought that the Arctic Ocean may absorb a significant amount of CO_2 during the winter. Although initial order–of–magnitude estimates indicate that the total winter flux is smaller than the open water flux (10^{12}gC yr^{-1} vs. 10^{14}gC yr^{-1}), the area through which this exchange occurs is smaller by a similar magnitude. Thus, if the area of winter open water increases, absorption of CO_2 via this pathway could become more significant. The potential for increased winter open water is a distinct possibility, given the recent decline of multi–year ice [Maslanik et al., 2011], drastic decreases in summer sea ice extent (e.g. Stroeve et al. [2007]), and observations of increased winter ice motion [Hakkinen et al., 2008]. However, testing of this hypothesis requires a better understanding of the flux enhancements that occur in winter open water features, and an extensive survey of winter ΔpCO_2 throughout the Arctic.

Chapter 6

Summary and Conclusions

6.1 Summary of Major Findings

Major Finding 1: Enhanced air–sea CO_2 exchange can occur in winter leads.

The first results chapter of this thesis (Chapter 2) focused on ship–based eddy covariance measurements of air–sea CO_2 exchange collected during a late fall/early winter occupation of western Amundsen Gulf in 2007–08. The measurements revealed strong (1–2 orders of magnitude higher than expected) fluxes of CO_2 associated with lead events, typically directed towards the surface. High rates of CO_2 exchange in such environments had previously been inferred from water column observations [Anderson et al., 2004] and tank studies [Loose et al., 2009], but our work provided the first real–time observation of the effect in a natural environment.

Based on ancillary observations and current understandings of gas transfer at water surfaces, we hypothesized that high water side turbulence (driven by wind, brine rejection, and surface instability) is likely driving this effect, with modification of the chemical properties of the surface (solubility, CO_2 concentration) also potentially playing a role.

A preliminary extrapolation of the eddy covariance measurements showed that CO_2 uptake through leads in the region may be of a similar order of magnitude to the uptake that occurs during the ice free months. Although very high, we were able to show that the amount of air–sea CO_2 exchange occurring during these months fits within dissolved inorganic carbon budgets for the region.

Major Finding 2: Annual cycles of pCO_{2sw} in polynya regions are more complex than previous studies have suggested.

In Chapter 3 we described pCO_{2sw} measurements made in Amundsen Gulf and the Mackenzie and Banks Island Shelves. The study used the first ever year–long pCO_{2sw} dataset collected in a polynya region to provide a comprehensive test of the Yager et al. [1995] "seasonal rectification" hypothesis of air–sea CO_2 exchange. It also provided context for the fluxes that we measured in Chapter 2, and allowed us to examine the processes important in controlling pCO_{2sw} over an annual cycle.

In Amundsen Gulf, we found that pCO_{2sw} was undersaturated with respect to the atmosphere at freeze–up, likely due to surface water cooling and fall phytoplankton blooms. Through the winter a gradual under–ice accumulation of pCO_{2sw} occurred as a result of biological respiration, air–sea gas exchange and rejection of carbon–rich brine, but saturation was never reached. In late March the beginnings of an ice algae phytoplankton bloom began to reduce pCO_{2sw}, and as ice was exported out of the region an open water bloom was initiated, resulting in fairly strong undersaturation at the start of the open water season. This undersaturation was eroded through the summer as sea surface temperature warmed by about 10°C, and we observed a brief, low–magnitude supersaturation in mid–July.

We observed a similar cycle on the Banks Island Shelf, but significantly different processes occurred on the Mackenzie Shelf. In fall of 2007 we found high–magnitude

supersaturations along the Mackenzie Shelf, which we were able to identify as the result of wind–driven shelf break upwelling. In the spring and summer, $p\mathrm{CO}_{2sw}$ was lower over most of the Mackenzie Shelf in comparison to Amundsen Gulf, potentially as a result of higher nutrient supply from upwelling and riverine sources. One exception to this general pattern was supersaturation near the coast, where the influence of heterotrophic river water was strongest.

The combined results of this Chapter and Chapter 2 show that the seasonal rectification hypothesis does not hold in the southeastern Beaufort Sea. We found significant deviations from this simple model in all three regions, and furthermore found distinct differences between each of the regions despite their close geographic proximity. These results show that we cannot expect to use a "one–size–fits–all" model for air–sea CO_2 exchange in polynya regions, and that many processes which influence $p\mathrm{CO}_{2sw}$ need to be considered to assess the annual CO_2 budget of a given region.

Major Finding 3: The seasonal evolution of $p\mathrm{CO}_{2sw}$ along landfast ice edges in Amundsen Gulf is complex, but suggests net annual uptake of atmospheric CO_2.

In Chapter 4, we extended the results and discussion of Chapter 3 into the landfast ice regions surrounding Amundsen Gulf. These regions were studied less frequently, but experienced very different ice and $p\mathrm{CO}_{2sw}$ cycles, allowing for additional insights into the nature of air–sea carbon cycling in coastal Arctic seas.

Similar to the Mackenzie Shelf, we found strong fall $p\mathrm{CO}_{2sw}$ supersaturations associated with wind–driven coastal and ice edge upwelling. This supersaturation would have permitted a certain amount of CO_2 outgassing during the fall, although it is difficult to quantify its significance. It is possible that the enhanced exchange

that we observed in Chapter 2 was occurring in these regions, but the formation of landfast ice by late November would have limited such exchange to a relatively short time period.

When we returned to the region in May we once again encountered supersaturated pCO_{2sw}, which was either remnant from the fall, or the result of a subsequent upwelling event. Again, the presence of landfast ice probably restricted any significant outgassing. Further interesting results were obtained in June, when we observed the ice edges as they decayed. In early June, pCO_{2sw} was significantly undersaturated as a result of biological production and the beginnings of dilution from ice melt. Following a brief episode of supersaturation (driven by yet another short–lived upwelling event), we observed a strong influence of ice melt, which resulted in some of the lowest pCO_{2sw} readings that we measured throughout the entire field project. This effect (coupled with strong under–ice biological production) conditioned the sea surface for strong CO_2 uptake when the sea ice finally began to break up in late June.

The cycle of suppression of outgassing during late fall and early spring followed by strong uptake through the summer is reminiscent of the seasonal rectification hypothesis proposed by Yager et al. [1995]. However, it does not match well with other studies of pCO_{2sw} in landfast ice regions, which typically show persistent undersaturation throughout the year [Gibson and Trull, 1999; Sejr et al., 2011]. That discrepancy forced us to consider whether the conditions which drove spring and fall upwelling were typical for the region. An analysis of wind and pressure patterns in 2007–08 compared to the long term average suggest that particularly strong easterly winds occurred during the study year, possibly making the upwelling anomalous.

Major Finding 4: The Cape Bathurst polynya region was a remarkably effective CO_2 sink in 2007–08, due in part to strong winds and light ice conditions.

In Chapter 5, we once again focused on offshore Amundsen Gulf, combining the results of Chapters 2 and 3 to derive an annual air–sea CO_2 exchange budget for the Cape Bathurst polynya region. The budget combined a rough estimate of enhanced winter gas exchange with conventional methods of estimating air–sea gas exchange in the open water season. The results of the exercise showed that the Cape Bathurst polynya region was indeed a significant net annual sink of CO_2 in 2007–08. By including the rough estimate of winter air–sea gas exchange, our estimate of net annual uptake more than doubled a preliminary estimate made by our collaborators [Shadwick et al., 2011]. The results compare well with estimates made for a polynya in Svalbard by Omar et al. [2005], lending support to their theory that coastal polynyas around the circumpolar Arctic may constitute an important sink for atmospheric CO_2.

In this Chapter, we further investigated the idea that 2007–08 may have been a somewhat anomalous year. By comparing ice, wind, and pCO_{2sw} conditions to observations made over the past decade, we found that 2007–08 was indeed an anomalously windy year, which resulted in "light" ice conditions characterized by a late freeze–up and early break–up. Although limited, past observations of pCO_{2sw} suggest that the pCO_{2sw} cycle that we observed in 2007–08 was typical for the region, at least in years with similar ice conditions. We showed that the strong winds and light ice conditions may have been linked with a mode of climate variability known as the "Arctic Dipole," which existed in a strong phase throughout the study period. This Arctic Dipole pattern has been cited as a potentially emerging signal of high–

latitude climate change, and it is therefore possible that the conditions that we observed in 2007–08 may become normal (or may even become amplified) in the future.

6.2 Limitations and Future Work

Although Chapter 2 contains some of our most significant results, it is also the Chapter which was most severely limited by sampling constraints. Although eddy covariance instrumentation was deployed through the duration of the field program (October 2007 to August 2008), the only useful results were obtained between November 2007 – January 2008. To understand why, it is instructive to note that past measurements of air–sea CO_2 exchange (conducted at lower latitudes) reveal fluxes that are extremely low in comparison to more commonly measured terrestrial surfaces. Although it is not often discussed in the literature, these flux magnitudes are at the low end of the detection capabilities of commonly used instruments. In an Arctic open ocean environment, the cold surface water reduces fluxes by about half in comparison to lower latitudes (due to the Schmidt number dependency), pushing instruments even closer to their detection limits. To compound this problem, the environment amplifies several sources of noise, including heating of the open path gas analyzer, salt and rime deposition, and ship motion. We found that only the exceptionally strong fluxes associated with leads could be detected above this noise, limiting our results to those instances. Retrievable data were further limited by the failure of the LI-7500 device in February, 2008. Although we attempted many modifications to the eddy covariance equipment on subsequent field projects, there are still several avenues of improvement that we can work towards. The use of short–line closed path systems (such as the commercially available LI-7200) may help solve

some of the instrument heating and salt/rime deposition problems, while retaining many of the benefits of an open path system. Noise in such systems could be also be reduced by heating and drying the sample line. Also, the use of instruments employing cavity ring–down spectroscopy should be investigated. These instruments use mirrors to extend the path length of a near–infrared beam to several kilometres (as opposed to several centimetres), allowing for much more precise measurements, and possibly better detection of low–level CO_2 fluctuations.

Chapter 2 was also limited in its ability to relate the high CO_2 flux measurements to physical and chemical processes occurring at the surface. This is of course largely due to the logistical difficulty of sampling the open water of a cold, windy, and treacherous lead, but we also simply did not have equipment to measure some parameters that may be of interest. In the future, we should work towards examining the hypothesis that turbulence in leads is particularly high. The instrumental challenges could be addressed by using high–precision infrared videography techniques (e.g. Jessup et al. [2009]) or microscale turbulence profilers (e.g. Zappa et al. [2009]), while the logistical challenges could perhaps be first addressed with ice tank studies. We also need to refine our abilities to measure parameters such as temperature, salinity and pCO_{2sw} in the surface microlayer of leads. Once again, the adaptation of existing technologies coupled with laboratory tests could be helpful in achieving those goals.

In Chapters 3 and 4, our main limitations were caused by the infrequent sampling of the Banks Island Shelf, the Mackenzie Shelf, and the landfast ice regions. These limitations were inevitable in a project that attempted to cover such a broad spatio–temporal regime, but they nevertheless restricted our understandings of pCO_{2sw} cycles, and made it difficult to estimate annual air–sea CO_2 exchange budgets in

those regions. In both the Mackenzie Shelf and Amundsen Gulf landfast ice regions, it would be useful in the future to try and collect winter observations of pCO_{2sw}. Such observations may allow us to better understand if upwelled CO_2 rich waters persist for long periods of time, or if they sink back to depth once the wind forcing is removed. Given the potential for enhanced exchange throughout the winter, the persistence of this water on the Mackenzie Shelf may be an important factor in the region's source/sink status.

Chapter 5 was most strongly limited by uncertainties in the parameterization of air–sea CO_2 fluxes in Arctic seas. In order to estimate the winter contribution to the annual CO_2 budget, we were forced to rely on a simple arithmetic extrapolation of the measured eddy covariance fluxes. If future work can better understand the relationship between enhanced gas exchange and surface processes, then we may eventually be able to work towards more physically meaningful upscaling. Another limitation of this Chapter is that the role of sea ice on air–sea gas exchange in non–freezing seasons is also uncertain. In situations where the sea surface is composed of a mixture of open water and drifting floes, the presence of sea ice must have an effect on sea surface turbulence through reduced fetch (e.g. Woolf [2005]) and wave–ice interactions (e.g. Masson and LeBlond [1989]). In current air–sea gas exchange parameterizations, the effect of those processes are unquantified. The development of better parameterizations of air–sea gas exchange is quite possibly the most important knowledge gap that future studies should address, especially since the problem has important implications for gases other than CO_2.

6.3 Conclusions: A New Paradigm for Air–Sea CO_2 Cycling in Arctic Polynyas

Prior to this work, the existing paradigm of air–sea carbon cycling in Arctic polynya regions called for strong uptake of CO_2 in the open water season (driven by spring phytoplankton blooms and a windy fall season), and then a restriction of potential winter outgassing by the sea ice cover [Yager et al., 1995]. Our results show that this simple model is insufficient for our study region. In western Amundsen Gulf (where we have the most complete picture), we found persistent undersaturation of pCO_{2sw}, with the exception of a brief period of supersaturation in late summer. We also found evidence that air–sea gas exchange is surprisingly active through the winter via enhanced gas exchange through leads. By incorporating this effect into an estimate of the annual air–sea carbon exchange budget for the region, we found that a similar magnitude of CO_2 uptake can occur in both the winter and open–water seasons.

Given that other recent studies have found similar cycles of pCO_{2sw} [Gibson and Trull, 1999; Sejr et al., 2011] and enhanced winter gas exchange [Anderson et al., 2004; Omar et al., 2005], is the evidence pointing us towards a new paradigm of CO_2 exchange in seasonally ice covered Arctic seas? If we are referring to a paradigm where we consider Arctic seas to experience predominantly undersaturated pCO_{2sw} and strong CO_2 uptake through most of the year, then the answer is no. Evidence from the other regions that we studied show that significant spatial variability can exist, even between regions in close geographic proximity to one another. Both the landfast ice regions of southern Amundsen Gulf and broad expanses of the the Mackenzie Shelf region experienced episodes of wind–driven upwelling which caused

significantly elevated pCO_{2sw}. In addition, we observed supersaturated pCO_{2sw} in the near–shore areas of the Mackenzie Shelf as a result of river input. Thus, the new paradigm that this work is pointing towards is one in which many processes (i.e. timing of phytoplankton/ice algae blooms, sea surface temperature and salinity cycles, upwelling, continental shelf processes, and enhanced winter gas exchange), need to be considered in order to understand the source/sink status of a given Arctic region.

The advantage of this paradigm is that it allows us to see more starkly the multi–faceted impacts that climate change may have on air–sea carbon cycling in the Arctic. A warmer [Steele et al., 2008], fresher [McPhee et al., 2009; Morison et al., 2012] Arctic ocean may result in stronger summer supersaturations (Chapter 3), and a reduced capacity to absorb CO_2. A retreat of seasonal sea ice beyond the continental shelf break may permit enhanced upwelling along certain shelves [Carmack and Chapman, 2003; Tremblay et al., 2011], with the potential to elevate pCO_{2sw} in the spring and fall (Chapters 3 and 4). A lengthened phytoplankton growing season [Arrigo et al., 2008; Pabi et al., 2008], particularly one that extends into the fall, may help reduce pCO_{2sw} prior to freeze–up (Chapter 3). Increased winter ice motion [Hakkinen et al., 2008] and an increased seasonal ice area due to ice retreat (e.g. Comiso et al. [2008]) may make enhanced gas exchange associated with new ice formation (Chapter 2) increasingly relevant. Changing ice and atmospheric circulation patterns (e.g. Wang et al. [2009]; Zhang et al. [2008]) may cause later ice formation and earlier breakup in some regions, permitting a longer season for air–sea gas exchange (Chapter 5). These processes are likely already having a significant impact on air–sea CO_2 exchange in the Arctic, and can be expected to exert an increasing influence in the future.

Working from this paradigm also allows us to identify the research that remains for the future. One of the main results of this work is that fall, winter, and early spring processes are very important in annual air–sea carbon budgets of Arctic seas. A series of questions therefore emerges regarding the air–sea CO_2 gradient during these time periods. For example, how widespread is persistent winter undersaturation of pCO_{2sw} in the Arctic? Can upwelling sustain supersaturated pCO_{2sw} in the winter season in some regions? Is pCO_{2sw} undersaturation at ice breakup common? If we can better understand these processes that control the air–sea CO_2 gradient, then we will also want to better understand how we can estimate the magnitude of exchange that occurs across that gradient. This raises a series of questions regarding gas exchange enhancement in polar seas. For example, what processes are actually responsible for this enhancement? Are those processes ubiquitous in freezing sea ice? Can we eventually develop parameterizations to create a better method of estimating enhanced gas exchange? Both of these avenues of research – into the processes that set the potential for air–sea CO_2 exchange in the polar winter, and the processes that determine the rate at which it occurs – will demand considerable ingenuity and effort from future researchers.

Appendix A: Contributions of Authors to Thesis Chapters

Chapter 2

In this Chapter, I collected much of the field data and processed the eddy covariance and pCO_{2sw} data. The ideas for presenting the results and the ensuing discussion were largely my own. With the exception of the methods section on RADARSAT-1 imagery, all of the writing is my own. Tim Papakyriakou provided expertise and discussion regarding eddy covariance, and logistical and financial support for the field work. Ryan Galley performed RADARSAT-1 analysis, wrote the methods section on RADARSAT-1 imagery, and helped with the interpretation and presentation of RADARSAT-1 images. Will Drennan provided technical support for correction of eddy covariance data for ship motion effects. Lisa Miller and Helmuth Thomas reviewed the manuscript, and provided expertise regarding the DIC budget implications of our results.

Chapter 3

In this chapter, I collected much of the field data and processed the pCO_{2sw} data. The ideas for presenting the results and the ensuing discussion were largely my own. All of the writing is my own. Tim Papakyriakou provided expertise and discussion regarding the results, and logistical and financial support for the field work. Ryan

Galley provided discussion and expertise regarding sea ice conditions in the study area, created Figure 3.7, and assisted with Figure 3.8. Al Mucci and Lisa Miller provided very valuable reviews of early manuscript drafts, which helped shape the presentation and discussion of results. Michel Gosselin provided chlorophyl-a data, and helped with interpretation of those results. Elizabeth Shadwick and Helmuth Thomas provided seawater carbonate system data and helped with the interpretation of those results.

Chapter 4

In this chapter, I collected much of the field data and processed the pCO_{2sw} data. The ideas for presenting the results and the ensuing discussion were largely my own. All of the writing is my own. Ryan Galley provided expertise regarding landfast sea ice conditions in the region, created Figures 4.2, 4.4 and 4.5, and provided comments on manuscript drafts. Tim Papakyriakou provided expertise and discussion regarding the results, and logistical and financial support for the field work. Al Mucci and Lisa Miller provided very valuable reviews of early manuscript drafts, which helped shape the presentation and discussion of results. Dave Barber provided financial support for Ryan Galley, and provided reviews of manuscript drafts.

Chapter 5

In this chapter, I collected the various data products and performed the flux calculations myself. The ideas for presenting the results and the ensuing discussion were largely my own. All of the writing is my own. Tim Papakyriakou provided expertise and discussion regarding the results, and logistical and financial support for the analysis. Matthew Asplin and Ryan Galley provided discussion regarding atmosphere and ice conditions, respectively. Lisa Miller and Al Mucci provided

external reviews and useful comments on manuscript drafts. Dave Barber provided financial support for Ryan Galley, and provided reviews of manuscript drafts.

Appendix B: Additional Contributions to the Peer Reviewed Literature

In addition to the four papers contained in the body of this thesis, I also co–authored seven peer–reviewed articles. The articles and my contributions are detailed below.

Geilfus, N.-X., Carnat, G., Papakyriakou, T.N., Tison, J.-L., **Else, B.**, Thomas, H., and E. Shadwick (2012). pCO_2 dynamics and related air-ice CO_2 fluxes in the Arctic coastal zone (Amundsen Gulf, Beaufort Sea). *Journal of Geophysical Research*, 117, C00G10, doi: 10.1029/JC007118.

In this paper, I assisted the lead author with field sampling, and provided comments and suggestions on manuscript drafts.

Rempillo, O., Seguin, A., Norman, A.-L., Scarratt, M., Michaud, S., Sjostedt, S., Abbatt, J., **Else, B.**, Papakyriakou, T., Sharma, S., Grasby, S., and M. Levasseur (2011). DMS air-sea fluxes and biogenic sulfur as a source of new aerosols in the Arctic Fall. *Journal of Geophysical Research*, 116, D00S04, doi: 10.1029/2011JD016336.

In this paper, I provided expertise regarding the air–sea exchange of gases in Arctic environments. I also provided processed, quality controlled wind velocity data (collected in the field) to allow calculation of air–sea DMS exchange.

Galley, R.J., **Else, B.G.T.**, Lukovich, J., Howell, S. and D. Barber (in press). Fast ice in the Canadian Arctic: 1983-2009. Accepted to *Arctic*, MS# 11-148

In this paper, I helped the lead author with the writing of the manuscript, and provided comments on the presentation and interpretation of results.

Galley, R.J., **Else, B.G.T.**, Prinsenberg, S.J. and D. Barber (in review). Summer sea ice concentration, motion and thickness near areas of proposed offshore oil and gas development in the Canadian Beaufort Sea - 2009. Submitted to *Arctic*, October 2011, MS# 11-175.

In this paper, I helped the lead author conceptualize the work, in addition to helping with the writing and editing of the manuscript. I also collaborated with the lead author to help come up with effective ways to present the ideas contained within the manuscript.

Miller, L.A., Carnat, G., **Else, B.G.T.**, Sutherland, N. and T. Papakyriakou (2011). Carbonate system evolution in autumn sea ice. *Journal of Geophysical Research*, 116, C00G04, doi:10.1029/2011JC007143.

I was heavily involved in the data collection for this paper, and provided significant comments and suggestions on manuscript drafts.

Shadwick, E.H., Thomas, H., Chierici, M., **Else, B.**, Fransson, A., Michel, C., Miller, L.A., Mucci, A., Niemi, A., Papakyriakou, T.N., and J.-É. Tremblay (2011). Seasonal variability of the inorganic carbon system in the Amundsen Gulf region of the southeastern Beaufort Sea. *Limnology and Oceanography* 56(1), 303-322, doi:10.4319/lo.2011.56.1.0303.

In this paper, I provided quality controlled, processed pCO_{2sw} field data which I played a significant role in collecting. I also provided comments and suggestions on draft manuscripts.

Mundy, C.J., Gosselin, M., Ehn J., Gratton, Y., Rossnagel, A., Barber, D.G., Martin, J., Tremblay, J.-É., Palmer, M., Arrigo, K., Darnis, G., Fortier, L., **Else, B.**, and T. Papakyriakou (2009). Contribution of under-ice primary production to an ice-edge upwelling phytoplankton bloom in the Canadian Beaufort Sea. *Geophysical Research Letters*, Vol. 36, L17601, doi:10.1029/2009GL038837.

In this paper, I provided a figure illustrating the wind velocity and direction recorded in the field during an ice–edge upwelling event.

References

ACIA (2004). *Impacts of a warming Arctic: Arctic climate impact assessment*. Cambridge University Press. 3

Amiro, B. (2010). Estimating annual carbon dioxide eddy fluxes using open-path analysers for cold forest sites. *Agricultural and Forest Meteorology*, 150(10):1366–1372, doi:10.1016/j.agrformet.2010.06.007. 21

Anctil, F., Donelan, M. A., Drennan, W. M., and Graber, H. C. (1994). Eddy-correlation measurements of air-sea fluxes from a discus buoy. *Journal of Atmospheric and Oceanic Technology*, 11:1144–1150. 21

Anderson, L. G., Falck, E., Jones, E. P., Jutterström, S., and Swift, J. H. (2004). Enhanced uptake of atmospheric CO_2 during freezing of seawater: A field study in Storfjorden, Svalbard. *Journal of Geophysical Research*, 109:C06004, doi:10.1029/2003JC002120. 4, 13, 38, 82, 122, 127, 133, 149, 157

Anderson, L. G., Jutterström, S., Hjalmarsson, S., Wåhlström, I., and Semiletov, I. P. (2009). Out-gassing of CO_2 from Siberian Shelf seas by terrestrial organic matter decomposition. *Geophysical Research Letters*, 36:L20601, doi:10.1029/2009GL040046. 77, 88, 146

Anderson, L. G., Tanhua, T., Björk, G., Hjalmarsson, S., Jones, E. P., Jutterström, S., Rudels, B., Swift, J. H., and Wåhlstöm, I. (2010). Arctic Ocean shelf-basin interaction: an active continental shelf CO_2 pump and its impact on the degree of calcium carbonate solubility. *Deep Sea Research Part I: Oceanographic Research Papers*, 57:869–879, doi:10.1016/j.dsr.2010.03.012. 53, 63, 82

Andreas, E. L. (1980). Estimation of heat and mass fluxes over arctic leads. *Monthly Weather Review*, 108:2957–2063. 46

ArcticNet (2010). Impacts of environmental change in the Canadian Coastal Arctic: A compendium of research conducted during ArcticNet Phase I (2004–2008). 94, 123

Arrigo, K. R., van Dijken, G., and Pabi, S. (2008). Impact of a shrinking Arctic ice cover on marine primary production. *Geophysical Research Letters*, 35(19):L19603, doi:10.1029/2008GL035028. 3, 89, 158

Arrigo, K. R. and van Dijken, G. L. (2004). Annual cycles of sea ice and phytoplankton in Cape Bathurst polynya, southeastern Beaufort Sea, Canadian Arctic. *Geophysical Research Letters*, 31:L08304, doi:10.1029/2003GL018978. 56, 67, 82

Asher, W. E., Karle, L. M., Higgins, B. J., Farley, P. J., Monahan, E. C., and Leifer, I. S. (1996). The influence of bubble plumes on air-seawater gas transfer velocities. *Journal of Geophysical Research*, 101(C5):12,027–12,041, doi:10.1029/96JC00121. 12

Barber, D. G., Asplin, M. G., Gratton, Y., Lukovich, J. V., Galley, R. J., Raddatz, R. L., and Leitch, D. (2010). The International Polar Year (IPY) Circumpolar Flaw Lead (CFL) System Study: Overview and the physical system. *Atmosphere–Ocean*, 48(4):225–243, doi:10.3137/OC317.2010. 58, 94, 123

Barber, D. G. and Massom, R. A. (2007). The role of sea ice in Arctic and Antarctic polynyas. In Smith Jr, W. O. and Barber, D. G., editors, *Polynyas: Windows to the World*, volume 74 of *Elsevier Oceanography Series*, pages 1–54. Elsevier. 51, 52, 80, 121, 144

Bates, N., Moran, S., Hansell, D., and Mathis, J. (2006). An increasing CO_2 sink in the Arctic Ocean due to sea–ice loss. *Geophysical Research Letters*, 33:L23609,doi:10.1029/2006GL027028. 3, 47

Bates, N. R., Cai, W. J., , and Mathis, J. T. (2011). The ocean carbon cycle in the western Arctic Ocean: Distributions and air–sea fluxes of carbon dioxide. *Oceanography*, 24(3):186–201, doi:10.5670/oceanog.2011.71. 77, 79

Bates, N. R. and Mathis, J. T. (2009). The Arctic Ocean marine carbon cycle: evaluation of air-sea CO_2 exchanges, ocean acidification impacts and potential feedbacks. *Biogeosciences*, 6(11):2433–2459 , doi:10.5194/bg–6–2433–2009. 3, 89, 134, 146, 147

Bates, N. R., T, M. J., and Cooper, L. W. (2009). Ocean acidification and biologically induced seasonality of carbonate mineral saturation states in the western Arctic Ocean. *Journal of Geophysical Research*, 114:C11007, doi:10.1029/2008JC004862. 84

Bock, E. J., Hara, T., Frew, N. M., and McGillis, W. R. (1999). Relationship between air sea gas transfer and short wind waves. *Journal of Geophysical Research*, 104(C11):25,821–25,831, doi:10.1029/1999JC900200. 11

Bolin, B. (1960). On the exchange of carbon dioxide between the atmosphere and the sea. *Tellus*, 12(3):274–281. 12

Borges, A. V., Delille, B., and Frankignoulle, M. (2005). Budgeting sinks and sources of CO_2 in the coastal ocean: Diversity of ecosystems counts. *Geophysical Research Letters*, 32(14):L14601, doi:10.1029/2005GL023053. 52, 134

Bourgault, D., Hamel, C., Cyr, F., Tremblay, J. E., Galbraith, P. S., Dumont, D., and Gratton, Y. (2011). Turbulent nitrate fluxes in the Amunsen Gulf during ice-covered conditions. *Geophysical Research Letters*, 38:L15602, doi:10.1029/2011GL047936. 40

Bourgault, D., Kelley, D. E., , and Galbraith, P. S. (2008). Turbulence and boluses on an internal beach. *Journal of Marine Research*, 66:563–588, doi:10.1357/002224008787536835. 40

Brugel, S., Nozais, C., Poulin, M., Tremblay, J. E., Miller, L. A., Simpson, K. G., Gratton, Y., and Demers, S. (2009). Phytoplankton biomass and production in the southeastern Beaufort Sea in autumn 2002 and 2003. *Marine Ecology Progress Series*, 377:63–77, doi:10.3354/meps07808. 56, 59, 67, 82

Burba, G. G., McDermitt, D. K., Grelle, A. G., Anderson, D. J., and Xu, L. (2008). Addressing the influence of instrument surface heat exchange on the measurements of CO_2 flux from open-path gas analyzers. *Global Change Biology*, 14(8):14(8):1854–1876, doi:10.1111/j.1365–2486.2008.01606.x. 21, 22

Cai, W., Chen, L., Chen, B., Gao, Z., Lee, S., Chen, J., Pierrot, D., Sullivan, K., Wang, Y., Hu, X., Huang, W.-J., Zhang, Y., Xu, S., Murata, A., Grebmeier, J. M., Jones, E. P., and Zhang, H. (2010). Decrease in the CO_2 uptake capacity in an ice-free Arctic Ocean basin. *Science*, 329(5991):556–559, doi:10.1126/science.1189338. 3, 47

Cai, W. J., Dai, M., and Wang, Y. (2006). Air-sea exchange of carbon dioxide in ocean margins: A province-based synthesis. *Geophysical Research Letters*, 33(12):L12603, doi:10.1029/2006GL026219. 52, 134, 145

Carmack, E. and Chapman, D. C. (2003). Wind-driven shelf/basin exchange on an Arctic shelf: The joint roles of ice cover extent and shelf-break bathymetry.

Geophysical Research Letters, 30(14):L1778, doi:10.1029/2003GL017526. 70, 71, 78, 88, 158

Carmack, E. C. and Macdonald, R. W. (2002). Oceanography of the Canadian Shelf of the Beaufort Sea: a setting for marine life. *Arctic*, 55:29–45. 54, 74

Carmack, E. C., Macdonald, R. W., and Jasper, S. (2004). Phytoplankton productivity on the Canadian Shelf of the Beaufort Sea. *Marine Ecology Progress Series*, 277:37–50. 54, 74, 79

Carmack, E. C., Macdonald, R. W., and Papadakis, J. E. (1989). Water mass structure and boundaries in the Mackenzie shelf estuary. *Journal of Geophysical Research*, 94(C12):18,043–18,055, doi:10.1029/JC094iC12p18043. 54

Chen, C.-T. A. and Borges, A. V. (2009). Reconciling opposing views on carbon cycling in the coastal ocean: Continental shelves as sinks and near–shore ecosystems as sources of atmospheric CO_2. *Deep Sea Research Part II: Topical Studies in Oceanography*, 56(8–10):578–590, doi:10.1016/j.dsr2.2008.12.009. 52, 77, 86, 88, 134

Chierici, M., Fransson, A., Lansard, B., Miller, L. A., Shadwick, E., Thomas, H., Tremblay, J. E., and Papakyriakou, T. N. (2011). Impact of biogeochemical processes and environmental factors on the calcium carbonate saturation state in the Circumpolar Flaw Lead in the Amundsen Gulf, Arctic Ocean. *Journal of Geophysical Research*, 116:C00G09, doi:10.1029/2011JC007184. 56, 62, 67

Comiso, J. C., Parkinson, C. L., Gersten, R., and Stock, L. (2008). Accelerated decline in the arctic sea ice cover. *Geophysical Research Letters*, 35:L01703, doi:10.1029/2007GL031972. 3, 158

Denman, K., Brasseur, G., Chidthaisong, A., Ciais, P., Cox, P., Dickinson, R., Hauglustaine, D., Heinze, C., Holland, E., Jacob, D., Lohmann, U., Ramachandran, S., da Silva Dias, P., Wofsy, S., and Zhang, X. (2007). Couplings between changes in the climate system and biogeochemistry. In Solomon, S., Qin, D., Manning, M., Marquis, M., Averyt, K., Tignor, M., and Miller, H., editors, *Climate Change 2007, the Physical Science Basis*, chapter 7. Cambridge University Press, United Kingdom and New York, NY, USA. 2, 11

Dickson, A. G. and Millero, F. J. (1987). A comparison of the equilibrium constants for the dissociation of carbonic acid in seawater media. *Deep Sea Research Part A: Oceanographic Research Papers*, 34(10):1733–1743, doi:10.1016/0198–0149(87)90021–5. 60

Dieckmann, G. S., Nehrke, G., Papadimitriou, S., Göttlicher, J., Steininger, R., Kennedy, H., Wolf-Gladrow, D., and Thomas, D. N. (2008). Calcium carbonate as ikaite crystals in Antarctic sea ice. *Geophysical Research Letters*, 35:L08501, doi:10.1029/2008GL033540. 93

Dugan, J. P., Panichas, S. L., and DiMarco, R. L. (1991). Decontamination of wind measurements from buoys subjected to motions in a seaway. *Journal of Atmospheric and Oceanic Technology*, 8:85–95. 21

Edson, J. B., Hinton, A. A., Prada, K. E., Hare, J. E., and Fairall, C. W. (1998). Direct covariance flux estimates from mobile platforms at sea. *Journal of Atmospheric and Oceanic Technology*, 15:547–562, doi:10.1175/1520–0426(1998)015. 21

Else, B. G. T., Galley, R. J., Papakyriakou, T., Miller, L. A., Mucci, A., and Barber, D. G. (2012a). Sea surface pCO_2 cycles and CO_2 fluxes at landfast sea ice edges in Amundsen Gulf, Canada. *Journal of Geophysical Research*, in press:doi:10.1029/2012JC007901. 125, 126, 146

Else, B. G. T., Papakyriakou, T. N., Galley, R. G., Mucci, A., Gosselin, M., Miller, L. A., Shadwick, E. H., and Thomas, H. (2012b). Annual cycles of pCO_{2sw} in the southeastern Beaufort Sea: New understandings of air–sea CO_2 exchange in Arctic polynyas. *Journal of Geophysical Research*, 117:C00G13, doi:10.1029/2011JC007346. 14, 92, 93, 96, 99, 103, 114, 122, 125, 126, 129, 130, 133, 146

Else, B. G. T., Papakyriakou, T. N., Galley, R. J., Drennan, W. M., Miller, L. A., and Thomas, H. (2011). Wintertime CO_2 fluxes in an Arctic polynya using eddy covariance: Evidence for enhanced air–sea gas transfer during ice formation. *Journal of Geophysical Research*, 116:C00G03, doi:10.1029/2010JC006760. 68, 82, 96, 97, 98, 114, 121, 122, 123, 125, 127, 128

Else, B. G. T., Papakyriakou, T. N., Granskog, M., and Yackel, J. (2008a). Observations of sea surface fCO_2 distributions and estimated air-sea CO_2 fluxes in the Hudson Bay region (Canada) during the open water season. *Journal of Geophysical Research*, 113(C8):C08026, doi:10.1029/2007JC004389. 135

Else, B. G. T., Papakyriakou, T. N., and Yackel, J. (2008b). Application of satellite remote sensing techniques for estimating air–sea CO_2 fluxes in Hudson Bay, Canada during the ice–free season. *Remote Sensing Environment*, 112:3550–3562, doi:10.1029/2007JC004389. 146

Forest, A., Bélanger, S., Sampei, M., Saski, H., Lalande, C., and Fortier, L. (2010). Three–year assessment of particulate organic carbon fluxes in Amundsen Gulf (Beaufort Sea): Satellite observations and sediment trap measurements. *Deep Sea Research Part I*, 57:125–142, doi:10.1016/j.dsr.2009.10.002. 89

Fowler, C. (2003, updated 2010). Polar pathfinder daily 25 km ease–grid sea ice motion vectors. Boulder, Colorado, USA: National Snow and Ice Data Center, Digital media. 63

Francis, J. A. and Hunter, E. (2007). Changes in the fabric of the arctic's greenhouse blanket. *Environmental Research Letters*, 2(4):045011, doi:10.1088/1748–9326/2/4/045011. 3

Fransson, A., Chierici, M., and Nojiri, Y. (2009). New insights into the spatial variability of the surface water carbon dioxide in varying sea ice conditions in the Arctic Ocean. *Continental Shelf Research*, 29(10):1317–1328, doi:10.1016/j.csr.2009.03.008. 92

Frew, N. M. (1997). The role of organic films in air-sea gas exchange. In Liss, P. S. and Duce, R. A., editors, *The Sea Surface and Global Change*. Cambridge University Press. 11

Frew, N. M., Bock, E. J., Schimpf, U., Hara, T., Haußecker, H., Edson, J. B., McGillis, W. R., Nelson, R. K., McKenna, S. P., Uz, B. M., and Jähne, B. (2004). Air-sea gas transfer: Its dependence on wind stress, small-scale roughness, and surface films. *Journal of Geophysical Research*, 109(C8):C08S17, doi:10.1029/2003JC002131. 11

Fujitani, T. (1981). Direct measurement of turbulent fluxes over the sea during AMTEX. *Papers in Meteorology and Geophysics*, 32(3):119–134. 21

Galley, R. J., Barber, D. G., Key, E., and Prinsenberg, S. (2009). A physical explanation of the formation of the Cape Bathurst polynya, NWT, Canada. In *Sea ice thermodynamic and dynamic processes in the ocean-sea ice-atmosphere system of the Canadian Arctic*, pages 205–240. University of Mantioba PhD Thesis. 141, 143

Galley, R. J., Else, B. G. T., Lukovich, J. V., Howell, S. E. L., and Barber, D. G. (2012). Landfast sea ice conditions in the Canadian Arctic: 1983–2009. *Arctic*, page In Press. 92, 94, 118

Galley, R. J., Key, E., Barber, D. G., Hwang, B. J., and Ehn, J. K. (2008). Spatial and temporal variability of sea ice in the southern Beaufort Sea and Amundsen Gulf: 1980–2004. *Journal of Geophysical Research*, 113(C5):C05S95, doi:10.1029/2007JC004553. 13, 56, 94, 117, 143

Geilfus, N. X., Carnat, G., Papakyriakou, T., Tison, J. L., Else, B., Thomas, H., Shadwick, E., and Delille, B. (2012). pCO_2 dynamics and related air–ice CO_2 fluxes in the Arctic coastal zone (Amundsen Gulf, Beaufort Sea). *Journal of Geophysical Research*, 117:C00G10, doi:10.1029/2011JC007118. 108

Gibson, J. A. E. and Trull, T. W. (1999). Annual cycle of fCO_2 under sea-ice and in open water in Prydz Bay, East Antarctica. *Marine Chemistry*, 66:187–200, doi:10.1016/S0304–4203(99)00040–7. 92, 93, 115, 118, 152, 157

Golden, K., Ackley, S., and Lytle, V. (1998). The percolation phase transition in sea ice. *Science*, 282(5397):2238–2241, doi:10.1126/science.282.5397.2238. 36

Gosink, T. A., Pearson, J. G., and Kelley, J. J. (1976). Gas movement through sea ice. *Nature*, 263:41–42, doi:10.1038/263041a0. 12, 93

Graversen, R. G., Mauritsen, T., Tjernstrom, M., Kallen, E., and Svensson, G. (2008). Vertical structure of recent arctic warming. *Nature*, 451:53–56, doi:10.1038/nature06502. 3

Gruber, N., Keeling, C. D., and Stocker, T. F. (1998). Carbon-13 constraints on the seasonal inorganic carbon budget at the BATS site in the northwestern Sargasso Sea. *Deep Sea Research Part I*, 45(4–5):673–717, doi:10.1016/S0967–0637(97)00098–8. 62, 63

Hakkinen, S., Proshutinsky, A., and Ashik, I. (2008). Sea ice drift in the arctic since the 1950s. *Geophysical Research Letters*, 35:L19704, doi:10.1029/2008GL034791. 47, 88, 148, 158

Hansen, J., Sato, M., Ruedy, R., Kharecha, P., Lacis, A., Miller, R., Nazarenko, L., Lo, K., Schmidt, G. A., Russell, G., et al. (2007). Dangerous human-made interference with climate: a GISS modelE study. *Atmospheric Chemistry and Physics*, 7:2287–2312, doi:www.atmos–chem–phys.net/7/2287/2007/. 1

Hirata, R., Hirano, T., Saigusa, N., Fujinuma, Y., Inukai, K., Kitamori, Y., Takahashi, Y., and Yamamoto, S. (2007). Seasonal and interannual variations in carbon dioxide exchange of a temperate larch forest. *Agricultural and Forest Meteorology*, 147(3–4):110–124, doi:10.1016/j.agrformet.2007.07.005. 21

Ho, D. T., Law, C. S., Smith, M. J., Schlosser, P., Harvey, M., and Hill, P. (2006). Measurements of air-sea gas exchange at high wind speeds in the Southern Ocean: Implications for global parameterizations. *Geophysical Research Letters*, 33:L23503, doi:10.1029/2006GL026817. 12

Ho, D. T., Zappa, C. J., McGillis, W. R., Bliven, L. F., Ward, B., Dacey, J. W., Schlosser, P., and Hendricks, M. B. (2004). Influence of rain on air-sea gas exchange: Lessons from a model ocean. *Journal of Geophysical Research*, 109:C08S18, doi:10.1029/2003JC001806. 11

Jacobs, J. D., Barry, R. G., and Weaver, R. L. (1975). Fast ice characteristics, with special reference to the eastern Canadian Arctic. *Polar Record*, 17:521–536, doi:10.1017/S0032247400032484. 92

Jähne, B. (1987). On the parameters influencing air-water gas exchange. *Journal of Geophysical Research*, 92(C2):1937–1950, doi:10.1029/JC092iC02p01937. 11

Jähne, B., Gerhard, H., and Dietrich, W. (92). Measurement of the diffusion coefficients of sparingly soluble gases in water. *Journal of Geophysical Research*, C10:10,767–10,776, doi:10.1029/JC092iC10p10767. 98

Järvi, L., Mammarella, I., Eugster, W., Ibrom, A., Siivola, E., Dellwik, E., Keronen, P., Burba, G., and Vesala, T. (2009). Comparison of net CO_2 fluxes measured with open-and closed-path infrared gas analyzers in an urban complex environment. *Boreal Environment Research*, 14:499–514. 21

Jessup, A. T., Asher, W. E., Atmane, M., Phadnis, K., Zappa, C. J., and Loewen, M. R. (2009). Evidence for complete and partial surface renewal at an air–water interface. *Geophysical Research Letters*, 36:L16601, doi:10.1029/2009GL038986. 155

Kaimal, J. C. and Gaynor, J. E. (1991). Another look at sonic thermometry. *Boundary-Layer Meteorology*, 56:401–410. 21

Kalnay, E. and co authors (1996). The NCEP/NCAR reanalysis 40–year project. *Bull Amer Meteor Soc*, 77:437–471. xvii, 116, 142

Keeling, C. D., Piper, S. C., Bacastow, R. B., Wahlen, M., Whorf, T. P., Heimann, M., and Meijer, H. A. (2001). Exchanges of atmospheric CO_2 and $^{13}CO_2$ with the terrestrial biosphere and oceans from 1978 – 2000. In *Global Aspects*, volume No. 01-06 of *SIO Reference Series*. Scripps Institution of Oceanography, San Diego. 125

Kohsiek, W. (2000). Water vapor cross-sensitivity of open path H_2O/CO_2 sensors. *Journal of Atmospheric and Oceanic Technology*, 17:299–311. 22

Körtzinger, A., Thomas, H., Schneider, B., Gronau, N., Mintrop, L., and Duinker, J. C. (1996). At-sea intercomparison of two newly designed underway pCO_2 systems–encouraging results. *Marine Chemistry*, 52(2):133–145, doi:10.1016/0304–4203(95)00083–6. 15

Kuss, J. and Schneider, B. (2004). Chemical enhancement of the CO_2 gas exchange at a smooth seawater surface. *Marine Chemistry*, 91(1–4):165–174, doi:10.1016/j.marchem.2004.06.007. 12

Kwok, R. (2006). Exchange of sea ice between the Arctic Ocean and the Canadian Arctic Archipelago. *Geophysical Research Letters*, 33:L16501, doi:10.1029/2006GL027094. 57, 143

Lansard, B., Mucci, A., Miller, L. A., MacDonald, R. W., and Gratton, Y. (2012). Seasonal variability of water mass distribution in the southeastern Beaufort Sea determined by total alkalinity and $\delta^{18}O$. *Journal of Geophysical Research*, 117:C03033, doi:10.1029/2011JC007299. 62, 99, 105

Le Quéré, C., Rödenbeck, C., Buitenhuis, E. T., Conway, T. J., Langenfelds, R., Gomez, A., Labuschagne, C., Ramonet, M., Nakazawa, T., Metzl, N., Gillett, N., and Heimann, M. (2007). Saturation of the Southern Ocean CO_2 sink due to recent climate change. *Science*, 316(5832):1735–1738, doi:10.1126/science.1136188. 2

Leuning, R. (2004). Measurements of trace gas fluxes in the atmosphere using eddy covariance: WPL corrections revisited. In Lee, X., Massman, W. J., and Law, B. E., editors, *Handbook of micrometeorology: A guide to surface flux measurement and analysis*, pages 119–132. Kluwer. 21

Lindsay, R. W. and Rothrock, D. A. (1995). Arctic sea ice leads from advanced very high resolution radiometer images. *Journal of Geophysical Research*, 100(C3):4533–4544, doi:10.1029/94JC02393. 46

Liss, P. S. and Merlivat, L. (1986). Air-sea gas exchange rates: Introduction and synthesis. In Buat-Menard, P., editor, *The role of air–sea exchange in geochemical cycling*, pages 113–127. D. Reidel Publishing Company. 12

Loose, B., McGillis, W. R., Schlosser, P., Perovich, D., and Takahashi, T. (2009). Effects of freezing, growth, and ice cover on gas transport processes in

laboratory seawater experiments. *Geophysical Research Letters*, 36(5):L05603, doi:10.1029/2008GL036318. 13, 38, 82, 127, 149

Loose, B., Schlosser, P., Perovich, D., Ringelberg, D., Ho, D., Takahashi, T., Richter-Menge, J., Reynolds, C., McGillis, W., and Tison, J. L. (2010). Gas diffusion through columnar laborator sea ice: implications for mixed layer ventilation of CO_2 in the seasonal sea ice zone. *Tellus B*, 63(1):23–39, doi:10.1111/j.1600–0889.2010.00506.x. 36, 93, 98

Lukovich, J. V. and Barber, D. G. (2006). Atmospheric controls on sea ice motion in the southern Beaufort Sea. *Journal of Geophysical Research*, 111:D18103, doi:10.1029/2005JD006408. 143

Macdonald, R. W., Carmack, E. C., McLaughlin, F. A., Iseki, K., Macdonald, D. M., and O'Brien, M. C. (1989). Composition and modification of water masses in the Mackenzie shelf estuary. *Journal of Geophysical Research*, 94(C12):18,057–18,070, doi:10.1029/JC094iC12p18057. 70

Macdonald, R. W., Wong, C. S., and Erickson, P. E. (1987). The distribution of nutrients in the southeastern Beaufort Sea: Implications for water circulation and primary production. *Journal of Geophysical Research*, 92:2939–2952, doi:10.1029/RG025i005p00905. 54, 71

Magen, C., Chaillou, G., Crowe, S. A., Mucci, A., Sundby, B., Gao, A., Makabe, R., and Sasaki, H. (2010). Origin and fate of particulate organic matter in the southern Beaufort Sea-Amundsen Gulf region, Canadian Arctic. *Estuarine, Coastal and Shelf Science*, 86(1):31–41, doi:10.1016/j.ecss.2009.09.009. 56

Martin, J., Tremblay, J. E., Gagnon, J., Tremblay, G., Lapoussière, A., Jose, C., Poulin, M., Gosselin, M., Gratton, Y., and Michel, C. (2010). Prevalence, structure and properties of subsurface chlorophyll maxima in Canadian Arctic waters. *Marine Ecology Progress Series*, 412:69–84, doi:10.3354/meps08666. 67

Maslanik, J., Drobot, S., Fowler, C., Emery, W., and Barry, R. (2007). On the Arctic climate paradox and the continuing role of atmospheric circulation in affecting sea ice conditions. *Geophysical Research Letters*, 34:L03711, doi:10.1029/2006GL028269. 117, 118, 144

Maslanik, J., Stroeve, J., Fowler, C., and Emery, W. (2011). Distribution and trends in Arctic sea ice age through 2011. *Geophysical Research Letters*, 34:L03711, doi:10.1029/2006GL028269. 148

Massom, R. A. (1988). The biological significance of open water within the sea ice covers of the polar regions. *Endeavour*, 12(1):21–27. 51

Masson, D. and LeBlond, P. H. (1989). Spectral evolution of wind–generated surface gravity waves in a dispersed ice field. *Journal of Fluid Mechanics*, 202:43–81. 156

Maykut, G. A. (1978). Energy exchange over young sea ice in the Central Arctic. *Journal of Geophysical Research*, 83(C7):3646–3658, doi:10.1029/JC083iC07p03646. 34, 46, 51

McGillis, W. M., Edson, J. B., Ware, J. E., Dacey, J. H. W., Hare, J. E., Fairall, C. W., and Wanninkhof, R. (2001). Carbon dioxide flux techniques performed during GasEx-98. *Marine Chemistry*, 75:267–280, doi:10.1016/S0304–4203(01)00042–1. 22

McGillis, W. R., Edson, J. B., Zappa, C. J., Ware, J. D., McKenna, S. P., Terray, E. A., Hare, J. E., Fairall, C. W., Drennan, W. M., Donelan, M., DeGrandpre, M. D., Wanninkhof, R., and Feely, R. A. (2004). Air-sea CO_2 exchange in the equatorial Pacific. *Journal of Geophysical Research*, 109:C08S02, doi:10.1029/2003JC002256. 11, 39, 129

McPhee, M., Kwok, R., Robins, R., and Coon, M. (2005). Upwelling of Arctic pycnocline associated with shear motion of sea ice. *Geophysical Research Letters*, 32:L13502, doi:10.1029/2011GL047735. 146

McPhee, M. G., Proshutinsky, A., Morison, J. H., Steele, M., and Alkire, M. B. (2009). Rapid change in freshwater content of the arctic ocean. *Geophysical Research Letters*, 36:L10602, doi:10.1029/2009GL037525. 4, 158

McPhee, M. G. and Stanton, T. P. (1996). Turbulence in the statically unstable oceanic boundary layer under arctic leads. *Journal of Geophysical Research*, 101(C3):6409–6428, doi:10.1029/95JC03842. 12, 40

Mehrbach, C., Culberson, C. H., Hawley, J. E., and Pytkowicz, R. M. (1973). Measurement of the apparent dissociation constants of carbonic acid in seawater at atmospheric pressure. *Limnology and Oceanography*, 18(6):897–907, doi:10.4319/lo.1973.18.6.0897. 60

Melling, H., Gratton, Y., and Ingram, G. (2001). Ocean circulation within the North Water Polynya of Baffin Bay. *Atmosphere–Ocean*, 39(3):301–325. 84

Melling, H. and Moore, R. (1995). Modification of halocline source waters during freezing on the Beaufort Sea shelf: evidence from oxygen isotopes and dissolved nutrients. *Continental Shelf Research*, 15(1):89–113, doi:10.1016/0278–4343(94)P1814–R. 42

Miller, L. A. and DiTullio, G. R. (2007). Gas fluxes and gas dynamics in polynyas. In Smith Jr, W. O. and Barber, D. G., editors, *Polynyas: Windows to the World*, volume 74 of *Elsevier Oceanography Series*, pages 163–192. Elsevier. 121, 122

Miller, L. A., Papakyriakou, T. N., Collins, R. E., Deming, J. W., Ehn, J. K., Macdonald, R. W., Mucci, A., Owens, O., Raudsepp, M., and Sutherland, N. (2011). Carbon dynamics in sea ice: A winter flux time series. *Journal of Geophysical Research*, 116:C02028, doi:10.1029/2009JC006058. 71, 103, 115, 117, 118, 126

Miller, L. A., Yager, P. L., Erickson, K. A., Amiel, D., Bâcle, J., Cochran, J. K., Garneau, M.-E., Gosselin, M., Hirschberg, D. J., Klein, B., LeBlanc, B., and Miller, W. L. (2002). Carbon distributions and fluxes in the North Water, 1998 and 1999. *Deep Sea Research Part II*, 49:5151–5170, doi:10.1016/S0967–0645(02)00183–2. 52, 92, 122, 146

Mitsuta, Y. and Fujitani, T. (1974). Direct measurement of turbulent fluxes on a cruising ship. *Boundary-Layer Meteorology*, 6:203–217, doi:10.1007/BF00232485. 21

Morison, J., Kwok, R., Peralta-Ferriz, C., Alkire, M., Rigor, I., Anderson, R., and Steele, M. (2012). Changing arctic ocean freshwater pathways. *Nature*, 451:66–70, doi:10.1038/nature10705. 4, 158

Mucci, A., Lansard, B., Miller, L. A., and Papakyriakou, T. N. (2010). CO_2 fluxes across the air–sea interface in the southeastern Beaufort Sea: Ice–free period. *Journal of Geophysical Research*, 115:C04003, doi:10.1029/2009JC005330. 14, 54, 56, 75, 117, 135

Mundy, C. J., Gosselin, M., Ehn, J., Gratton, Y., Rossnagel, A., Barber, D. G., Martin, J., Tremblay, J. E., Palmer, M., Arrigo, K. R., Darnis, G., Fortier, L., Else, B., and Papakyriakou, T. (2009). Contribution of under–ice primary production to an ice–edge upwelling phytoplankton bloom in the Canadian Beaufort Sea (2009). *Geophysical Research Letters*, 36:L17601, doi:10.1029/2009GL038837. 105, 107, 117

Murata, A. and Takizawa, T. (2003). Summertime CO_2 sinks in shelf and slope waters of the western Arctic Ocean. *Continental Shelf Research*, 23(8)::753–776, doi:10.1016/S0278–4343(03)00046–3. 14

Nightingale, P. D., Malin, G., Law, C. S., Watson, A. J., Liss, P. S., Liddicoat, M. I., Boutin, J., and Upstill-Goddard, R. C. (2000). In situ evaluation of air-sea gas exchange parameterizations using novel conservative and volatile tracers. *Global Biogeochemical Cycles*, 14:373–387, doi:10.1029/1999GB900091. 12

Nomura, D., Eicken, H., Gradinger, R., and Shirasawa, K. (2010). Rapid physically driven inversion of the air–sea ice CO_2 flux in the seasonal landfast ice off Barrow, Alaska after onset of surface melt (2010). *Continental Shelf Research*, 30(19):1998–2004, doi:10.1016/j.csr.2010.09.014. 94, 126

Nomura, D., Yoshikawa-Inoue, H., and Toyota, T. (2006). The effect of sea-ice growth on air–sea CO_2 flux in a tank experiment. *Tellus B*, 58(5):418–426, doi:10.1111/j.1600–0889.2006.00204.x. 36, 126

Omar, A., Johannessen, T., Bellergy, R. G. J., Olsen, A., Anderson, L. G., and Kivimäe (2005). Sea–ice and brine formation in Storfjorden: Implications for the Arctic wintertime air–sea CO_2 flux. In Drange, H., Dokken, T., Furevik, T., Gerdes, R., and Berger, W., editors, *The Nordic Seas: an Integrated Perspective*, volume 158 of *Geophysical Monograph*. American Geophysical Union. 46, 47, 122, 145, 146, 153, 157

Omstedt, A. (1985). On supercooling and ice formation in turbulent sea-water. *Journal of Glaciology*, 31:263–271. 40

Ono, K., Miyata, A., and Yamada, T. (2008). Apparent downward CO_2 flux observed with open-path eddy covariance over a non-vegetated surface. *Theoretical and Applied Climatology*, 92(3):195–208, doi:10.1007/s00704–007–0323–3. 21

Overland, J. E. and Wang, M. (2005). The Arctic climate paradox: The recent decrease of the Arctic Oscillation. *Geophysical Research Letters*, 32:L06701, doi:10.1029/2004GL021752. 144

Overland, J. E. and Wang, M. (2010). Large–scale atmospheric circulation changes are associated with the recent loss of Arctic sea ice. *Tellus*, 62A:1–9, doi:10.1111/j.1600–0870.2009.00421.x. 115, 117, 118, 144

Pabi, S., van Dijken, G. L., and Arrigo, K. R. (2008). Primary production in the Arctic Ocean, 1998–2006. *Journal of Geophysical Research*, 113(C8):C08005, doi:10.1029/2007JC004578. 3, 56, 74, 158

Papakyriakou, T. and Miller, L. (2011). Springtime CO_2 exchange over seasonal sea ice in the Canadian Arctic Archipelago. *Annals of Glaciology*, 52(57):215–224. 94, 126

Perovich, D. K. and Richter-Menge, J. A. (2008). Loss of sea ice in the Arctic. *Annual Review of Marine Science*, 1:417–441, doi:10.1146/annurev.marine.010908.163805. 89

Perovich, D. K., Richter-Menge, J. A., Jones, K. F., and Light, B. (2008). Sunlight, water and ice: Extreme Arctic sea ice melt during the summer of 2007. *Geophysical Research Letters*, 35:L11501, doi:10.1029/2008GL034007. 115

Pierrot, D., Neill, C., Sullivan, K., Castle, R., Wanninkhof, R., Lüger, H., Johannessen, J., Olsen, A., Feeley, R., and Cosca, C. E. (2009). Recommendations for autonomous underway pCO_2 measuring systems and data–reduction routines. *Deep Sea Research Part II*, 56:512–522, doi:10.1016/j.dsr2.2008.12.005. 135

Prytherch, J., Yelland, M. J., Pascal, R. W., Moat, B. I., Skjelvan, I., and Neill, C. C. (2010). Direct measurements of the CO_2 flux over the ocean: Development of a novel method. *Geophysical Research Letters*, 37(3):L03607, doi:10.1029/2009GL041482. 21, 22, 37

Robbins, L., Hansen, M., Kleypas, J., and Meylan, S. (2010). CO2calc - a user-friendly seawater carbon calculator for Windows, Mac OS X, and iOS (iPhone). *U S Geological Survey Open–File Report*, 1280:17. 60

Rysgaard, S., Bendtsen, J., Pedersen, L. T., Ramløv, H., and Glud, R. N. (2009). Increased CO_2 uptake due to sea ice growth and decay in the Nordic Seas. *Journal of Geophysical Research*, 114:C09011, doi:10.1029/2008JC005088. 13, 93

Rysgaard, S., Glud, R. N., Sejr, M. K., Bendtsen, J., and Christensen, P. B. (2007). Inorganic carbon transport during sea ice growth and decay: A carbon pump in polar seas. *Journal of Geophysical Research*, 112:C03016, doi:10.1029/2006JC003572. 4, 13, 38, 71, 93

Sabine, C. L., Feely, R. A., Gruber, N., Key, R. M., Lee, K., Bullister, J. L., Wanninkhof, R., Wong, C. S., Wallace, D. W. R., Tilbrook, B., Millero, F. J., Peng, T.-H., Kozyr, A., Ono, T., and Rios, A. F. (2004). The oceanic sink for anthropogenic CO_2. *Science*, 305(5682):367–371, doi:10.1126/science.1097403. 1

Sakshaug, E. (2004). Primary and secondary production in the Arctic Seas. In Stein, R. and Macdonald, R., editors, *The organic carbon cycle in the Arctic Ocean*, pages 57–81. Springer. 78

Sarmiento, J. L. and Gruber, N. (2006). *Ocean biogeochemical dynamics*. Cambridge University Press. 53

Sarmiento, J. L., Hughes, T. M., Stouffer, R. J., and Syukuro, M. (1998). Simulated response of the ocean carbon cycle to anthropogenic climate warming. *Nature*, 393:245–249, doi:10.1038/30455. 2

Sarmiento, J. L. and Sundquist, E. T. (1992). Revised budget for the oceanic uptake of anthropogenic carbon dioxide. *Nature*, 356:589–593, doi:10.1038/356589a0. 2

Schuster, U. and Watson, A. J. (2007). A variable and decreasing sink for atmospheric CO_2 in the North Atlantic. *Journal of Geophysical Research*, 112:C11006, doi:10.1029/2006JC003941. 2

Schweiger, A. J., Lindsay, R. W., Vavrus, S., and Francis, J. A. (2008). Relationships between arctic sea ice and clouds during autumn. *Journal of Climate*, 21(18):4799–4810, doi:10.1175/2008JCLI2156.1. 3

Screen, J. A. and Simmonds, I. (2010). The central role of diminishing sea ice in recent arctic temperature amplification. *Nature*, 464:1334–1337, doi:10.1038/nature09051. 3

Sejr, M. K., Krause-Jensen, D., Rysgaard, S., Sørensen, L. L., Christensen, P. B., and Glud, R. N. (2011). Air–sea flux of CO_2 in arctic coastal waters influenced by glacial melt water and sea ice. *Tellus*, 63B:815–822, doi:10.1111/j.1600–0889.2011.00540.x. 92, 115, 118, 152, 157

Semiletov, I., Makshtas, A., Akasofu, S. I., and Andreas, E. L. (2004). Atmospheric CO_2 balance: the role of Arctic sea ice. *Geophysical Research Letters*, 31:L05121, doi:10.1029/2003GL017996. 94, 126

Semiletov, I. P., Pipko, I. I., Repina, I., and Shakova, N. E. (2007). Carbonate chemistry dynamics and carbon dioxide fluxes across the atmosphere–ice–water interfaces in the Arctic Ocean: Pacific sector of the Arctic. *Journal of Marine Systems*, 66:204–226, doi:10.1016/j.jmarsys.2006.05.012. 146

Serreze, M. C., Barrett, A. P., Stroeve, J. C., Kindig, D. N., and Hollan, M. M. (2009). The emergence of surface-based arctic amplification. *The Cyrosphere*, 3:11–19. 3

Shadwick, E., Thomas, H., Chierici, M., Else, B., Fransson, A., Michel, C., Miller, L., Mucci, A., Niemi, A., Papakyriakou, T., and J É, T. (2011). Seasonal variability of the inorganic carbon system in the Amundsen Gulf region

of the southeastern Beaufort Sea. *Limnology and Oceanography*, 56(1):303–322, doi:10.4319/lo.2011.56.1.0303. 14, 16, 42, 43, 44, 45, 53, 59, 61, 62, 63, 65, 67, 68, 69, 70, 71, 84, 92, 93, 99, 103, 105, 123, 126, 132, 133, 134, 147, 153

Skogseth, R., Fer, I., and Haugen, P. M. (2005). Dense–water production and overflow from an Arctic coastal polynya in Storfjorden. In Drange, H., Dokken, T., Furevik, T., Gerdes, R., and Berger, W., editors, *The Nordic Seas: an Integrated Perspective*, volume 158 of *Geophysical Monograph*, pages 73–88. American Geophysical Union. 145

Skogseth, R., Nilsen, F., and Smedsrud, L. H. (2009). Supercooled water in an arctic polynya: observations and modeling. *Journal of Glaciology*, 55(189):43–52, doi:10.3189/002214309788608840. 41

Smith, S. D., Muench, R. D., and Pease, C. H. (1990). Polynyas and leads: An overview of physical processes and environment. *Journal of Geophysical Research*, 95(C6):9461–9479, doi:10.1029/JC095iC06p09461. 51

Spreen, G., Kaleschke, L., and Heygster, G. (2008). Sea ice remote sensing using AMSR–E 89–GHz channels. *Journal of Geophysical Research*, 113:C02S03, doi:10.1029/2005JC003384. xiv, 66, 124

Steele, M., Ermold, W., and Zhang, J. (2008). Arctic Ocean surface warming trends over the past 100 years. *Geophysical Research Letters*, 35:L02614, doi:10.1029/2007GL031651. 4, 89, 158

Stroeve, J., Holland, M. M., Meier, W., Scambos, T., and Serreze, M. (2007). Arctic sea ice decline: Faster than forecast. *Geophysical Research Letters*, 34(9):L9501, doi:10.1029/2007GL029703. 47, 89, 148

Sweeney, C. (2003). *The annual cycle of surface water CO_2 and O_2 in the Ross Sea: A model for gas exchange on the continental shelves of Antarctica*, pages 295–312. Number 78 in Antarctic Research Series. American Geophysical Union. 122

Sweeney, C., Gloor, E., Jacobson, A. R., Key, R. M., McKinley, G., Sarmiento, J. L., and Wanninkhof, R. (2007). Constraining global air-sea gas exchange for CO_2 with recent bomb ^{14}C measurements. *Global Biogeochemical Cycles*, 7:843–878, doi:10.1029/2006GB002784. 12, 60, 98, 127

Sweeney, C., Hansell, D., Carlson, C. A., Codispoti, L. A., Gordon, L. I., Marra, J., Millero, F. J., Smith, W. O., and Takahashi, T. (2000). Biogeochemical regimes,

net community production and carbon export in the Ross Sea, Antarctica. *Deep Sea Research Part II*, 47:3369–3394, doi:10.1016/S0967–0645(00)00072–2. 122

Takagaki, N. and Komori, S. (2007). Effects of rainfall on mass transfer across the air-water interface. *Journal of Geophysical Research*, 112(C6):C06006, doi:10.1029/2006JC003752. 11

Takahashi, T., Olafsson, J., Goddard, J. G., Chipman, D. W., and Sutherland, S. C. (1993). Seasonal variation of CO_2 and nutrients in the high-latitude surface oceans: a comparative study. *Global Biogeochemical Cycles*, 7(4):843–878, doi:10.1029/93GB02263. 4, 16, 58, 61, 96, 126

Takahashi, T., Sutherland, S. C., Wanninkhof, R., Sweeney, C., Feely, R. A., Chipman, D. W., Hales, B., Friederich, G., Chavez, F., Sabine, C., Watson, A., Bakker, D. C. E., Schuster, U., Metzi, N., Yoshikawa-Inoue, H., Ishii, M., Midorikawa, T., Nojiri, Y., Körtzinger, A., Steinhoff, T., Hoppema, M., Olafsson, J., Arnarson, T. S., Tilbrook, B., Johannessen, T., Olsen, A., Bellerby, R., Wong, C. S., Delille, B., Bates, N. R., and de Barr, H. J. W. (2009). Climatological mean and decadal change in surface ocean pCO_2, and net sea-air CO_2 flux over the global oceans. *Deep Sea Research Part II: Topical Studies in Oceanography*, 56(8–10):554–577, doi:10.1016/j.dsr2.2008.12.009. 11

Thomas, H., Bozec, Y., Elkalay, K., and de Baar, H. J. W. (2004). Enhanced open ocean storage of CO_2 from shelf sea pumping. *Science*, 304(5673):1005–1008, doi:10.1126/science.1095491. 52, 53

Thomas, H., Shadwick, E., Dehairs, F., Lansard, B., Navez, J., Gratton, Y., Prowe, F., Mucci, A., Chierici, M., Fransson, A., Papakyriakou, T. N., Sternberg, E., Miller, L. A., and Monnin, C. (2011). Barium and Carbon fluxes in the Canadian Arctic Archipelago. *Journal of Geophysical Research*, 116:C00G08, doi:10.1029/2011JC007120. 56

Tremblay, J. E., Bélanger, S., Barber, D. G., Asplin, M., Martin, J., Darnis, G., Fortier, L., Gratton, Y., Link, H., Archambault, P., Sallon, A., Michel, C., Williams, W. J., Philippe, B., and Gosselin, M. (2011). Climate forcing multiplies biological productivity in the coastal Arctic Ocean. *Geophysical Research Letters*, 38:L18604, doi:10.1029/2011GL048825. 71, 74, 85, 88, 99, 103, 105, 107, 117, 158

Tremblay, J. E., Simpson, K., Martin, J., Miller, L., Gratton, Y., Barber, D., and Price, N. M. (2008). Vertical stability and the annual dynamics of nutrients

and chlorophyll fluorescence in the coastal, southeast Beaufort Sea. *Journal of Geophysical Research*, 113:C07S90, doi:10.1029/2007JC004547. 5, 56, 79, 84, 89

Tsang, G. and Hanley, T. O. (1985). Frazil formation in water of different salinities and supercoolings. *Journal of Glaciology*, 31(108):74–85. 41

Tsunogai, S., Watanabe, S., and Sato, T. (1999). Is there a "continental shelf pump" for the absorption of atmospheric CO_2? *Tellus B*, 51(3):701–712, doi:10.1034/j.1600–0889.1999.t01–2–00010.x. 52, 53, 84

Ushio, S. and Wakatsuchi, M. (1993). A laboratory study on supercooling and frazil ice production processes in winter coastal polynyas. *Journal of Geophysical Research*, 98(C11):20,321–20,328, doi:10.1029/93JC01905. 40, 42

Vallières, C., Retamal, L., Ramlal, P., Osburn, C. L., and Vincent, W. F. (2008). Bacterial production and microbial food web structure in a large arctic river and the coastal Arctic Ocean. *Journal of Marine Systems*, 74:756–773, doi:10.1016/j.jmarsys.2007.12.002. 59, 77

Wadhams, P. (2000). *Ice in the Ocean*. Gordon and Breach Science Publishers. 46

Wallace, D. W. R., Minnett, P. J., and Hopkins, T. S. (1995). Nutrients, oxygen, and inferred new production in the Northeast Water Polynya. *Journal of Geophysical Research*, 100(C3):4323–4340, doi:10.1029/94JC02203. 84

Wang, J., Zhang, J., Watanabe, E., Ikeda, M., Mizobata, K., Walsh, J., Bai, X., and Wu, B. (2009). Is the Dipole Anomaly a major driver to record lows in Arctic summer sea ice extent? *Geophysical Research Letters*, 36:L05706, doi:10.1029/2008GL036706. 144, 158

Wanninkhof, R. (1992). Relationship between wind speed and gas exchange over the ocean. *Journal of Geophysical Research*, 97(C5):7373–7382, doi:10.1029/92JC00188. 12

Wanninkhof, R., Asher, W. E., Ho, D. T., Sweeney, C., and McGillis, W. R. (2009). Advances in quantifying air-sea gas exchange and environmental forcing. *Annual Review of Marine Science*, 1:213–244, doi:10.1146/annurev.marine.010908.163742. 11, 12

Wanninkhof, R. and McGillis, W. R. (1999). A cubic relationship between gas exchange and wind speed over the ocean. *Geophysical Research Letters*, 26:7373–7381, doi:10.1029/1999GL900363. 12

Watson, A. J., Metzl, N., and Schuster, U. (2011). Monitoring and interpreting the ocean uptake of atmospheric co_2. *Philosophical Transactions of the Royal Society A – Mathematical, Physical and Engineering Sciences*, 369:1997–2008, doi:10.1098/rsta.2011.0060. 2

Webb, E. K., Pearman, G. I., and Leuning, R. (1980). Correction of flux measurements for density effects due to heat and water vapour transfer. *Quarterly Journal of the Royal Meteorological Society*, 106(447):85–100, doi:10.1002/qj.49710644707. 21

Weiss, R. F. (1974). Carbon dioxide in water and seawater: the solubility of a non-ideal gas. *Marine Chemistry*, 2(3):203–215. 60

Weiss, R. F. and Price, B. A. (1980). Nitrous oxide solubility in water and seawater. *Marine Chemistry*, 8(4):347–359, doi:10.1016/0304–4203(80)90024–9. 96

Williams, W. J. and Carmack, E. C. (2008). Combined effect of wind-forcing and isobath divergence on upwelling at Cape Bathurst, Beaufort Sea. *Journal of Marine Research*, 66(5):645–663, doi:10.1357/002224008787536808. 59, 74, 99, 117

Williams, W. J., Melling, H., Carmack, E. C., and Ingram, R. G. (2008). Kugmallit Valley as a conduit for cross–shelf exchange on the Mackenzie Shelf in the Beaufort Sea. *Journal of Geophysical Research*, 113:C02007, doi:10.1029/2006JC003591. 74

Woolf, D. K. (1997). Bubbles and their role in gas exchange. In Liss, P. S. and Duce, R., editors, *The Sea Surface and Global Change*, pages 173–207. Cambridge University Press. 12

Woolf, D. K. (2005). Parametrization of gas transfer velocities and sea-state-dependent wave breaking. *Tellus B*, 57(2):87–94, doi:10.1111/j.1600–0889.2005.00139.x. 12, 97, 156

Woolf, D. K., Leifer, I. S., Nightingale, P. D., Rhee, T. S., Bowyer, P., Caulliez, G., De Leeuw, G., Larsen, S. E., Liddicoat, M., Baker, J., and Andreae, M. O. (2007). Modelling of bubble-mediated gas transfer: Fundamental principles and a laboratory test. *Journal of Marine Systems*, 66(1–4):71–91, doi:10.1016/j.jmarsys.2006.02.011. 12

Yager, P. L., Wallace, D. W. R., Johnson, K. M., Smith Jr, W. O., Minnett, P. J., and Deming, J. W. (1995). The Northeast Water Polynya as an atmospheric CO_2 sink: A seasonal rectification hypothesis. *Journal of Geophysical Research*,

100(C3):4389–4398, doi:10.1029/94JC01962. xv, 5, 45, 51, 52, 53, 80, 81, 82, 84, 85, 86, 114, 118, 121, 122, 146, 147, 150, 152, 157

Yamamoto-Kawai, M., McLaughlin, F. A., Carmack, E. C., Nishino, S., and Shimada, K. (2009). Aragonite undersaturation in the arctic ocean: Effects of ocean acidification and sea ice melt. *Science*, 326(5956):1098–1100, doi:10.1126/science.1174190. 5

Zappa, C. J., Asher, W. E., Jessup, A. T., Klinke, J., and Long, S. R. (2004). Microbreaking and the enhancement of air-water transfer velocity. *Journal of Geophysical Research*, 109:C08S16, doi:10.1029/2003JC001897. 11

Zappa, C. J., Ho, D. T., McGillis, W. R., Banner, M. L., Dacey, J. W. H., Bliven, L. F., Ma, B., and Nystuen, J. (2009). Rain-induced turbulence and air-sea gas transfer. *Journal of Geophysical Research*, 114:C07009, doi:10.1029/2008JC005008. 11, 155

Zappa, C. J., McGillis, W. R., Raymond, P. A., Edson, J. B., Hintsa, E. J., Zemmelink, H. J., Dacey, J. W. H., and Ho, D. T. (2007). Environmental turbulent mixing controls on air-water gas exchange in marine and aquatic systems. *Geophysical Research Letters*, 34(10):10601, doi:10.1029/2006GL028790. 11, 40

Zemmelink, H., Delille, B., Tison, J. L., Hintsa, E., Houghton, L., and Dacey, J. (2006). CO_2 deposition over the multi-year ice of the western Weddell Sea. CO_2 deposition over the multi-year ice of the western Weddell Sea. *Geophysical Research Letters*, 33:L13606, doi:10.1029/2006GL026320. 126

Zhang, X., Sorteberg, A., Zhang, J., Gerdes, R., and Comiso, J. C. (2008). Recent radical shifts of atmospheric circulations and rapid changes in the Arctic climate system. *Geophysical Research Letters*, 35:L22701, doi:10.1029/2008GL035607. 144, 158

1.1